UNIVERSITY OF MODENA AND REGGIO EMILIA

DEPARTMENT OF BIOMEDICAL, METABOLIC AND NEURAL SCIENCES

PhD School in Clinical and Experimental Medicine

Coordinator: Prof. Giuseppe Biagini

XXXII Cycle

ROS-responsive polymer conjugates and prodrugs as innovative DDS aiming for the treatment of brain diseases

Supervisor:

Prof. Giovanni Tosi

Co-supervisor:

Prof. Barbara Ruozi

PhD Candidate: **Natalia Oddone**

The PhD candidate was financially supported by The School of Clinical and Experimental Medicine and the thesis project financially supported by FAR UNIMORE and MAECI grant 2019 (Nanomedicine for BBB crossing in CNS Oncologic Pathologies).

The thesis was performed in collaboration between the Biomaterials Laboratory, Institute Bernal, Laboratory of University of Limerick, (Ireland) under the supervision of Prof. Andreas M. Grabrucker, and “Center for Research in Cancerology and Immunology Nantes” (CRCINA), INSERM, University of Angers (France), under the supervision of Prof. Frank Boury and Prof. Emmanuel Garcion.

Acknowledgements

I would like to sincerely thank my Ph.D. supervisors Professors Giovanni Tosi and Barbara Ruozi for their guidance, inspiration and advice provided throughout the years of Ph.D. On the other hand, I would also like to recognize the valuable support that Professors Andreas Grabrucker, Frank Boury and Emmanuel Garcion provided to me during my mobility period abroad. I have learned a lot from all of them, and I am deeply grateful for the time they dedicated to my Ph.D. project. In addition, I would like to thank Professors Anna Janaszewska and Barbara Klajnert-Maculewicz for welcoming me to their Laboratory in behalf of COST (European Cooperation in Science and Technology) Action CA17140 | Nano2Clinic, and from whom I received training and learned valuable techniques, adding new skills to my scientific formation in Nanomedicine.

I would also thank Cinzia Restani, Diego Pinetti and Filippo Genovese from CIGS ("Centro Interdipartamentale Grandi Strumenti"), UNIMORE, for their valuable assistance in terms of characterization measurements as well as to Emmet O'Reilly and Javed Iqbal from Bernal Institute, University of Limerick, for bringing their time to perform GPC measurements. In addition, I wish to thank to Francesca Pederzoli, Jason Duskey, Chiara Alessia De Benedictis, Stephanie Grabrucker, Ann Katrin Sauer, Mathie Najberg, Muhammad Hajimansor, Helene Gregoire and Nela Buchtova, whom assistance was a milestone in regards to my Ph.D. project.

I am grateful to all the colleagues from the Department of Life Sciences (UNIMORE), Bernal Institute (University of Limerick) and INSERM (University of Angers), who were very supportive not only in terms of sharing their knowledge and being helpful regarding the use of new equipment and protocols, but also for encouraging me in the difficult times.

I wish to express my deepest gratitude to my family and friends from Uruguay who supported me and were understandable, demonstrating that they are always there for me beyond distance, and to my little nephew, Lara, that brought me her love from the first time I met her. Finally, I am also deeply grateful to the new friends I made in Europe from several nationalities, from whom I learned that there is no cultural limit when it comes to friendship.

I dedicate this Ph.D. thesis to my parents, sister and grandmothers who I love so much. During these years of Ph.D., they were very supportive and strong enough to overcome long periods without seeing me.

Abstract

In order to obtain more selective and tunable Drug Delivery Systems (DDS), "Smart" DDS that can release their drugs in response to a specific stimulus (e.g. pH, GSH and ROS), are currently under investigation. Inflammatory diseases, neurodegenerative diseases and cancer, including Glioblastoma (GBM) are all sharing a relevant oxidative stress; therefore the design of ROS- responsive DDS for the treatment of these conditions could be a smart and very encouraging approach to access to a selective and specific delivery mediated by a pathological stimulus. Thus, the aim of this PhD thesis was to develop ROS-responsive polymeric conjugates and prodrugs linked to a ROS cleavable group, namely Thioketal (TK) diacid linker that could be used for the treatment of brain diseases.

Aiming to validate the use of TK- containing ROS- responsive polymers and prodrugs, we firstly performed proof-of-concept studies by synthesizing a ROS-responsive methoxy polyethylene glycol (mPEG) polymer (mPEG-TK-COOH) and, by exploiting Cy5 fluorescent dye, ROS-responsive (mPEG-TK-Cy5) and non-ROS-responsive (mPEG-Cy5) polymer conjugates. Full chemical-physical and technological characterization was performed to confirm the success in polymer conjugation and to describe chemical-physical properties of the obtained conjugates; then the ability of these conjugates to respond to ROS was validated in ROS-simulated conditions as well as assessed *in vitro* on Glioblastoma multiforme (GBM) cell lines. These tests were performed in close collaboration with Prof. Grabrucker, University of Limerick, Ireland, and with Prof. Boury, University of Angers, France, during a period of international mobility. Results clearly indicated that mPEG-TK-Cy5 could be selectively released in "pathological" conditions (C6 GBM cells) over "healthy" conditions (DI TNC1 astrocyte cells). Secondly, a prodrug (mPEG-TK-MPH) for the ROS- responsive release of Melphalan (MPH), which is a poorly soluble and non-selective anticancer drug, was synthetized aiming to GBM treatment. A non-ROS responsive prodrug (mPEG-MPH) was also prepared through a similar synthetic procedure. Both prodrugs were characterized and demonstrated to undergo spontaneous auto- assembling into spherical nanometric structures. *In vitro* cytotoxicity assays performed on GBM cells, showed that mPEG-TK-MPH was significantly more cytotoxic than mPEG-MPH on High- ROS GBM cells (C6 and U251MG cells). Remarkably, none of the prodrugs showed to be cytotoxic on Low- ROS astrocyte cells (DI TNC1), demonstrating their safety.

Finally, since PLGA (polylactic-co-glycolic acid) NPs demonstrated to be promising DDS for their application in several diseases, we produced and characterized other ROS-responsive polymeric conjugates with PLGA: PLGA-TK-COOH and PLGA-TK-PLGA, for the selective release of surface attached and encapsulated drugs into oxidative stress featuring diseases. We were able (starting from the PLGA conjugates produced) to formulate ROS-responsive TK-surface functionalized PLGA and PLGA-TK-PLGA NPs, respectively.

We can conclude that due to its selective cytotoxicity in High-ROS GBM cells without being toxic to "healthy" cells, our developed ROS-responsive prodrugs show encouraging results for GBM treatment. On the other hand, the ROS-responsive PLGA NPs developed during this PhD project, could be considered as promising starting point for their future application in GBM as well as in relevant neurodegenerative diseases as Alzheimer's disease.

Keywords: *ROS- responsive conjugates and prodrugs, Thioketal linker, oxidative stress, selective drug release, Glioblastoma*

Riassunto

"Coniugati e profarmaci polimerici "ROS- responsive" come DDS innovativo per il trattamento delle malattie cerebrali"

Al fine di ottenere sistemi di somministrazione di farmaci (DDS) più selettivi e regolabili, sono attualmente sotto studio DDS "intelligenti" in grado di rilasciare i farmaci in risposta ad uno stimolo specifico (pH, GSH, ROS, etc). Ad esempio lo stress ossidativo caratterizza malattie infiammatorie, neurodegenerative e il cancro; la progettazione di DDS "ROS-responsive" potrebbe dimostrarsi quindi un approccio interessante per il rilascio selettivo di farmaci per il trattamento di queste malattie. Pertanto, lo scopo di questa tesi di dottorato è stato quello di sviluppare coniugati e profarmaci polimerici "ROS-responsive" collegati a Tiochetale (TK) diacido, come linker sensibile ai ROS, che potrebbe essere sfruttato per il trattamento delle malattie cerebrali.

Con l'obiettivo di convalidare l'uso di polimeri e profarmaci ROS-responsive contenenti TK, abbiamo eseguito studi preliminari sintetizzando un polimero mPEG (metossi polietilenglicole) sensibile ai ROS (mPEG-TK-COOH). Sfruttando un marker fluorescente come farmaco modello (Cy5), abbiamo realizzato coniugati polimerici sensibili (mPEG-TK-Cy5) e non sensibili (mPEG-Cy5) ai ROS. La completa caratterizzazione chimico-fisica e tecnologica è stata eseguita per confermare il successo della coniugazione polimerica e per descrivere le proprietà chimico-fisiche dei coniugati ottenuti. La capacità di questi coniugati di rispondere ai ROS è stata validata in condizioni simulate dai ROS e valutata *in vitro* su linee cellulari di Glioblastoma multiforme (GBM). Questi test sono stati condotti in collaborazione con il Prof. Grabrucker dell'Università di Limerick e con il Prof. Boury dell'Università di Angers, durante un periodo di mobilità internazionale. I risultati hanno indicato chiaramente che mPEG-TK-Cy5 potrebbe rilasciare selettivamente il farmaco modello in condizioni "patologiche" (cellule C6 GBM) rispetto a condizioni "sane" (cellule di astrociti DI TNC1). In secondo luogo, per il rilascio "ROS-responsive" di Melphalan (MPH), un farmaco antitumorale scarsamente solubile e non selettivo, mirato al trattamento del GBM, è stato sintetizzato un profarmaco (mPEG-TK-MPH) sensibile ai ROS ed il suo controllo non sensibile ai ROS (mPEG-MPH). Entrambi i profarmaci sono stati caratterizzati e si sono sintetizzate strutture nanometriche sferiche autoassemblanti. I saggi di citotossicità *in vitro* eseguiti su cellule GBM hanno dimostrato come mPEG-TK-MPH sia significativamente più citotossico su cellule GBM con elevati livelli di ROS (cellule C6 e U251MG) rispetto al controllo (mPEG-MPH). Sorprendentemente, nessuno dei profarmaci ha mostrato di essere citotossico su cellule di astrociti con bassi livelli di ROS (DI TNC1), confermando la loro *safety*.

Infine, con l'obiettivo di ottenere un rilascio selettivo (nelle malattie con stress ossidativo) e sfruttando la potenzialità di NPs polimeriche (a base di acido polilattico-co-glicolico, PLGA) abbiamo prodotto e caratterizzato altri coniugati polimerici "ROS-responsive" con PLGA (PLGA-TK-COOH e PLGA-TK-PLGA) e formulati in NPs funzionalizzate.

Possiamo concludere quindi che a prescindere dal successo di coniugazione chimica e formulazione tecnologica, per i risultati *in vitro* ottenuti, l'approccio "ROS-responsive prodrug" si è dimostrato promettente per un possibile trattamento del GBM, caratterizzato da elevati livelli di ROS; approccio che può essere ulteriormente ampliato sfruttando anche altri polimeri (come il PLGA) e applicato non solo al GBM ma anche ad altre patologie caratterizzte da alti livelli di ROS, come le patologie neurodegenerative.

Parole chiave: *ROS coniugati e profarmaci sensibili, linker tioketale, stress ossidativo, rilascio selettivo di farmaci, glioblastoma*

Table of contents

Abbreviations:

(1,4-phenyleneacetone dimethylene thioketal)
(PPADT); 37
1-palmitoyl-2- hydroxysn-glycero- 3-phosphocholine
(PPC); 42
3-Mercaptopropionic acid
(3-MPA); 62
3-morpholinosydnonimine
(SIN-1); 32
4-amino-1,8-napthalimide
(4-AN); 31
4-hydroxybenzoic acid
(HBA); 31
Adamantane
(ADA); 46
Alpha-tocopheryl succinate
(α-TOS); 46
Alternative magnetic field
(AMF); 18
Alzheimer's disease
(AD); 20
Blood Brain Barrier
(BBB); 21
Blood brain tumor barrier
(BBTB); 110
Brain-derived neurotrophic factor
(BDNF); 21
Camptothecin
(CPT); 39
Cervical cancer cells
(HeLa); 35
Chinese hamster ovary cells
(CHO); 50
Chlorambucil
(CHL); 33
Chlorin 6
(Ce6); 26
Cysteine-(proline)5-lysine
(CP5K); 32
Diaxophosopholane
(PBYP); 45
Dichloromethane
(DCM); 62
Dihydroethidium
(DHE); 94
Dimethylformamide
(DMF); 62
Distearoyl phosphatidylethanolamine (DSPE)- Polyethylene glycol
(DSPE-PEG); 43
Docetaxel
(DTX); 33
Drug Delivery Systems
(DDS); 14
Ethidium homodimer
(EthD); 98
Fluorogens with aggregation-induced emission
(AIEgens); 48
Fullerene
(C60); 46
Glioblastoma
GBM; 56
Glutathione
(GSH); 14
Human breast cancer cells
(MCF-7); 28
Human glioma cells
(U87); 48
Human prostate cancer cells
(PC-3); 28
Huntington's disease
(HD); 20
Hyalurinuc acid
(HA); 16
Hyaluronidase
(HAase); 16
Inflammatory bowel disease
(IBD); 22
Ionizing radiation
(IR); 29
Ischemic-reperfusion injury
(I/R); 22
Lipopolysaccharide
(LPS); 32
Matrix metalloproteinases
(MMPs); 16
Mesoporous NPs
(MSNs); 46
Mesoporous titanium oxide nanoparticles
(MTN); 48
Methoxy polyethylene glycol

Chapter 1:

General introduction

1.1. “Smart” Drug Delivery Systems (DDS)

With the objective to obtain more efficacious pharmaceutical formulations for a site targeted drug release with minimal undesirable effects, DDS (as liposomes, polymeric nanoparticles, block co-polymer micelles, hydrogels, dendrimers, etc.) have been developed and *in vitro*/*in vivo* tested. These systems showed a remarkable ability to minimize degradation, prevent harmful side-effects, increase solubility, bioavailability and the fraction of drug accumulated at the target site [1,2]. Despite being demonstrated to be efficient, certain shortcomings must be attained in order to refine them. For instance, since the release of drugs from nanocarriers is frequently modulated by diffusion or degradation, *in vivo* results are variable, being greatly influenced by the physio-pathological conditions of the patient. Moreover, the stabilization of drugs incorporated into polymeric or lipid nanocarriers results low and the drug can be lost during storage or in blood circulation, leading to off-target effects and a poor effectiveness of drugs [3,4]. A possible approach to solve this problem could be to adopt chemical/technological strategies that change the stability and properties of the material that forms the DDS, so that they respond to an stimulus, leading to drug release [2]. Generally, these new DDS are known as “Smart” DDS, in which the term “Smart” refers to the process in which drugs are selectively released from these DDS when they reach their target tissues or organs in response to a stimulus. The selective release of drugs from “Smart” DDS also implies that at off-target sites, the drug is not release or released but an extremely low rate [6].

Thus, by means of exploiting these type of DDS, the aforementioned issues of conventional nanoformulations, can be broadly improved [7,8]. Accordingly, “Smart” DDS in response to a) endogenous (e.g. enzyme, pH, redox: Glutathione (GSH) and Reactive Oxygen Species (ROS)), b) endo-exogenous (temperature), and c) exogenous stimuli (e.g. temperature, light, ultrasonic wave and electric/magnetic field), are currently being widely explored [8–11] (Figure 1).

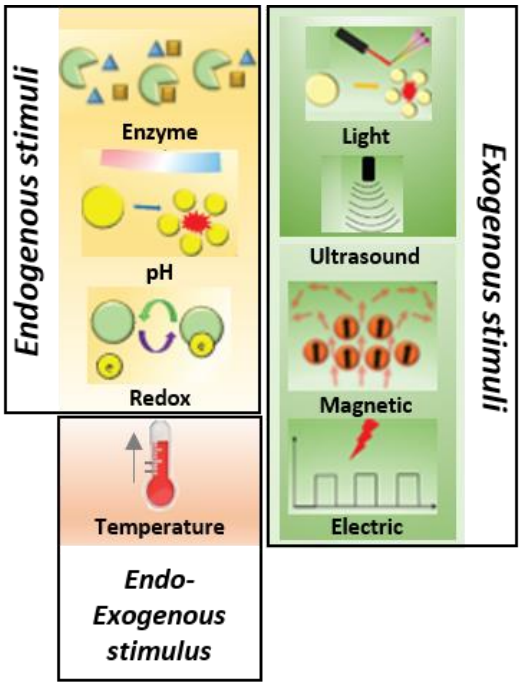

Figure 1: Main stimuli exploited for the formulation of "Smart" DDS (Adapted and modified from refs. [12,13]).

While endogenous stimuli have a direct association with pathological state, exogenous stimuli are artificially applied in order to trigger controlled on demand drug release [12]. Furthermore, in order to achieve better efficacy, dual and multi-stimuli responsive DDS, have also been developed [14].

The possibility of a "Smart" DDS to respond to a given stimulus or stimuli, is achieved by the integration of "sensitive" or "responsive" materials that are prone to suffer chemical modifications (structural changes or cleavage), promoting drug release. Several materials such as polymers, lipids and inorganic NPs as well as natural occurring polymers, such as dextran, hyaluronic acid, chitosan and their blends as well as cyclodextrin and derivatives, are being employed to produce "Smart" DDS [6,15,16]. Noteworthy, a prodrug strategy that consists of the covalent conjugation of a drug to a polymer through a stimulus sensitive linker [17], that creates amphiphilic structures with self-assembly features, is currently being exploited for the design of these type of DDS. Since prodrugs can prevent premature drug leakage as well as rapid release, this strategy could be relevant in a number of clinical applications in order to impact on undesired effects produced by rapid and un-controlled diffusion of drugs in non-target sites [18].

1.2. Types of stimuli exploited in the design of "Smart" DDS

1.2.1. Endogenous stimuli

Enzyme. In numerous diseases, it is frequent to find an overexpression of enzymes that are related to metabolic processes (glycosidases, lipases, phospholipases and proteases) and thus, this feature can be exploited to trigger drug release into disease sites [5,19]. DDS that respond to this stimulus, contain at least one component in their structure that is a substrate of an enzyme or a substrate mimic, undergoing chemical/physical change upon enzymatic action [13]. In tumors, for example, high concentrations of hyaluronidase (HAase), matrix metalloproteinases (MMPs), β-glucuronidase and esterases, are generally common and therefore, DDS that are made up from a substrate/s of any of these enzymes can be designed. For example, the presence of hyaluronidases in tumor tissues has been exploited for gene delivery application by including in the formulation a protective hyaluronic acid (HA) that degrades enzymatically in tumor tissue [20].

pH. Among the different stimuli that can be exploited for the release of therapeutics, pH is one of the most employed. In normal physiological conditions, the pH is maintained at around 7.4, but in certain disease conditions as cancer and inflammation, microenvironment's pH turned into acidic values. On the other hand, endosomal/lysosomal cellular compartments as well as the stomach, are acidic. Thus, pH-responsive DDS can be exploited for the delivery of drugs in cancer, inflammation or into endo/lysosomes as well as for the selective administration of an orally administrated drug in the stomach or intestine [21].

The strategies that are used for the design of pH-sensitive DDS can be:

1. Using acid or basic polymers which undergo conformational changes in response to a variation of pH. For instance, the polymers that respond to acidic pH, contain multiple protonatable groups, and include histidine, tertiary amine and sulfonamide-containing groups [17,21,22].
2. Using pH cleavable linkers for the release of polymer attached molecules. Linkers containing hydrazone, orthoester, acetal, imine and vinyl ether chemical groups, have been generally used to obtain pH-sensitive prodrugs and can be readily hydrolyzed in mild acidic conditions (pH ~ 4.0−6.5). Their hydrolyzation kinetics

is dependent of the pH (the lower the pH, the fastest the cleavage), being accelerated at higher temperatures [22,21,23].

3. Using peptides that at neutral pH present low interaction with cell membranes; these peptides at slightly acidic environments form transmembrane complexes with the subsequent permeabilization of cell membranes [22].

Redox. Since in pathological conditions redox status is unbalanced with respect to normal tissues, the design of redox DDS in therapy gained attention [6]. In this regard, DDS which respond to reductive or oxidative stimulus as GSH and ROS were developed [24]. As in certain tumors (i.e. breast, ovarian, head, neck and lung cancers) the GSH amounts are higher in comparison to normal tissue, GSH-sensitive linkages were extensively exploited. DDS sensitive to GSH are made of di-sulfide bridges and mimic a stimuli sensitive response that already exists in nature. For instance, HIV virus uses the reduction of disulfide bonds to interact with host target cells [5]. This linker can be conjugated to the main chain or side chain of linear polymers or onto NPs surface for the selective release of drugs, nucleic acids, imaging agents and proteins [17]. The exploitation of ROS stimulus is more recent, and it will be explained in a separate section.

1.2.2. Endo-exogenous stimuli

Temperature. In diseases such as inflammation and cancer, microenvironment's temperature is increased with respect to normal body temperature (~37 °C); thus, temperature responsive delivery systems can be used to triggered drug release [6]. The increase in temperature in tumor sites (~40-42 °C) allows for the possibility of using thermo-responsive polymers that undergo a temperature-dependent morphological change inside tumor tissues [25,26]. Due to their low critical solution temperature, poly(N-isopropylacrylamide) (PNIPAM) polymers are the most widely used thermo-responsive materials and can be used in the formulation of micelles, liposomes and polymeric NPs [27]. On the other hand, in order to increase drug release from temperature sensitive DDS, the temperature can be further increased by means of exogenous triggers (e.g. light, ultrasound and magnetic field) [6,24,25]. This process, known as induced hyperthermia, apart from increasing the sensitivity of tumors to therapeutics, can also permeabilize membranes and therefore enhance DDS cell uptake [28].

1.2.3. Exogenous stimuli

Light. Since light is not an invasive stimulus, it was widely investigated in cancer therapy for forced production of toxic concentrations of ROS by means of light absorbing molecules, known as photosensitizers (PSs), that generates singlet oxygen upon light stimulus [29]. As an example, the use of light in therapy, known as photodynamic therapy (PDT) was successfully employed for the treatment of skin diseases in the clinic [30]. Besides, the efficiency in treatment of solid tumors through this technique can be also achieved by the use of near-infrared (NIR) light (650–900 nm) that provides a deep tissue penetration without tissue damage [31]. PDT can be used in combination with other stimulus as ROS or GSH to induce drug release from appropriate designed stimuli-responsive DDS [32].

Ultrasound. This stimulus is being applied in clinical practice for diagnosis and treatment, by means of the application of low and high frequencies, respectively. The possibility to regulate tissue penetration as well as the non-invasive nature of this stimulus, with lack of ionizing radiation, make the application of this stimulus very straightforward. In addition, the cavitation phenomena as well as the radiation forces (generated by ultrasounds) trigger mechanical and/or thermal effects that can promote drug release from DDS as well as the permeability of biological barriers [13,27].
The use of chemical agents, known as sonosensitizers, can be also used to respond to ultrasound stimulus in Sonodynamic Therapy (SDT), an approach derived from PDT as non-invasive cancer therapy [33]. As it has better tissue penetration in comparison with PDT, SDT was therefore recently proposed to achieve synergistic antitumoral effect with DDS that respond to endogenous stimuli as ROS [34].

Magnetic field. Since the magnetic interaction with the body is scarce, the use of magnetic-sensitive DDS is a good choice aiming to decrease at the minimum level possible side-effects or toxic effects on endogenous pathways. Materials that respond to magnetism can undergo a real-time response to a brief pulse [13]. A radiofrequency of alternative magnetic field (AMF) can be used for controlled drug release through structure disassembly of magneto-thermally responsive DDS [12] and used for controlled drug release, guidance, targeting, imaging (MRI and fluorescence) as well as hyperthermal therapy [13] inducing a selective heating of tumors [27].

Electric pulses. The introduction of polyelectrolytes that contain large numbers of ionizable groups confers responsiveness to electrical stimulus through polymer shrinking or swelling [12]. The drawback of using electric field as a stimulus is the possibility to get undesired induction from heat and a non-ON/OFF reproducibility of the stimulus [13]. In particular, a critical point lies on the selection of the electric current which has to be sufficient to trigger drug release, but not to lead to an undesired stimulation of local tissue nerve endings [35].

1.3. ROS and oxidative stress

Reactive oxygen species (ROS) are small oxygen containing molecules that have a single unpaired electron in their outermost shell of electrons [23]. These species are mainly generated endogenously during aerobic cellular metabolism, but they can be also derived from the presence of xenobiotics, cytokines, bacterial invasion as well as produced in response to exogenous sources (air pollutants, tobacco smoke, ionizing and nonionizing radiations, food and drugs) [11,36–38]. ROS consist of free radical and non-radical compounds. The first ones are molecules which have unpaired electrons as superoxide anion, hydroxyl and peroxide radicals, while the second ones, as H_2O_2, singlet molecular oxygen and nitric oxide, can easily be transformed to free radicals. For instance, H_2O_2 leads to hydroxyl radical formation, in the presence of transition metals.

As known, ROS, and in particular H_2O_2, are involved in cell signaling, cell cycle progression, differentiation and apoptosis [23,24,26]. The presence of physiological ROS scavengers (e.g.: superoxide dismutase, catalase and glutathione peroxidase), therefore plays a fundamental role on redox balance and regulation of signaling pathways.

When alteration on redox balance occurs due to an accumulation of reducing molecules (e.g., GSH, NAD+, and NADP+) or ROS, biomolecules as DNA, lipids and proteins are prone to suffer modifications, thus hampering their functions and leading to pathological conditions (Figure 2A-C) [2,11,26–28]. In addition, ROS overproduction was confirmed to directly contribute to tissue injury due to continuous lipid peroxidation, inflammatory cascade initiations and systemic disturbances [29]. Although it is still on debate whether ROS play a causative role or acts in association with other factors during the pathogenesis of a given disease, it is almost clear that a molecular damage induced by ROS is closely related to the birth and even the progression of several diseases [30,22].

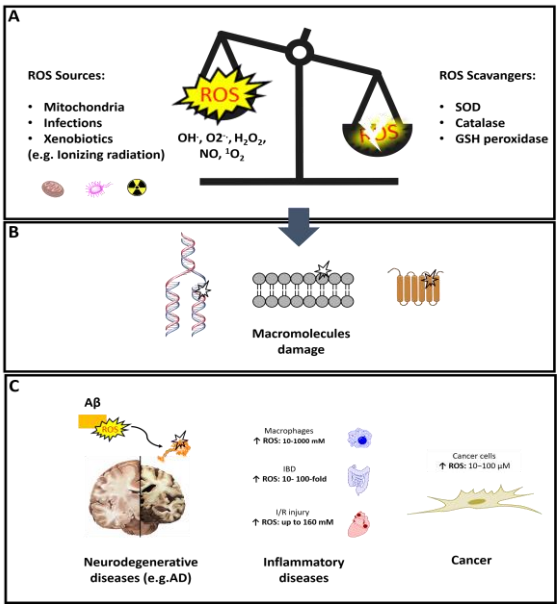

Figure 2: Scheme showing the relationship among unbalanced ROS **(A)** and the macromolecular triggered damage **(B)**. **C)** Diseases featured by ROS. The estimated concentrations of H_2O_2 in certain diseases are shown.

1.4. Diseases featuring oxidative stress. Opportunities for the design of ROS-responsive DDS

1.4.1. Neurodegenerative diseases

Oxidative stress in the Central Nervous System (CNS) is present and involved in aging and neurodegenerative diseases [45]. The high oxygen demand in the brain, along with a limited antioxidant defense make neurons and glial cells to be highly susceptible to ROS [46,47].

An overproduction of ROS was therefore proven in several neurodegenerative diseases: as an example, in Huntington's disease (HD), the high concentrations of ROS contribute to several alterations (e.g. mitochondrial DNA mutation, respiratory chain damage and membrane permeability) of the pathological brain. In the case of Parkinson's disease (PD), the overproduction of cytokines, inflammatory mediators and ROS by microglial cells in substantia nigra are common features in patients with this disease [35, 36].

Lastly, Alzheimer's disease (AD) is another example of a disease featured by ROS, in which, in contraposition to normal brains, higher levels of ROS are present in brains from patients with this disease [49]. At a deeper level of investigation, as AD is mainly characterized by extracellular Aβ oligomerization, aggregation and plaque formation,

ROS production is induced by metal ions associated to Aβ plaques (copper, iron, zinc). Furthermore, around these plaques, microglial cells stimulated by inflammatory cytokines produce more ROS [49,50], leading to neuronal death (Figure 2C) [47].
In all these neurodegenerative diseases, a promising strategy could be directed against the overproduction of ROS, for example, by means of antioxidants [51]. But in addition, this peculiar high ROS concentration can also be exploited as a stimulus to selectively release antioxidant or other therapeutics in these sites.
Even though the undoubtedly role of ROS in all these pathologies, ROS-responsive DDS for the selective release of therapeutics in neurodegenerative diseases were scarcely explored. The need of reaching the brain by crossing the Blood-Brain Barrier (BBB) might be the reason that explains why the design of these smart DDS is still elusive. It is not surprising if we consider that the first priority in CNS delivery consists of overcoming the BBB and, therefore, a tailored design of DDS with surface modification with a BBB-targeting ligand is often required [52]. Nevertheless, some examples in the literature are reporting the use of ROS-responsive DDS for the treatment of cerebral ischemia (stroke). In this condition, featured by a strong alteration in BBB permeability, the ischemic neurons produce ROS that not only cause detrimental effect on neuronal connections, but also contribute to BBB damage and therefore disability [53,54]. For instance, Lv and co-workers developed a ROS-responsive DDS for the delivery of neuroprotective agent (NR2B9C), demonstrating a reduction of the damaged brain after ischemia in a rat model of middle cerebral artery occlusion [54]. As neural stem cells (NSC) promote proliferation and differentiation to neurons and regeneration, and can migrate into ischemic regions, the intravenous injection of NSC demonstrated potentially application in stroke [40,41]. In this regard, Jiang and co-workers, proposed to transfect NSC with ROS- responsive gene delivery system for the release of brain-derived neurotrophic factor (BDNF) expressing plasmid. After intravenous administration, these transfected cells migrated into ischemic regions, and demonstrated to dramatically increase mice survival with respect to non-treated mice, up to 60% [53].

1.4.2. Inflammatory diseases

Inflammation microenvironment is characterized by amplified levels of ROS (Figure 2C) [56,57]. As part of the inflammatory response, leukocytes release multiple pro-

inflammatory cytokines (e.g. IL-1 and IL-6) as well as ROS [58]. The leukocytes that migrate into inflammation sites produce ROS, which in turn lead to the recruitment of more leukocytes and, therefore stimulate further production of ROS [59]. For instance, the local H_2O_2 concentration in activated macrophages can reach 10-1000 mM [60] with respect to physiological level of ROS, around 0.1–1 μM. For example, in inflammatory bowel disease (IBD), which is characterized by a continuous inflammation state of the intestine [61], the levels of ROS may increase from 10- to 100-fold in comparison to healthy intestine [36]. Similarly, ROS play an important role also in inflammatory lung diseases, in which the concentration of H_2O_2, can increase up to 20-fold if compared with normal conditions (0.1–1 μM) [60]. Similarly, in an ischemic-reperfusion (I/R) injury condition, where an exacerbated production of mitochondrial ROS during reperfusion phase leads to vascular dysfunction, acute inflammation and tissue cell death [64,65], the H_2O_2 levels can achieve a concentration as high as 160 mM [66].

Exacerbated levels of ROS are also related to the pathogenesis and progression of atherosclerotic vascular disease [57], being the elimination of H_2O_2 suggested as an antithrombotic therapy for the treatment of vascular diseases [67]. For instance, due to a failure of the response to an ischemic event, diabetic patients have a 4-fold risk of developing peripheral artery disease (PAD). It has been demonstrated that by reducing the oxidative stress, this response can be improved [59]. Thus, the restoration of H_2O_2 from pathological to physiological levels could be also a promising strategy to alleviate inflammation [68].

1.4.3. Cancer

Numerous stimuli-responsive platforms exploit the extracellular environments of tumors for triggered drug delivery in cancer. Taking into account the acidic pH in tumor tissues, “Smart” DDS which respond to acidic pH were intensively explored for cancer application [35]. Despite their effectiveness [36], as lysosomes acidic pH is present in both tumor and normal cells, their selectivity is limited [37].

GSH, is another stimulus that has been taken into consideration for the design of “Smart” DDS in cancer therapy [38]. However, as this stimulus can be found at high concentrations (2–10 mM) in both cancer and normal cells, the selectivity of this stimulus in cancer cells over normal ones is also limited [37,39].

On the other hand, ROS levels in cancer cells are higher than in normal cells. Cancer cells can tolerate concentrations of H_2O_2 that are in the range of 10−100 μM (Figure 2C), while in normal cells an H_2O_2 concentration of 1 μM is already toxic [21]. Only during apoptosis, normal cells can reach the physiological concentrations of H_2O_2 found in cancer cells [22]. This substantial difference on H_2O_2 concentration suggests that ROS-responsive DDS could confer selectivity in cancer therapy. In addition, H_2O_2 is not only present in the cytosol, but also can diffuse into lysosomes [41], being the reported high levels of ROS inside endo/lysosomes able to trigger both drug release and endo/lysosomal escape of endocytosed ROS-responsive DDS [42].

1.5. ROS- responsive materials

In order to design efficient ROS-responsive DDS, several ROS-sensitive materials were studied. In particular, the synthesis and oxidation properties of poly (propylene sulfide) (PPS), selenium and tellurium containing polymers (monoselenide/telluride (Se/Te) and diselenide/ditelluride (Se-Se/Te-Te), polyoxalate, poly(proline), phenyl boronic acid/ester, and thioketal (TK), were well documented in the literature [76] and are shown in Figure 3.

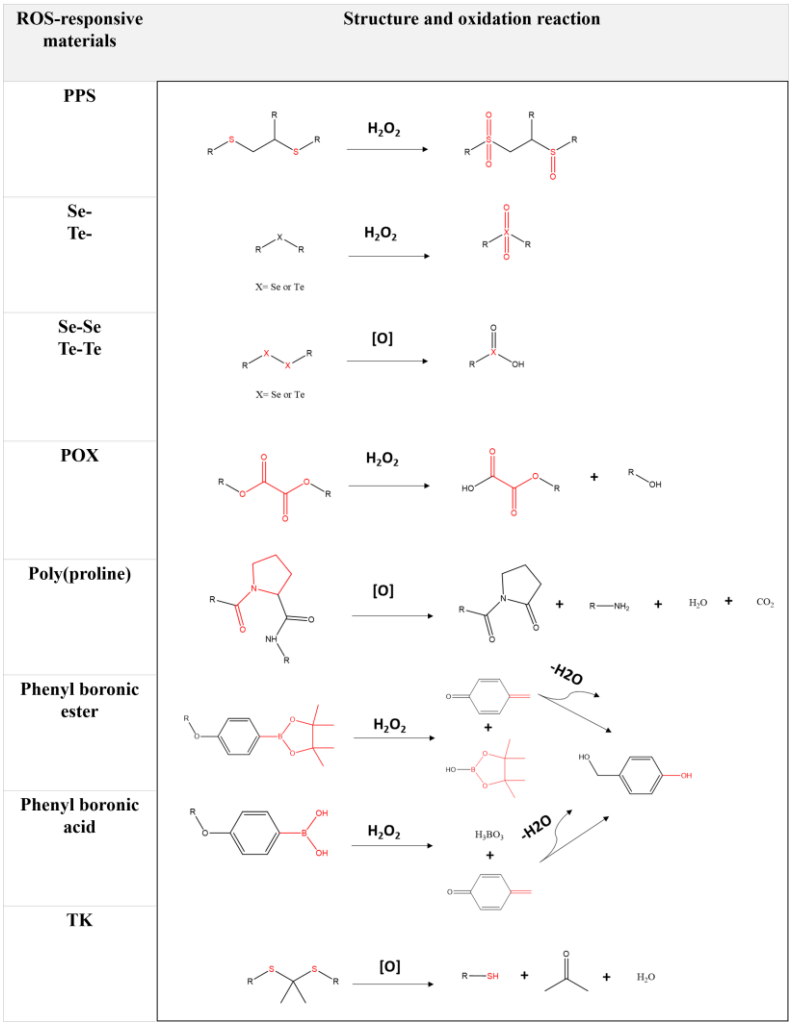

Figure 3: Summary of ROS-sensitive materials described, and the products and by-products resulting from their structural modifications upon oxidation by ROS. In red are highlighted the atoms/bonds that take part in the reaction with ROS. [O] refers to the ability to be oxidized upon all types of ROS (adapted and modified from refs. [25,77,78]).

Depending on the material and on the formulation, the release of drugs can occur by a) disassembly of carriers due to a conformation transition of polymers upon ROS exposure with subsequent polymer solubilization in aqueous media or b) carrier degradation after backbone breakdown of polymers mediated by the cleavage of ROS sensitive bonds (Figure 4). PPS and Se/Te- containing polymers are included in the first group, while Se-Se/Te-Te- containing polymers, polyoxalate, poly(proline), phenyl boronic ester/acid and TK, are comprised in the second group [4,22,37].

In this section, examples of ROS-responsive DDS designed by exploiting these ROS-sensitive materials will be shown. The ROS-responsive cleavable TK material will be discussed in a separate section.

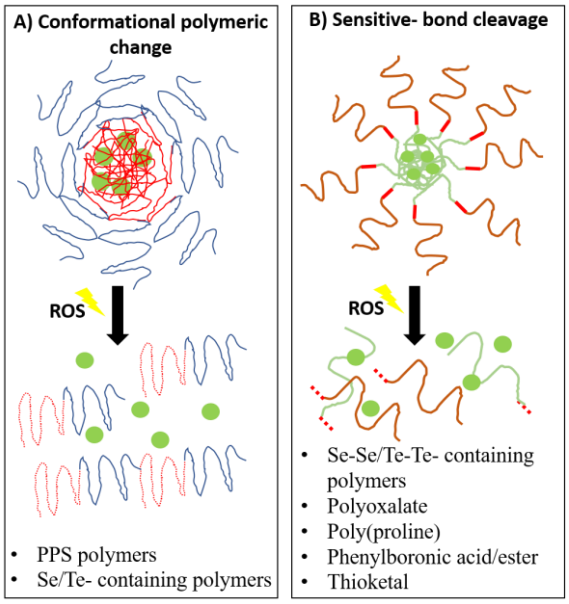

Figure 4: Graphical and simplified representation of the mechanism by which ROS-responsive DDS interact in the presence of ROS. A) DSS that respond to ROS through a structural change. **B)** DDS that respond to ROS by cleavage. In both cases, the polymers or chemical units that respond to ROS are represented in red.

1.5.1. Poly (propylene sulfide) (PPS).

Polypropylene sulfide (PPS), composed of repeating units of sulfide, was the first ROS-sensitive material to be employed in the design of ROS- responsive DDS, being sensitive to H_2O_2 [11,79]. Under oxidative conditions, PPS is transformed to sulfones and sulfoxide with an abrupt hydrophobic-to-hydrophilic transition which leads to morphological disruption, swelling and solubilization of PPS-based DDS [80,41,77].

The physical-chemical properties of PPS polymers make them appropriate for the preparation of ROS-responsive amphiphilic blocks, and therefore, open the possibility of formulating ROS-responsive micelles, NPs and hydrogels. Nevertheless, they have not been used for the preparation of prodrugs, in which materials that are prone to be cleavable are well suited for this application.

This ROS-responsive material was also proposed to be used alone, or in combination with other stimulus (as light, temperature variation and specific enzyme) for the treatment of cancer and inflammatory conditions, respectively [81–85].

Regarding cancer application, PPS-based DDS were proposed to be used in combination with light. For instance, PPS-PEG co-polymer micelles conjugated with Chlorin 6 (Ce6) and loaded with DOX were used for combined chemo and PDT. *In vitro* and *in vivo* studies on colon cancer cells and melanoma tumor bearing mice showed that upon irradiation, these micelles showed the highest DOX cytotoxicity as well the highest decrease of tumor volumes upon light irradiation with respect to control samples [81]. Dai and co-workers used the same co-polymer (PPS-PEG) to co-encapsulate DOX and ZnPc into micelles targeted against tumor by means of a specific ligand, namely folic acid (FA). In comparison to free DOX and empty micelles, the cytotoxicity of human liver carcinoma cells (HepG) treated with these micelles was the highest upon irradiation, being this result in accordance with the inhibition of tumor growth and survival prolongation seen in treated mice [82]. In another example, an anti-hypoxia-inducible factor-1 alpha (HIF-1α) inhibitor (Doxy) was co- encapsulated along with the photosensitizer IR780 in mPEG-PPS NPs, demonstrating high *in vivo* antitumor efficacy [83].

Regarding their application in inflammation, PPS-based DDS were proposed for the specific treatment of sepsis-induced liver injury [42], PAD in diabetes [59] and for the potential treatment of I/R injury [85]. For the treatment of sepsis-induced liver injury, Melatonin (Mel) encapsulated in PEG-b-PPS NPs lead to a higher attenuation of inflammatory response (lower lipid peroxidation, tissue neutrophil accumulation and inflammatory cytokine levels) and liver injury in comparison to free Mel after 12 h of LPS mice exposure [42]. In the case of PAD in diabetes, the use of Curcumin encapsulated in PPS microparticles showed protection against H_2O_2-induced fibroblast (NIH 3T3) cell cytotoxicity. Interestingly, protection against H_2O_2-triggered cytotoxicity was also observed with blank PPS microparticles, which can be explained by the ability of these microparticles to scavenge H_2O_2. Similarly, the ROS levels on activated macrophages treated with Cur-PPS were significantly decreased in comparison to blank PPS, showing an additive effect. On the other hand, the levels of ROS in gastrocnemius muscle of mice model of PAD, treated with either blank or Cur-PPS microspheres, were significantly reduced [59].

An example that combines ROS response with a secondary stimulus, was reported by Gupta and co-workers. These researchers developed a dual ROS and temperature responsive micelles made up from PSS di-block and poly[(propylenesulfide)-block-(N,N-dimethylacrylamide)-block-NIPAAM] (PPS-b-PDMA-b-PNIPAAM) that can be transformed into hydrogel when the temperature transition to 37 °C. These hydrogels demonstrated to be able to decrease ROS mediated cell death and be biocompatible on mice fibroblast cells (NIH 3T3) [84]. Interestingly, in these two last examples, it has been observed that cells exposed to either blank PPS microspheres or hydrogels can improve cell viability under oxidative conditions. Thus, in some cases, PPS-based DDS not only act as drug reservoirs, but also as ROS scavengers, preventing ROS-induced cell death [59,84].

Regarding the PPS- based DDS safety, some formulations reported in the literature showed to be biocompatible while others showed to have certain cytotoxicity, depending on the concentration range. For example, polypropylene sulfide-block-N,N-dimethylacrylamide (poly (PSS-b-DMA)) micelles developed by Gupta and co-workers did not demonstrate to be cytotoxic across different concentrations on macrophages (RAW 264.7 cells) [86] as well as Poly[(propylenesulfide)-block-(N,N-dimethylacylamide)-block-NIPAAM] (PPS-b-PDMA-b-PNIPAAM) tri-block co-polymer micelles did not show to be cytotoxic on fibroblasts [84]. On the other hand, PPS microspheres can be cytotoxic to normal cells at 50-1000 μg/mL concentration [85].

1.5.2. Selenium and Tellurium containing DDS

1.5.2.1. Selenide (Se)/Telluride (Te)

Polymers containing Monoselenium and monotellurium bonds (Se/Te) respond to ROS by undergoing a transition change from hydrophobic to hydrophilic that is caused by changes on the oxidized state of Se/Te atoms [87,88]. In comparison to thioether bonds, selenide and telluride are much more sensitive to ROS [89].

The difference between Se- based DDS and Te- based DDS is related to their ROS-sensitivity [87]. For example, Yu and co-workers developed Se and Te- containing polycarbonate NPs encapsulating DOX and Ce6, for combined chemo and PDT application, observing the highest oxidation rate from ethyl telluride over ethyl and phenyl selenide, with enhanced NP cytotoxicity on human breast cancer cells (MCF-7) due to an accelerated release of DOX triggered by light and synergistic effect with PDT [89].

1.5.2.2. Diselenide (Se-Se)/Ditelluride (Te-Te)

Di- selenide bonds (Se-Se) respond to ROS (H_2O_2, hydroxyl radical, singlet oxygen, etc.) by a cleavage mechanism and based on the quantity of Se-Se repeating units, the ROS sensitivity of this platform can be amplified [90]. Upon ROS, they can be degraded into seleninic acids or selenonic acids [91,92], and like monoselenide, diselenium-containing polymers can also respond to reductive environments and thus, being redox responsive [25,90]. On the other hand, selenide bonds demonstrated to be 10-fold more sensitive to ROS than monoselenide [90]. For instance, Deepagan and co-workers designed diselenide-crosslinked micelles encapsulating DOX for cancer treatment, and demonstrated better *in vitro* cytotoxicity than non-crosslinked micelles on human prostate cancer cells (PC-3) with high levels of ROS, showing less cytotoxicity on normal cells [93].

Regarding Te-Te- based DDS, the energy of Te-Te bond is estimated to be 149 KJ/mol and lower than that of Se-Se (192 KJ/mol) and S-S bond (240 KJ/mol), respectively, suggesting that Te-Te-containing polymers are more predisposed to be cleaved [48]. For example, Te- containing polymer micelles demonstrated to promptly respond to H_2O_2 at the physiological concentration of ROS in tumors (100 μM) [94]. For instance, Wang and co-workers prepared self-assembled PEG-PUTeTe-PEG NPs encapsulating DOX for cancer treatment, demonstrating concentration- dependent cytotoxicity on mouse breast cancer cells (4T1) *in vitro* and higher inhibition of tumor volumes *in vivo* on 4T1 tumor bearing mice [87].

1.5.2.3. Selenium and Tellurium based ROS-responsive DDS in combination with other stimuli

Attractively, the use of γ-ray ionizing radiation (IR) as a second stimulus with diselenide and ditellurium containing polymers has been proposed. Radiation chemistry revealed that ROS, as H_2O_2 and hydroxyl radicals, could be generated by means of irradiating water with ionizing radiation [92,94]. For instance, Ma and co-workers explored the combination of PEG-PUSe-Se-PEG micelles with a γ-ray dose of 5 Gy, demonstrating that these micelles swelled at this dose as well as can release about 45% DOX. In addition, *in vitro* results performed with empty micelles demonstrated cytocompatibility [92]. Later on, Cao and co-workers, prepared Te- containing micelles which were irradiated with γ-ray at a dose that is used in patients (2 Gy) and observed a reduction in the diameter of the micelles (from 200 nm to 35 nm) and thus, as in the case of diselenide, demonstrating that the ROS produced by means of γ-ray radiation can trigger the response of Te-based DDS [94].

Regarding the combination of DDS based on these ROS-responsive materials with PDT, a recent work used diselenide to prepare HA-Se-Se-Ce6 co-polymers that self-assemble into micelles for a light triggered amplified release of Ce6 for an enhanced PDT in cancer. The micelles demonstrated a higher *in vitro* toxicity than free Ce6 on light exposed 4T1 cells, without significant toxicity in the dark. *In vivo* studies with these micelles demonstrated a 5-fold and 10-fold inhibition of tumor growth with respect to free Ce6 treated and non-treated mice. Furthermore, these micelles were not toxic to breast cancer cells when they were not exposed to irradiation [95].

Despite the potentiality of DDS developed from these materials to be applied in the treatment of High-ROS diseases, the lack of *in vitro* and *in vivo* studies focused on toxicity and bioavailability of ROS- responsive selenium and tellurium- based DDS is a major limitation, since poor number of data regarding their safety is present. Thus, their cytotoxicity is a crucial factor that needs to be evaluated in the next future [11,49].

Since Se is an essential element that is a component of selenoproteins [97], it can be hypothesized that Se-containing DDS might be biocompatible. On the other hand, differently from Se, Te does not represent an essential element, being the available data regarding its toxicity scarce [98]. From the examples given here, safety issues were not

found with neither Selenium nor Tellurium containing DDS. For instance, blank crosslinked selenide micelles did not show to be cytotoxic up to 200 mg/ml [93]. On the other hand, Wang and co-workers observed that both mouse fibroblast cells (NIH/3T3) and 4T1 cells incubated with blank Te-Te NPs were viable even at a high concentration of 0.4 mg/mL [87]. Yu and co-workers reported the design of ROS- responsive aliphatic polycarbonates containing different selenides and telluride groups [89]. NPs prepared from these copolymers were evaluated in terms of their cytocompatibility using a tumor and a non-tumor cell lines (concentration range: 0-0.5 mg/mL), showing negligible cytotoxicity. Furthermore, oxidation derivatives of ethylselenyl and ethyltellanyl co-polymers showed cytocompatibility. Nevertheless, the oxidation derivative of phenyl selenyl co-polymers showed to be cytotoxic in a concentration-dependent manner [89].

1.5.3. Polyoxalate (POX)

Polyoxalate (POX) containing polymers, are formed by a backbone of peroxalate linkages and can be degraded preferentially upon H_2O_2 exposure [99], being responsive even to nanomolar concentrations of this type of ROS [1,4,100]. Since POX can be degraded in response to H_2O_2, but also in water, producing biocompatible products, POX DDS are best suited to be used in body locations where fast degradation is necessary, as they can degrade even in the absence of ROS [101].

POX have been proposed to be used in tissue engineering applications [102] and also for the encapsulation of drugs into NPs [1]. For instance, hybrid polyvinyl alcohol (PVA)/POX nanofibers (NFs) for the potential application of inflammatory diseases were prepared. Proof-of-concept studies performed on NFs loaded with Rhodamine B (RB) showed a faster degradation in comparison to those exposed to PBS and high cumulative RB release. These NFs demonstrated to be compatible with both cells and macrophages [102].

This ROS-responsive material was mainly exploited to prepare NPs for the treatment of inflammatory conditions or for the treatment of asthma and hind limb ischemia/reperfusion in mice models, without showing any side-effect thanks to their high biodegradability and biocompatibility [101]. Interestingly, HPOX NPs that integrate an antioxidant and anti-inflammatory herbal agent, Phenolic acid 4-hydroxybenzoic acid

(HBA), into the polyoxalate polymer backbone were prepared and intended for the treatment of asthma [100] as well as I/R injury [103].

Stimulated macrophages treated with HPOX have reduced their ROS levels in a short exposure time with almost a complete inhibition of mRNA expression of inflammation markers. Minimal inflammatory alterations were detected in lungs extracted from mice model of asthma; reduction of inflammation, lung epithelial damage and airway wall thickness [100]. For the treatment of I/R injury, the antioxidant effect of HPOX NPs was complemented by encapsulating the anti-apoptotic drug, 4-amino-1,8-napthalimide (4-AN). In animal models of I/R injury, i.v. injection of 4-AN/HPOX, in comparison to vehicle group, lead to apoptotic markers significantly reduced [103].

Few examples are present in the literature on the use of POX in cancer therapy. For instance, Höcherl and co-workers integrated diethylstilbestrol into polyoxalate polymer to prepare ROS- responsive polyprodrug NPs [4]. These polydiethylstilbestrol (PDEB) NPs were applied for cancer treatment and *in vitro* experiments on human prostate (LnCaP and PC3) and breast (MCF-7) cancer cells demonstrating that these systems hold great promise to achieve specific drug release into tumors, lowering the required drug dose in estrogen-dependent hormone therapy. PDEB NPs cytotoxicity was higher on MCF-7 than on human fibroblast, being the free drug, DEB, equally toxic to both cell types. Likewise, on human prostate cancer cells (LnCaP and PC3), PDEB polyprodrug NPs significantly lowered the required minimal DEB effective concentration, demonstrating superior cytotoxicity towards the free drug [4].

In relation to safety, the use of POX-based ROS-responsive DDS has not been reported results that indicated their unsafety. The products from POX H_2O_2- induced cleavage, produces oxalic acid, carbon dioxide and 1,4- Cyclohexanedimethanol. This last compound was approved by the FDA to be used as a food additive, being non- toxic and easily excreted [1,52,53]. An excellent safety profile of HPOX blends, with significantly higher cell viability in comparison to blends made up form PLGA was demonstrated *in vitro* in mouse fibroblast cells (NIH/3T3) [105].

1.5.4. Poly (Proline)

Amino acids such as proline, histidine, arginine, and lysine are susceptible to ROS-mediated and metal-catalyzed oxidation. Proline is the only amino acid that can form

tertiary amide bonds and is known to be more susceptible to oxidation than secondary amide bonds. Then, proline oligomers or polyproline have been employed to fabricate ROS- responsive materials [11]. Of interest, proline oligomer has a relatively slower degradation rate under ROS than other ROS-sensitive groups, and thus it can be used for sustained release [78].

As an example, a ROS-cleavable polycaprolactone scaffold crosslinked with oligoproline was developed, confirming ROS-induced degradation by exposing them to Nitric Oxide (NO), superoxide and 3-morpholinosydnonimine (SIN-1). In detail, poly(ε-caprolactone) (PCL) polymers were carboxylated to form a terpolymer (4% PEG-86% PCL-10% cPCL), which was further cross-linked with the biaminated PEG-P(n)-PEG, with P(n) referring to the length of the polyproline oligomer, and used to form scaffolds. The erosion of scaffolds was evaluated after immersion in a buffer with or without 1 mM of ROS generator, 3-morpholinosydnonimine (SIN-1) (that produces nitric oxide and superoxide leading to the production of peroxynitrite and hydroxyl radicals) for 28 days at 37 °C, and the study confirmed the loss of about 30% of their mass, while the mass of materials incubated without ROS showed only minimal changes. These results are in accordance to those obtained *in vitro* on IFN-γ and/or lipopolysaccharide (LPS) stimulated bone marrow-derived macrophages, in which the scaffolds were slowly degraded as a result of the exacerbated ROS produced and released by the stimulated cells. In a subsequent study, this group performed *in vivo* assays in mice by implanting the scaffold subcutaneously, observing that the released cargo from the scaffold also promoted angiogenesis [11,106,107].

Despite its biocompatibility, ROS- responsive DDS based on polyproline were mainly confined only to scaffold's design and technological characterization. As far as we are concerned, the design of a ROS-responsive vehicle was only reported by the group of Gupta, that designed a pH- and ROS-responsive nanocarrier for the release of DNA. This dual responsive nanocarrier was prepared from a co-polymer obtained from a pH-responsive co-polymer N,N-dimethylaminoethyl methacrylate (DMAEMA) and the ROS-responsive proline oligomer, cysteine-(proline)5-lysine (CP5K). This nanocarrier demonstrated uptake, endosomal escape and improved gene expression in an *in vitro* model of vascular smooth muscular cells (VSMCs) pathology and thus it has been suggested as a promising gene delivery DDS for preventing or treating high ROS sites, as atherosclerotic lesions [108].

1.5.5. Phenyl boronic ester/acids

Phenyl boronic ester/acids, ROS-responsive molecules, were extensively applied in drug delivery [25]. They can be selectively cleaved by H_2O_2 at a physiological pH and temperature, with a cleavage stoichiometry of one molecule of Phenyl boronic ester/acid cleaved by molecule of H_2O_2 [93,109]. Owing to their high affinity towards H_2O_2, they have been primarily used to prepare H_2O_2 detecting probes as well as small H_2O_2 responsive prodrugs [75].

Phenyl boronic esters were generally used to obtain ROS-responsive polymers for the preparation of micelles, but on the other hand they have been also proposed to prepare prodrugs. For instance, a polyprodrug that integrated the chemotherapeutic drug Chlorambucil (CHL) into the side chains of poly (acrylic acid) of poly (ethylene glycol)-g-poly (acrylic acid) co-polymer, PPAHC, was used to prepare NPs for cancer therapy application. The *in vitro* and *in vivo* antitumor efficiency of these NPs was demonstrated on MCF-7 cells as well as in MCF-7 tumor bearing mice in comparison to free CHL [110].

1.5.6.1. Phenyl boronic esters/acids- based DDS and their applications in disease

The use of phenyl boronic esters/acids for the engineering of ROS- responsive DDS is more recent and mostly used as a cleavable group for the building of degradable materials and polymer prodrugs [44,109] for the obtention of ROS-responsive DDS in cancer treatment application and inflammatory conditions (e.g. IBD, atherosclerosis and stroke). Examples on the application of these ROS-sensitive material in stroke have been previously mentioned in section 1.4.1 [54,53].

In more details, Zhang and co-workers conjugated boronic ester molecules to hydrophilic β-cyclodextrin (β-CD) thus creating amphiphilic β-CD-boronic ester conjugates which can undergo self-assembly into ROS-responsive β-CD NPs.

Docetaxel (DTX) loaded in these ROS-responsive β-CD NPs (DTX/Ox-β-CD-NPs) were comparatively evaluated with acid responsive β-CD NPs (Ac-β-CD) *in vitro* and *in vivo* for efficacy. *In vivo* assays in B16F10 melanoma-bearing mice treated with DTX/Ox-β-CD NPs, demonstrated that the tumor volumes were remarkably reduced in comparison

to DTX/Ac-β-CD NPs as well as other DTX formulations [111]. Similarly, β-CD-boronic ester conjugates were exploited to encapsulate the anti-atherosclerotic drug Rapamycin (RAP) for the treatment of atherosclerosis. Since macrophages have a close association with all the phases of the disease, these researchers treated activated macrophages with RAP/Ox-β-CD NPs and showed that these NPs reduced the levels of ROS and suppressed significantly the proliferation of macrophages in comparison to control, non-ROS responsive RAP/PLGA NPs. Evaluation of RAP/Ox-β-CD NPs in an *in vivo* mice model of atherosclerosis (ApoE -/- mice) confirmed a 2-fold reduction on the average atherosclerosis plaque area in comparison to control NPs, an thus the efficacy of the treatment [57].

1.5.6.2. Dual/Multistimuli responsive Phenyl boronic esters/acids -based DDS

Regarding the combination of phenyl boronic ester/acids with light, for instance, Liu and co-workers co-encapsulated Ce6 and hypoxia activated prodrug, tirapazamine (TPZp), in red blood cell membranes surface modified with iRGD peptide. These engineered nanocarriers effectively suppressed tumor growth without causing off-target undesired effects, configuring this approach as a promising strategy to treat hypoxic tumors [112].

On the other hand, a cascade amplification strategy consisting of the use of β-Lapachone (Lapa), that produces ROS by means of NADPH quinone oxidoreductase 1 (NQO1) (overexpressed in certain tumors) was exploited by Ye and co-workers. This approach consisted of the production of a boronic ester-DOX prodrug co-encapsulated along with Lapa in poly (ethylene glycol)–poly[2-(methylacryloyl) ethylnicotinate] (PEG–PMAN) NPs. *In vivo* results on multidrug resistance (MDR) mice tumor model showed an enhanced antitumor efficacy in comparison to control samples [71].

Regarding inflammation application, for instance, Bertoni and co-workers reported the design of NPs that were made up from phenylboronic esters grafted dextran with chitosan protecting coating (OxiDEX NPs) encapsulating rifampicin (RIF), for the potential treatment of IBD. The architecture of these systems is very complex and could be summarized in nano-in-micro composites which should maintain their morphology at stomach environment (pH=1.2), then disrupted at intestinal pH (pH=6.8) and therefore useful in inflammatory bowel diseases. *In vitro* studies showed a 10-fold decrease on drug

permeability across intestinal cell monolayer, which implies less drug absorbed by the bloodstream and thus, less undesired effects with potential used for the treatment of IBD [113].

1.5.6.3. Phenyl boronic esters/acids based- siRNA/DNA delivery systems

Boronic esters/acids have also been used in the design of nanocarriers for the delivery of siRNA for gene therapy. For instance, Li and co-workers took advantage of the exclusive interaction between pendant phenylboronic acid (PBA) groups with siRNA 3'- end ribose that promotes the formation of polymer/siRNA stable complexes. With this aim, the authors prepared a ROS- responsive vehicle based on a PBA- containing cationic polymer with lipid envelope for the ROS-responsive systemic delivery of anti-vascular endothelial growth factor (VEGF) siRNA for cancer therapy. *In vivo* results demonstrated the efficacy of this approach as ROS-responsive systems showed the highest effectivity in inhibiting tumor growth in cervical cancer cells (HeLa) tumor-bearing mice, in comparison with non-treated group, 5-Fluorouracil- treated and non-responsive polymer siRNA complex PDP/siRNA that showed moderate effect [114].

1.5.6.4. Safety considerations of phenyl boronic/acid materials

The mechanism of boronic ester degradation by ROS produces quinone methide (QM) intermediates (Figure 3) that tend to react efficiently with biomolecules. Despite it was demonstrated that they can be quenched by water *in vitro*, generating hydroxymethylphenol derivatives, they might be harmful for *in vivo* applications [49]. As the increased GSH levels in cancer cells play a role in the inactivation of alkylating agents inside tumor cells, such as CHL, inducing drug resistance mechanisms; Luo and co-workers took advantage of QMs by-products obtained from ROS-triggered phenyl boronic degradation, for a synergistic effect in cancer treatment by means of ROS-induced CHL release and GSH depletion by QM intermediates. Consequently, this group hypothesized that, in addition to the intracellular oxidation-triggered released of CHL, the anticancer effect of this drug could be improved by QM- induced GSH depletion [57].

On the other hand, Song and co-workers, explored another solution for the scavenging of QM molecules by developing aryl boronic ester-based ROS-responsive polymers conjugated to poly (amino ester). Since amine groups are nucleophilic, they can catch QM intermediates. Furthermore, due to the presence of secondary or tertiary amino groups in their structure, these copolymers are also pH sensitive. The QM generated by the degradation of the boronic ester on the polymer, could be subsequently captured by the secondary amines; this evidence is important to assure biocompatibility, and thus it should be considered for *in vivo* application [43]. Nevertheless, cyclodextrin NPs containing phenylboronic acid did not induced inflammatory response *in vitro* nor *in vivo* and most importantly, the products of their degradation by ROS did not cause an inflammatory response in mice and rabbits when intravenously injected or applied on ocular mucosa tissue [57]. On the other hand, the OxiDEX NPs obtained by Zhang and co-workers did not show to be cytotoxic, showing cytocompatibility even at a NP concentration of 2000 μg/mL [113].

1.6. Thioketal

The synthesis of TK, which is a sulfur analogue of ketal [115], can be carried out by the condensation of thiols with ketones or by the acid catalyzed replacement of a ketal with thiols, in which steps of polymerization can occur in the presence of di- or multi-thiols [116]. Due to their known stability to enzymes, like proteases, as well as acidic and basic conditions, TKs are commonly used as carbonyl protecting groups in organic synthesis. Despite their stability in these conditions, TKs can be readily cleaved upon oxidation into non-toxic thiols and acetone [96,117–119] (Figure 3). *In vitro* studies have shown the ability of this chemical group to be cleaved by the most relevant ROS (encountered in pathological states), such as superoxide, H_2O_2 and hydroxyl radical, being this last one the most efficient ROS to cleave TK [120].

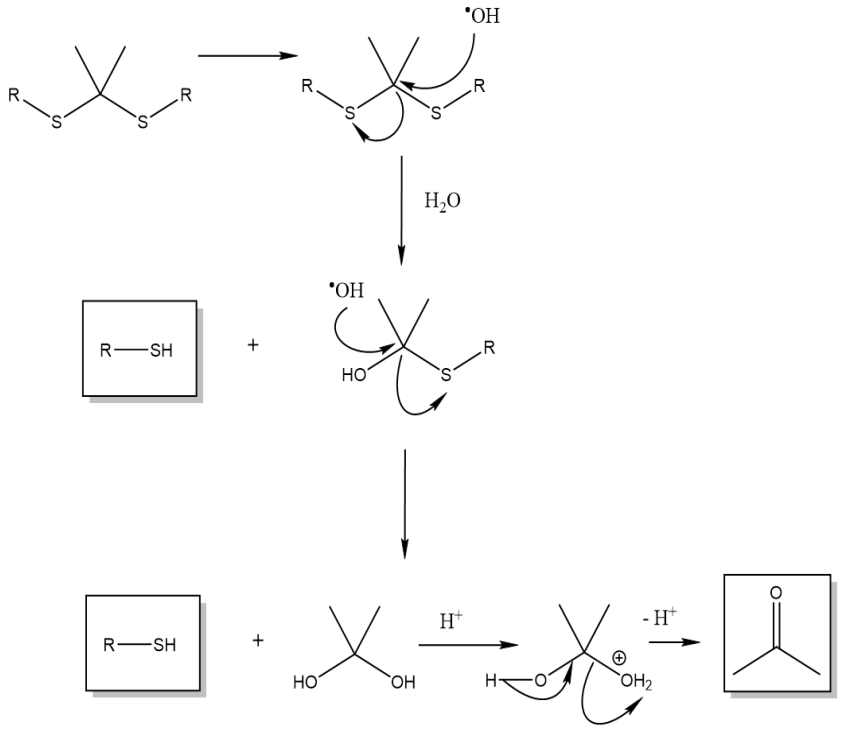

Figure 5: Mechanism of chemical degradation of TK groups by hydroxyl radicals. Detached molecules have a sulfhydryl chemical group and the by-product of ROS- TK cleavage is acetone. (adapted from Ref. [121]).

1.6.1. TK-containing polymers and linkers

TK groups can be integrated inside a polymer chain or a linker, being TK containing linkers more widely used for the design of TK-based DDS. Concerning the incorporation of TK groups in polymers, the pioneer that prepared nanoparticles based on polyTK polymers was the group of Murthy [116]. They used poly (1,4-phenyleneacetone dimethylene TK) (PPADT) which was obtained by a reaction of polycondensation of ketal with dithiol molecules, to encapsulate anti-TNF-α siRNA into NPs for the treatment of ulcerative colitis (Table 1, polymer 1) [62]. Zhang and co-workers also employed these polymers to prepare PPADT NPs in a different application [122].

Martin and co-workers prepare Polythioketal (PTK) diol co-polymer starting from dimetoxypropane and di-thiols molecules, butane dithiol and mercaptodiethylether to prepare scaffolds for tissue engineering by crosslinking of polyurethane (PU) with PTK (Table 1, polymer 2) [121]. More recently, in order to prepare microparticles for the treatment of colon inflammation, Regmi and co-workers synthesized an alternative TK

polymer obtained by growth polymerization of 4,4'Bis (mercaptomethyl) biphenyl and 2,2-dimethoxypropane (Table 1, polymer 3) [123]. On the other hand, TK-polymers were also prepared by combining monomers to each other through TK containing linkers. For instance, Chen and co-workers prepared an amphiphilic ROS-responsive poly (β-amino ester) (PBAE) for the preparation of NPs for cancer application (Table 1, polymer 4) [124]. Polyaminothioketal (PATK) represents another example of a TK-containing polymer prepared starting from diamine containing monomers and aminoacrylate TK linkers (Table 1, polymer 5) [120].

TK-containing polymer	Chemical structure	Ref.
1. PPADT	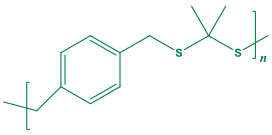	[62]
2. PTK Diol	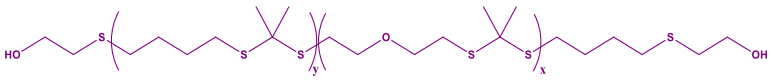	[121]
3.TK Polymer	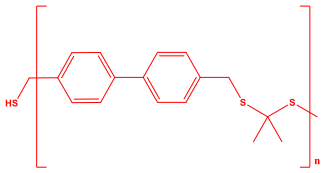	[123]
4. PBAE	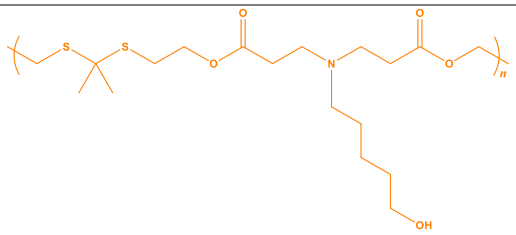	[124]
5. PATK	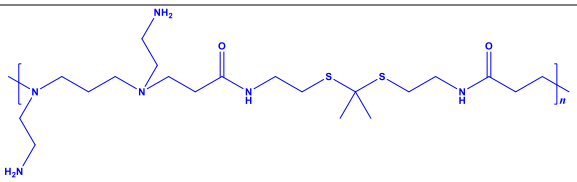	[120]

Table 1: PTKs that have been developed in the design of ROS-responsive DDS for different applications.

Regarding TK linkers, the most widely employed are TK diacid linkers with S, S' dimethyl TK moiety (Table 2, linker 1). Nevertheless, other linker types have been recently synthesized with alternative terminal chemical functionalities that are shown in Table 2. In addition, in order to design more efficient ROS-responsive DDS, linkers with an attached chemical moiety associated to the TK group, have been developed (Table 2, linkers 5-7). For instance, for an efficient encapsulation of DOX in mPEG-TK-PCL micelles, a TK linker with two conjugated aromatic groups was developed [125]. Due to the establishment of π-π interactions among the drug and the π-conjugated TK moieties, the loading of a drug such as DOX into micelles can be enhanced. On the other hand, Lin and co-workers developed a linker containing an aromatic thioacetal linker to form ROS-responsive polyplexes with DNA, suggesting that the conjugated aromatic ring, might help to improve the DNA condensation capacity of cationic polymers [126]. Another example was described by Liu and co-workers that developed hydrophobic "bola-lipid" core with a thioacetal group that apart from respond to high concentrations of ROS in cancer cells, this core can offer the outstanding property to mimic the assembly observed in extremophile archaebacteria [127].

Most of TK-linkers described up to now are homolinkers (Table 2, linkers 1-7). In order to improve the versatility of the molecules to be attached to the linker, the synthesis of TK heterolinkers has been proposed [128]. Thus, polymers and small molecules (drugs, PSs, fluorescent dyes, targeting ligands, etc.) with different terminal chemical groups can be simultaneously attached to the same linker molecule. For instance, Yin and co-workers employed a heterobifunctional linker (Table 2, linker 8) to synthesize a monomer with TK and Camptothecin (CPT), namely TCPT, that was then polymerized in the presence of PEG based macroRAFT agent, to finally obtain PEG-b-PTCPT ROS-responsive prodrug [129].

TK containing Linker	Chemical structure	Ref.
1. TK diacid linkers	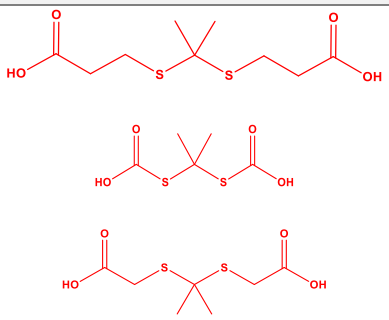	[31,130,131]
2. Diamine linker		[132–134]
3. Hydroxyl-terminated TK	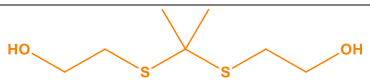	[115]
4. TK diazide linker	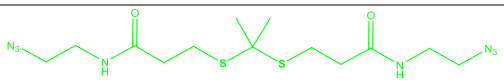	[135]
5. π-conjugated TK diacid linker	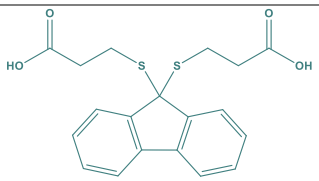	[125]
6. Aromatic Thioacetal linker	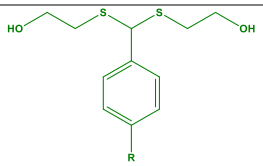	[126]
7. TK "Bola core"	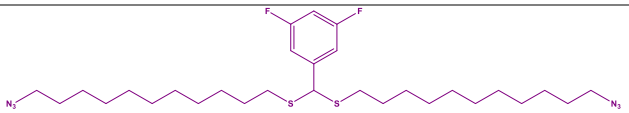	[127]
8. TK alcohol and methacrylate linker	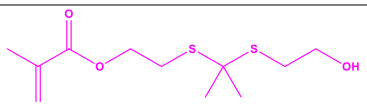	[129]

Table 2: TK containing linkers that have been used in the formulation of ROS-responsive DDS. Linkers 1-7 refer to homolinkers and 8 refers to heterolinker.

1.6.2. TK-based ROS-responsive DDS

PTKs and TK linkers, have been generally used for the synthesis of ROS- responsive polymers to be applied in the preparation of several DDS.

1.6.2.1. Scaffolds. Martin and co-workers prepared a series of PTK urethane (PTK-UR) scaffolds for tissue engineering applications. These scaffolds demonstrated to be stable in aqueous conditions for almost 6 months. When applied to subcutaneous wounds, evidences of cell infiltration and connective tissue/vessels formation were observed on the scaffold, with a degradation kinetics of about 1.5 months. The recovery of the wounds with this scaffold was significantly improved in comparison to control scaffold (without TK crosslinks) [121]. PTK-UR is very versatile as it was also investigated to prepare bone cements with mechanical properties, demonstrating that they could be degraded in the oxidative microenvironment generated by osteoclasts and macrophages during wound healing and bone remodeling [136].

1.6.2.2. Hydrogels. An innovative hydrogel that exploited the strong interactions among nucleic acids guanine (G) and cytosine (C) as well as the supramolecular host-guest interactions among PEG and α-CD has been investigated by Liu and co- workers. They synthesized TKs-modified guanines (G-TK-G) and terminal cytosine-functionalized PEGs (C-PEG-C) that self-assembly into hydrogels along α-CD in aqueous solution (Figure 6A). Proof-of-concept studies were performed with DOX-loaded hydrogels, demonstrating drug release ability in ROS-rich environments and, thus, making these hydrogels suitable to biomedical applications as tumor localized chemotherapy. Moreover, unloaded hydrogels demonstrated cytocompatibility [137]. Another example is a hydrogel that consisted of TK-crosslinked hyaluronic acid chains with pendant conjugated photosensitizer protoporphyrin IX (PpIX) and loaded DOX. These hydrogels were used for localized chemo-PDT combined therapy [138].

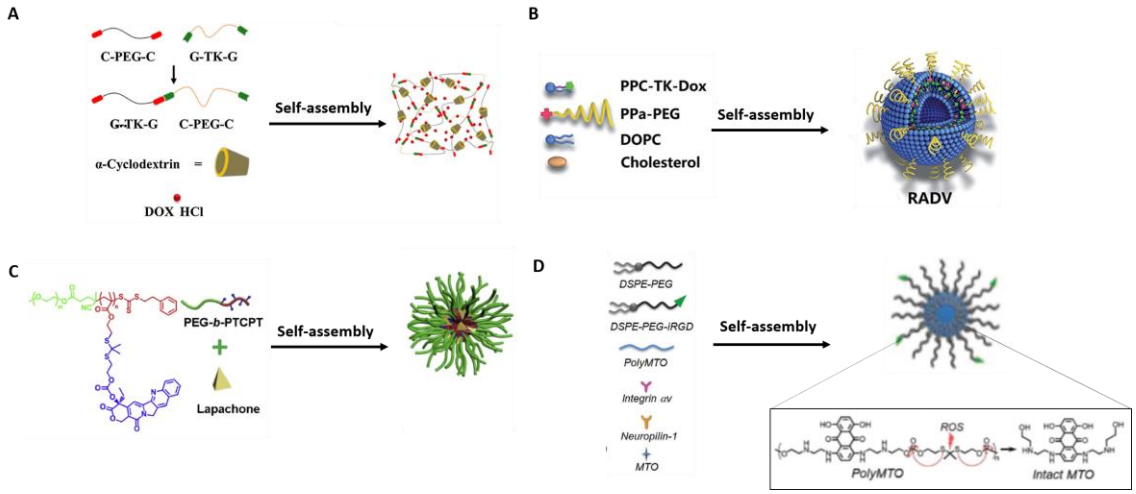

Figure 6: Examples of ROS-responsive DDS designed by applying TK linkers. A) Hydrogel **B)** ROS-reactive activatable DOX vesicles (RADV) **C)** Polymeric prodrug micelles and **D)** Polyprodrug made up from polymerized drugs that self-assembly forming micelles (adapted and modified from refs. [137,139,129,73]).

1.6.2.3. Liposomes. TK-lipids were recently used to formulate ROS-responsive liposomes by means of two approaches: a) integration of TK linkers into phospholipids and b) design of novel lipids containing TK linkages. The first approach was achieved by Zhou and co-workers that prepared ROS- reactive activatable DOX vesicles (RADV) from 1,2-dioleoyl-sn-glycero-3-phosphocholine (DOPC), cholesterol, PEG-photosensitizer pyropheophorbide-a (PPa) conjugate and a phospholipid-mimic DOX prodrug, which was synthesized by coupling DOX to the hydroxyl group of 1-palmitoyl-2-hydroxysn-glycero-3-phosphocholine (PPC) by means of TK. In addition, the presence of the unsaturated lipid, DOPC, can increase the liposome membrane permeability facilitating the escape of lipid detached DOX molecules. These liposomes were applied for the treatment of triple negative breast cancer with an image-guided and on-demand drug release approach, demonstrating highly antitumor efficiency *in vitro* and *in vivo*. Furthermore, they have demonstrated to be safe since they did not experience drug leakage in circulation and did not induce adverse effects (Figure 6B) [139].

The second approach is highly innovative and was described by Liang and co-workers and refers to cancer therapy. They prepared a library of novel TK-containing lipids, with the identification of a lipid, namely ROS-TK-5, that efficiently encapsulated siRNA and thus was selected for the design of ROS-responsive liposomes [140].

1.6.2.4. Prodrugs. Yue and co-workers prepared a prodrug consisting of PEG conjugated to CPT by means of TK, that was also modified with the mitochondrial targeting molecule, Tri-phenyl-phosphonium (TPP). This targeting polymeric prodrug along with a lipid conjugated PEG could self-assemble into blended NPs. To achieve synergistic effect with chemotherapy, photosensitizer molecules were also encapsulated into these NPs [7]. Following a similar strategy, a targeted polymeric prodrug with DOX, namely RGD-PEG-TK-DOX, was used to prepared encapsulated micelles with hematoporphyrin for a combined chemo-PDT against oral tongue squamous cell carcinoma (OTSCC) [141]. On the other hand, our group recently reported the synthesis of a fluorescent conjugate with Cy5 NIR dye (mPEG-TK-Cy5) with the aim to perform proof-of-concept studies that confirm the selective release of this dye in cancer cells towards normal cells. *In vitro* studies in rat Glioblastoma cells (C6) with high intrinsic levels of ROS, demonstrated Cy5 release, with no release on normal astrocyte cells (DI TNC1). In addition, by means of Cy5 release studies in simulated ROS-conditions with this fluorescent conjugate, we could observe that TK prevented Cy5 from being quenched [130].

Frequently, the term polyprodrug appears in the literature to describe: a) prodrugs in which multiple drug molecules are attached to the same polymer unit through TK linkages, and b) prodrugs in which multiple drug molecules are attached to each other also by means of TK. Regarding the first type of polyprodrug, for instance, Yin and co-workers prepared co-block polymers from PEG and polymerized methacrylate monomers with CPT, in which CPT has been conjugated to the side chains of methacrylate through TK. These co-block polymers, self-assembled into micelles encapsulating Lapa for ROS amplification cascade with enhanced CPT release [129] (Figure 6C). On the other hand, regarding the second type of polyprodrug, Xu and co-workers prepared mitoxantrone (MTO) polyprodrug by polymerization of MTO drug molecules mediated by TK linkers. This polyprodrug was then encapsulated by self-assembling in the presence of distearoyl phosphatidylethanolamine (DSPE)-Polyethylene glycol (DSPE-PEG) and RGD-DSPE-PEG in NPs for cancer therapy, showing *in vitro*/*in vivo* antitumor effect [73] (Figure 6D). Recently, the same research group combined the use of MTO polyprodrug with a cisplatin prodrug to prepare self-assembled NPs with DSPE-PEG. The NPs achieved synergistic anticancer effect against prostate cancer tumor model mice [142].

1.6.3. Overview of TK-linkages exploited to prepare ROS-responsive DDS

One of the possible reasons that accounts for the preference of TK linkers over PTKs, might be related to the high versatility of these linkers to be attached to either high or low molecular weight molecules. The exploitation of TK-linkers to obtain novel TK-linkages among nucleic acids and ROS-responsive lipids, prodrugs and polyprodrug has been already described in the previous section. Here, the alternative types of TK-linkages and their structure-function relationships that have been reported in the literature will be mentioned.

1.6.3.1. TK-linkages in co-polymers and crosslinked polymers. With the aim of obtaining block co-polymers suitable for the formulation of ROS- responsive micelles and NPs, TK-linkers have been widely used. For instance, the following block co-polymers mPEG-TK-PLA [133], PEG-TK-PLGA [143] and targeted RGD-PEG-TK-PLGA [144] were used to prepare ROS-responsive NPs for cancer application.

On the other hand, TK-containing block-copolymers have also been used to prepare NPs that instead of being decomposed upon ROS stimulus, are exploited as a NP de-shielding strategy. For instance, Mohammed and co-workers used two di-block copolymers, one containing a TK linkage and a long polydimethylacrylamide (PDMA) block (PCL-TK-PDMA), and a second one containing the small cell-penetrating block poly (2-guanidinoethyl methacrylate (PGEMA), namely PCL-PGEMA. These di-blocks were used to prepare self-assembled micelles for the encapsulation of Ce6 and PTX in which the light triggered production of ROS, can trigger the PDMA block de-shielding with the exposure of cell penetrating peptide for an enhanced cell uptake [145]. In addition, the de-shielding strategy has been also applied in the case of NPs that can undergo a conformational change upon ROS-mediated TK-cleavage. In this regard, Polyvinyl alcohol polymer side chains were modified with KLAK peptides, which is a cytotoxic peptide targeting mitochondria, and with di-block co-polymers of β-sheet-forming peptide (KLVFF) conjugated to PEG by means of TK linker (KLVFF-TK-PEG). These modified PVA chains can self-assemble in NPs. Once inside cells, the PEG chain is detached due to intracellular ROS with endosomal/lysosomal escape, and this PEG de-shielding induces a morphology NP switch into fibrous structures with the exposure of multiple KLAK molecules that interact cooperatively, enhancing mitochondrial

cytotoxicity. These NPs showed *in vitro* and *in vivo* antitumor efficacy, providing a new insight for theragnostic enhanced interaction with targeting site (Figure 7A) [146].
Finally, some works propose a TK-crosslinked strategy of cationic branched polymers in spite of obtaining high molecular branched polymers from small molecular ones and thus, overcome the undesired cytotoxicity of the cationic polymers used in gene therapy and siRNA silencing [117,126,147].

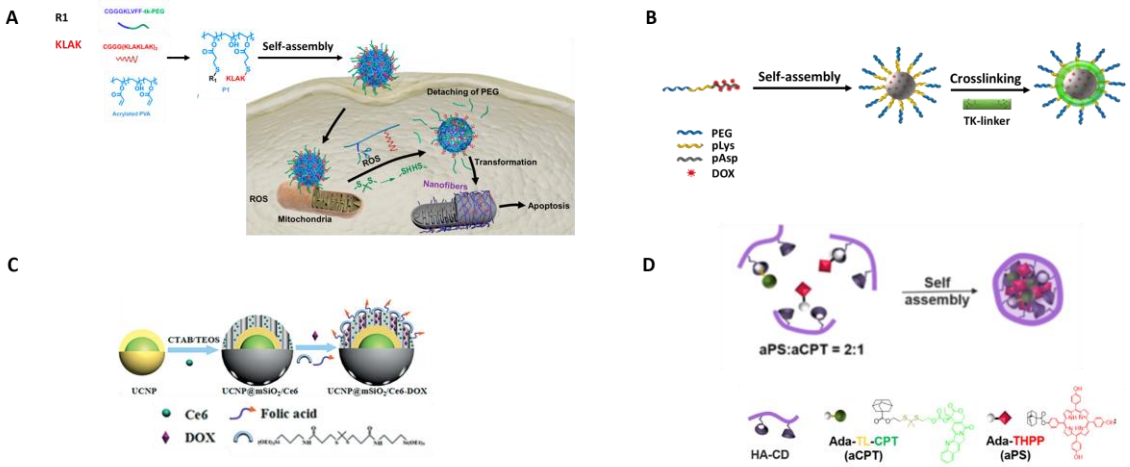

Figure 7: ROS-responsive DDS obtained by exploiting different types of TK-linkages. A) Di-block copolymer containing TK used for the obtention of NPs that undergo a conformational change upon ROS, exposing toxic peptide, **B)** Micelles in which TK act as a crosslinker that impedes the premature leakage of DOX, **C)** Inorganic NPs in which by means of TK-containing gate impedes premature release of loaded DOX and **D)** DOX linked to ADA form supramolecular complex with β-CD attached to HA chains self-assembling in micelles (adapted and modified from refs. [137,139,129,73]).

1.6.3.2.TK-linkages to prevent premature off-target drug release. Apart from prodrugs and polyprodrugs, in behalf of preventing premature off-target drug release from nanoformulations, crosslinked micelles, surface drug attached NPs, NP gates and host-guest interactions, have also been investigated.

<u>*Crosslinked micelles.*</u> One example of TK-crosslinked micelles was described by Li and co-workers that prepared crosslinked micelles for cancer application from PEG-diaxophosopholane (PBYP) co-polymers for the co-encapsulation of DOX and Ce6 into micelles. In order to prevent unspecific payload release, TK-linkers were then crosslinked to the side chains of the hydrophobic core [135]. Another work used a double strategy based on a co-polymer of PEG with poly (amino acids) (PEG−pLys−pBla), in which DOX

molecules were covalently attached to the side chains of pBla hydrophobic block (by means of pH sensitive hydrazone linker). These DOX co-polymer prodrugs self-assembled into micelles and subsequently TK linkers were crosslinked with pLys blocks (Figure 7B) [148].

Drug-surface attached NPs. Another approach consists of the covalent attach of drugs to the surface of inorganic NPs by means of TK linkers. For instance, Yue and co-workers functionalized upconverted NPs with Camptothecin through TK for chemo-PDT and fluorescence imaging [30]. In another example, DOX was surface attached to Fullerene (C60), through TK, obtaining an ON/OFF switch of drug release upon light stimulus [3].

NP Gates. The use of ROS-responsive gates was proposed to prevent the premature release of drugs from NPs. An example is represented by mesoporous NPs (MSNs), in which after DOX and alpha-tocopheryl succinate (α-TOS) encapsulation, the pores of the NPs were closed by conjugating β-CD to TK conjugated MSNs [149]. An additional example is represented by the work of Zhang and co-workers. This group used mesoporous silica coated upconverted NPs (UCNPs) for the co-loading of Ce6/DOX with subsequent NP gating achieved by TK linkages with silane groups (Figure 7C) [150].

Host-guest interactions. Due to their strong binding ability, the host-guest complexation between β-CD and adamantane (ADA) has been widely employed in macromolecular assembly [151]. This feature has also been exploited for the design of ROS- responsive NPs containing TK, in which drugs have been linked to either β-CD or ADA through this ROS-sensitive linker. This strategy might be considered as an alternative way to that of covalent TK linkages. An example in which host-guest interactions among β-CD-ADA was exploited, was proposed by Phua and co-workers. They used β-CD molecules attached to HA to guest PS-TK-ADA and CPT-TK-ADA conjugates with photosensitizer and drug, respectively, that self-assembled into NPs (Figure 7D) [31]. In another example, β-CD monomers attached to each other through TK linkers can self-assemble in the presence of Ruthenium (Ru)-ADA conjugates in response to host-guest interactions between β-CD and ADA. All the components were self-assembled into NPs along with CPT and Vitamin K3 for theragnostic cancer application [152].

1.6.4. TK-based ROS-responsive DDS used in association to other stimulus/i

TK- based ROS-responsive DDS have been used in combination with additional stimuli. The stimulus that have been most widely used is light, which is being proposed as a standard strategy to enhance the levels of ROS in tumor cells that improve the release of therapeutic drugs as well as to achieve synergistic chemo-PDT therapeutic effects. In addition, apart from light, ROS-responsive formulations have been also combined with temperature, sonodynamic therapy and pH for dual or multistimuli response. On the other hand, the combination of ROS-responsive DDS with chemical agents that induce an amplification cascade of ROS production has also been employed.

1.6.4.1. Light. Several PS have been exploited for the formulation of dual ROS and light-responsive DDS. Among them, Ce6 which can be excited at λ= 660 nm, has been the most widely used and this might be related to its high efficacy and low dark toxicity [95]. For instance, Ce6 has been co-encapsulated with PTX in mPEG-TK-PLA NPs [133] and PCL-TK-NP for ROS responsive deshielding [145], or with DOX in TK-core-crosslinked PEG-PBYP micelles [135] and PEGylated hyperbranched TK- polyphosphate NPs [132]. In all these examples it was confirmed *in vitro* and *in vivo* efficiency of the DDS even in highly resistant tumors.

In another example, Jin and co-workers prepared branched Ce6 conjugated by means of TK to TK- crosslinked phosphate polymers creating an amphiphilic co-polymer that can self-assemble into micelles encapsulating CPT for chemotherapy and PDT. The Ce6 inside the NPs can effectively generate ROS to kill cancer cells and cleave the TK units to sequentially reduce the size of NPs, promoting a more efficient tumor penetration with programmable CPT release. *In vitro/in vivo* experiments confirmed antitumor effect. Noteworthy, striking results were obtained in *in vivo* experiments, in which the tumor growth inhibition was of 96% with a complete elimination of one of the tumors. In addition, off-target undesirable effects in animals treated with these NPs were not observed [153]. Finally, Ce6 was also used in combination to Bilirubin (BR), that apart from generating singlet oxygen in response to light, undergoes a conformational change from hydrophobic to hydrophilic. These PSs were conjugated to FFVLK-PEG, in which FFVLK is a β-amyloid derived peptide that forms β-sheets and aggregate into fibers, to

form Ce6-FFVLK-PEG and BR-FFVLK-PEG co-polymers that self-assembly into co-polymer micelles, encapsulating TK-PTX dimers (PTX-TK-PTX). When PSs are detached from FFVLK block in response to ROS, the hydrogen bonds between FFVLK are weaker and thus, promoting the reorganization of these materials into nanofibers. These chimeric micelles shown to be biocompatible with high tumor accumulation and *in vitro* (82.6%)/*in vivo* (61.8%) efficacy [154].

Several other works have reported the use of other PSs types for the design of dual ROS and light responsive DDS based on TK [155,156,134,157–159]. It is worth to notice a recent work that proposed a different kind of photosensitizer by which, in addition to generate ROS, it is possible to monitor drug release by fluorescence. A novel ROS-responsive platform for theragnostic was developed to propose the use of a fluorogen with aggregation-induced emission (AIEgens) instead of the traditional PSs in which their fluorescence is quenched because of aggregation. This group used amphiphilic polymers made up of PEG and AIEgens consisting of an amphiphilic polymer that can self-assemble encapsulating DOX. These NPs not only can respond to ROS, but bring quality fluorescence imaging and monitor drug delivery, demonstrating a significant *in vitro* cytotoxicity on triple negative breast cancer cells [32].

1.6.4.2. Ultrasound. With the aim to trigger accelerated release from ROS-responsive TK-based DDS, a recent work used ultrasound stimulus to apply SDT. In this work, self-assembled ROS-responsive NPs obtained by self-assembling of PEG-TK-PTX prodrugs in combination with lipid-PEG and the sonosensitizer IR780 (IR780/PTL NPs) were prepared. *In vitro/in vivo* studies demonstrated an on-demand drug release, with high antitumor efficiency and cell apoptosis induction upon ultrasound stimulus in human glioma cells (U87) and U87 xenograft tumor mice [34]. On the other hand, Mesoporous titanium oxide nanoparticles (MTN), with low cytotoxicity and pores amenable for drug loading and suitability for both PDT and SDT, were used following the same approach already applied for MSN, in which after the encapsulation with DOX, the NPs pores were gated with β-CD. Apart from demonstrating excellent *in vitro/in vivo* antitumor efficacy, a reduction of DTX side effects without toxicity to the spleen and hemocompatibility, was observed [131].

1.6.4.3. Enzyme. For instance, Chen and co-workers attached TK to the surface of amine functionalized ZnO NPs to surface attach DOX and cell penetrating peptide (R8). These

positive charged NPs were then masked by HA for long circulation in blood as well as HAase sensitivity. Once the NPs reach the tumor, the presence of high concentrations of HAases in tumor microenvironment, will digest HA coating with the exposure of penetrating peptides, promoting cell uptake [160].

1.6.4.4. pH. The use of ROS and pH dual stimuli was reported by Zhang and co-workers for the preparation of crosslinked micelles previously commented in section 1.6.3.2. (Figure 7B). The treatment with these micelles demonstrated to improve the pharmacokinetics and biodistribution profiles of DOX, with around a 3-fold increase accumulation in breast cancer tumor mice model, antitumor efficacy and reduced systemic toxicity in comparison to free drug in these micelles [148].

1.6.4.5. Multiresponsive. pH stimulus was used along with PDT, in which the side chains of polymeric dextran, modified with histidine molecules, have been also covalently modified with DOX through TK linkages, encapsulating porphyrin (Zn-TPP). These acid-sensitive ROS-triggered dextran-based DDS, demonstrated to inhibit cell growth due to combined chemo-PDT [161]. An alternative nanocarrier that responds to ROS and pH was made up from TK-crosslinked polyphosphoester (PPE) functionalized with penetration peptide transactivator of transcription (TAT) that loads Ce6 and DOX and it is combined with a pH-responsive corona of monosaccharides. This corona serves to mask TAT peptide and also target cancer cells for nucleus targeted drug delivery. These NPs offered outstanding antitumor effect in an *in vivo* breast cancer mice model [162]. Regarding the combination of ROS-responsive DDS with light and temperature stimuli, Li and co-workers designed NPs made up from self-assembling PEG-TK-BODIPY encapsulating Iodine for simultaneous production of singlet oxygen and heat upon light illumination [163].

With the aim to achieve PDT treatment against hypoxic tumors, Li and co-workers conjugated simultaneously Cypate to the surface of polyamidoamine (PAMAM) dendrimers and Ce6 to obtain a multiresponsive DDS that respond to ROS, PDT and temperature stimuli. NPs made up from these conjugated dendrimers were self-assembled with PEG encapsulating H_2O_2, that in a first response to temperature stimulus, H_2O_2 decomposes into O_2 with the alleviation of hypoxia, and secondly to light with the production of ROS. After this last stimulus CC-PAMAM dendrimers are released from the NPs, with deep penetration in hypoxic pancreatic tumor with PDT damage. *In vivo*

studies in a mice model of pancreatic cancer showed an excellent result since by means of this treatment, a total removal of the pancreatic tumor could be obtained [164].

1.6.4.7. Cascade-amplification. The design of nanomedicines that undergo cascade reactions offers a promising strategy to enhance antitumor efficacy. For instance, Wang and co-workers prepared dual responsive nanomedicines that respond to ROS and pH made up from poly (ethylene glycol)-block-poly diisopropylamino ethyl methacrylate block-poly dopamine (PEG-PDPA-PDA) and ROS responsive PEG-PTK-DOX, containing β- lapachone (Lapa) and ferric ions. The nanomedicines transitioned from hydrophobic-to-hydrophilic in response to pH with the release of Lapa which is a substrate of a tumor-overexpressed enzyme, NQO1, that catalyzes the production of H_2O_2 by futile redox cycles of Lap, killing cells by combination of toxic ROS and DOX release from polyprodrug [165]. On the other hand, Vitamin K3 was also used for the amplification of ROS to promote the release of CPT from loaded Ruthenium-cyclodextrin (Ru-CD) NPs, showing striking *in vivo* results in which the total inhibition of tumors from breast cancer mice was achieved [152].

Another approach for self-amplification of intracellular ROS for an improved drug release consists of using alpha-TOS, an analog of vitamin E. Micelles prepared from RGD-PEG-TK-PLGA targeted polymers encapsulating DOX and α-TOS, demonstrated both *in vitro* and *in vivo* antitumor efficacy of DOX without increasing systemic cytotoxicity [144].

1.6.5. TK-based ROS-responsive siRNA/DNA delivery systems

Apart from being used for the delivery of drugs, TK- based delivery systems have been explored in gene therapy and gene silencing. For instance, Shim and Xia exploited the cationic and water-soluble PATK polymer for the ROS-responsive delivery of DNA, aiming for cancer therapy. They observed that the transfection of DNA/PATK polyplexes on high-ROS PC-3 cells was more effective than that obtained with DNA/non-degradable poly(amine) polyplexes and branched polyethyleneimine (b-PEI) polyplexes, showing less cytotoxicity in comparison to DNA/branched PEI. Interestingly, the transfection efficiency on Chinese hamster ovary cells (CHO), with low intrinsic ROS levels, was lower than on prostate cancer (PC-3) cells, while in the case of control polyplexes, the transfection efficiency did not differ among these two cell lines [73]. On the other hand,

an example in which PPADT polymer is used to prepare NPs was described by Wilson and co-workers. They designed PPADT NPs for oral TNF-α-siRNA delivery to inflamed intestine tissue, starting from PPADT polymer. These NPs showed TNF-α silencing and subsequent mice protection from ulcerative colitis. In addition, they confirmed that TNFα –TKNs have a cytotoxicity profile similar to that of FDA approved PLGA [62].
In this other example, the novel TK "Bola" linker used for on-demand siRNA delivery in cancer cells, showed that these polyplexes triggered selective gene silencing of target genes on PC-3 prostate cancer cells. In addition, the dendrimer obtained by applying TK-technology (Bola4A) was not cytotoxic nor hemolytic, suggesting its safety [127].

Alternatively, high MW bPEIs ROS-responsive DDS made up from TK-crosslinked low MW bPEI600Da were employed for an improved DNA/siRNA cell transfection and biocompatibility. For instance, Lin and co-workers prepared a series of bPEI polycations by this approach that also contains an aromatic Thioacetal linker, and evaluated DNA transfection efficiency of polyplexes on HeLa cells, identifying a polycation with enhanced DNA transfection [126]. Zheng and co-workers comparatively studied the transfection efficiency among DNA polyplexes obtained from TK-crosslinked bPEIs and acid sensitive bPEIs, observing that ROS-responsive polyplexes were more efficient in transfecting DNA than pH-responsive ones on cervical cancer (HeLa) cells [117]. In the case of the use of lipid NPs, Liang and co-workers showed a highly selective silencing on cancer cells than in normal cells, with efficient tumor cell growth inhibition of lipid NPs containing silencing lipid ROS-TK-5/siPlk-1, while those containing non-silencing lipid, ROS-TK-5/siGFP, showed high cytocompatibility (higher than 90%). In addition, *in vivo* studies on tumor-bearing mice showed an 80% suppression of tumor growth in comparison to controls [140].

1.6.5.1. ROS-responsive siRNA/DNA delivery systems in combination with other stimuli. Crosslinked TK-bPEI polymers were also used in combination with PDT. For instance, Wang and co-workers used PEGylated and Ce6 conjugated high MW TK-bPEIs for siRNA-mediated gene silencing in cancer therapy, demonstrating higher tumor volume reduction when used in combination with PDT [147]. Wang and co-workers, prepared high molecular weight bPEI (600) nanocomplexes with p53 tumor suppressor gene that was subsequently coated with hyaluronic acid linked to a photosensitizer (Pha), providing stability and cell targeting. Short time (8-min) and long-time (30-min) light

irradiation were used to program gene release first (triggered by a nonlethal concentration of ROS), and then (post-transfection stage) the induction of lethal concentration of ROS (PDT), demonstrating enhanced *in vivo* antitumor efficiency [166].

1.6.6. TK-based ROS-responsive DDS in the application of Inflammatory diseases

Generally, TK- based DDS have been widely used for cancer application, being several examples commented. An example previously given regarding their application in the treatment of inflammatory diseases have been also given with PPADT NPs for oral delivery of TNF-α-siRNA to inflamed intestine, showing excellent *in vitro/in vivo* results [62]. In another case, PPADT polymers were used for the preparation of PPADT NPs encapsulating Tacrolimus (FK506), a strong immunosuppressant used against tissue transplant rejection, to investigate the effect on the inflammatory induced effect of particulate matter. These NPs could suppress the ROS-related cytotoxicity on lung epithelial cells and RAW264.7 macrophages upon co- exposure with particulate matter (PM2.5) with confirmed *in vivo* suppression of their induced inflammatory effects [122]. Lately, Regmi and co-workers that used Tacrolimus (FK506) encapsulated in TK-based microparticles, confirmed an inhibition of the hyperactivation inflammatory response of inflamed colon [123].

The treatment of inflammatory bowel disease (IBD) for the simultaneous and ROS-responsive release of anti-inflammatory (Budesonide) and antioxidant drugs (Tempol) was proposed in another work in which they used self-assembled prodrugs consisting of Budesonide (B) conjugated to Tempol (T) through aromatized TK (TK), namely B-ATK-T, and PEGylated with DSPE-PEG, and established that more than 98% of drugs have been released in a mimicked inflammation microenvironment with *in vitro*/*in vivo* confirmed efficiency against inflammation [167].

Considering that systemic increase of iron induces the expression of iron-loading, oxidative-stress and inflammatory genes [168] and the current available treatments can be correlated to the appearance of adverse effects, new approaches based on ROS-responsive NPs may be appealing. Li and co-workers designed novel NPs for a ROS-responsive hydrogel containing molecules of the iron chelator Deferoxamine (DFO) in order to reduce the negative impact of the current treatment with free DFO. A reduction of the production of ROS by macrophages under oxidative conditions was demonstrated

in vitro/in vivo, and apart from their beneficial effect in preventing iron-related inflammation, the NPs can be degraded into fragments that favor the excretion of chelates [169].

1.6.7. Real applicability, safety and future prospective of TK-based ROS-responsive formulations

The use of TK in the design of ROS-responsive DDS is quite recent, being the scientific publications growing exponentially in the last years. The research articles recently published in this topic gives light regarding the possibilities of these delivery systems, mainly in cancer application. Regarding application to cancer, as not all cancer cells produce high intracellular concentrations of ROS, the levels of ROS must to be artificially enhanced to achieve a fast drug release from ROS-responsive DDS by taking advantage of ROS-responsive materials' sensitivity to 1 mM of H_2O_2, as recently reported [129].

In order to improve results in treating cancer, the application of a second or multistimuli approach has been used. Among all investigated stimuli, the use of light to produce singlet oxygen by means of PSs has been the most used, not only to bring higher ROS concentrations to trigger TK cleavage and drug release, but also to achieve synergistic effects with chemotherapy. Sonodynamic therapy was also employed in an analogous fashion showing promising results. On the other hand, the combination of pH and temperature stimuli, as well as the combination of chemical agents that generate intracellular cascade of ROS production, also showed to improve cancer therapy compliance. For instance, it was found in *in vivo* models that TK-based ROS-responsive DDS, without applying the exogenous light stimulus, result in antitumor effects comparable to that with analogous non-ROS-responsive DDS [133,145]. Excellent results have been observed with these DDS that, in some cases, not only reduced the tumor volume significantly, but also eliminated it [152,164].

On the other hand, other researchers have shown *in vivo* anticancer efficacy of NPs in response to endogenous ROS concentrations in tumor cells. In these cases, the NPs present TK linkages that are more accessible to ROS, as it is the case of MTO polyprodrugs and Ru-CD NPs. NPs in which the TK groups are more accessible to the intracellular ROS and with NPs that are made from polymerized drugs. MTO polyprodrug

NPs demonstrated significant antitumor effects that are triggered by the intrinsic ROS concentrations in tumors. In addition, tumor-targeted NPs showed a better antitumor effect than non-targeted NPs [73]. Similarly, in the case of self-assembled NPs made up from Ru-CD and CPT, a significant inhibition of tumor growth was observed even without receiving light stimuli, and it might be associated to accessibility of TK groups to cleavage by the intrinsic concentrations of ROS. Nevertheless, the maximal antitumor effect was achieved by the combination with PDT [152].

Concerning the use of ROS-responsive material in inflammatory disease, this has been less explored than cancer but there is an appreciate number of research articles that explored TK-based DDS for inflammatory bowel diseases, with promising results. Generally, secondary stimuli have not been applied for the treatment of these diseases and this might be due to the concentration of ROS in inflammation conditions is much higher than in cancer. For instance, macrophages can reach an intracellular concentration in the range of 10-1000 mM [60]. Another reason that accounts for their effectivity might be related to the fact that TK groups scavenge ROS and, thus, along with anti-inflammatory or/and antioxidants, can achieve a synergistic effect on reducing ROS and the inflammatory phenotype. It is worth to mention that the DDS designed against this disease are commonly based on PTK, with multiple TK units and thus more chances to interact with ROS to release drugs and concomitantly reduce ROS concentrations.

Regarding TK-based DDS safety, since one of the by-products of TK linker cleavage is acetone [75,76], and considering that it is also produced by normal metabolism, it is expected minimal linker toxicity. In addition, there have not been reported studies suggesting safety issues of the developed TK-based DDS [11]. Martin and co-workers predicted that the small MW by-products produced from TK cleavage would not cause cytotoxicity *in vivo* as they are rapidly cleared from circulation [121]. On the other hand, considering TK-based ROS- responsive DDS, the biocompatibility would also depend on features that are associated with the composition of the material, size, concentration, etc. Thus, safety should be evaluated for any design TK-based DDS. From the examples previously given, no adverse effect in normal cells or tissues have been observed for either cancer or inflammation application, demonstrating not only safety in terms of DDS materials but also in terms of preventing premature drug leakage in non-targeted cells/tissues/organs.

Chapter 2:

Research aim and objectives

2.1. Research aim

A **common feature in pathologies** such as inflammatory diseases, cancer and brain diseases (e.g. Glioblastoma (GBM) and neurodegenerative diseases), is represented by the **dysequilibrium in the production/elimination of ROS, with the consequent increase in ROS concentrations.**

Since the current trend in therapeutics is to create **more selective and effective DDS** directed to the targeted disease, it is possible to exploit these abnormally high concentrations of ROS by means of **"Smart" ROS-responsive DDS**.

Among all the ROS-sensitive materials that have been described, **TK is one of the most recent and promising**, with high potential in treatment, as confirmed by the growing number of articles on TK-based DDS application in cancer and inflammatory diseases.

Considering that TK-containing linkers can be cleaved by the most relevant types of ROS, generating non-toxic and excretable products, as well as harbor functional groups for the attachment of a variety of molecules (e.g. polymers, drugs, PSs, fluorophores, etc.), these molecules are **good candidates for the preparation of ROS-responsive DDS** based on TK-based polymers, prodrugs and block co-polymers.

The aim of this PhD thesis was therefore to investigate on TK-diacid linker and to design ROS-responsive polymers as well as ROS-responsive polymeric conjugates and prodrugs using FDA approved mPEG and PLGA polymers for the application of TK-technology in the treatment of brain diseases featured by high ROS concentration.

2.2. Specific objectives

2.2.1. a) Synthesis and characterization of TK- diacid containing linker, ROS-responsive mPEG polymer and ROS-responsive and non-ROS-responsive fluorescent polymeric conjugates: mPEG-TK-Cy5 and mPEG-Cy5, **b)** studies in simulated ROS conditions of ROS-responsive polymer and fluorescent conjugates in terms of TK-cleavage and Cy5 release, respectively, and **c)** comparative *in vitro* studies of fluorescent conjugates on

human neuroblastoma cells (SH SY5Y) and on rat Glioblastoma (C6) and astrocytes (DI TNC1) cells.

2.2.2. a) Synthesis and characterization of ROS-responsive and non-ROS-responsive prodrugs with Melphalan, namely mPEG-TK-MPH and mPEG-MPH, respectively. **b)** Physical characterization of prodrug self-assembling in water, **c)** *in vitro* cytotoxicity studies of prodrugs on C6 cells and human GBM cells (U87MG and U251MG), and **d)** study of the influence of X-ray IR on inducing the antitumor effect of mPEG-TK-MPH prodrug on human GBM cells.

2.2.3. a) Synthesis and characterization of ROS-responsive PLGA-TK-COOH polymer. **b)** Synthesis and characterization of ROS-responsive PLGA-TK-PLGA co-polymer. **c)** Preparation of ROS-responsive surface functionalized TK-PLGA NPs and PLGA-TK-PLGA NPs.

Chapter 3:

TK-technology: Proof-of-concept studies

3.1. Background and chapter aim

As it was already mentioned in the introduction section, polymer prodrugs that incorporates a cleavable linker that respond to a specific pathological stimulus, between the polymer and the drug, can be engineered to obtain selective drug release and premature drug release avoidance. Since current cancer therapies are not sufficiently effective and are accompanied by the appearance of adverse effects, the use of polymer prodrugs that release their drugs in response to tumor microenvironment, can improve the treatment of current cancer therapies. When it comes to the design of stimuli responsive prodrugs against cancer, the generally high ROS concentrations in tumor cells over normal cells ($[H_2O_2]_{tumor}$ = 10-100 μM vs. $[H_2O_2]_{normal}$ = 0.001 and 0.7 μM), make this stimulus appropriate to be exploited for the treatment of this disease.

Hence, the objective of this chapter is to investigate the feasibility of TK-technology in cancer application by performing proof-of-concept studies with a ROS-responsive fluorescent conjugate obtained from the conjugation of a NIR fluorescent dye (Cy5) to mPEG, through a TK linker. The ROS-triggered Cy5 release from ROS-responsive conjugate was evaluated by means of simulated ROS-conditions as well as *in vitro*, on rat GBM (C6), human neuroblastoma (SH SY5Y), and astrocyte (DI TNC1) cells.

3.2. Results

"ROS-responsive "smart" polymeric conjugate: synthesis, characterization and proof-of-concept study", published in: International Journal of Pharmaceutics 570 (2019) 118655.

Abstract

New approaches integrating stimuli-responsive linkers into prodrugs are currently emerging. These "smart" prodrugs can enhance the effectivity of conventional prodrugs with promising clinical applicability. Oxidative stress is central to several diseases,

including cancer. Therefore, the design of prodrugs that respond to ROS stimulus, allowing a selective drug release in this condition, is fairly encouraging. Aiming to investigate the ROS-responsiveness of prodrugs containing the ROS-cleavable moiety, Thioketal (TK), we performed proof-of-concept studies by synthesizing ROS-responsive conjugate, namely mPEG-TK-Cy5, through exploiting Cy5 fluorescent dye. We demonstrated that, differently to non-ROS-responsive control conjugate (mPEG-Cy5), mPEG-TK-Cy5 shows a selective release of Cy5 in response to ROS in both, ROS-simulated conditions and *in vitro* on glioblastoma cells. Our results confirm the applicability of TK-technology in the design of ROS-responsive prodrugs, which constitutes a promising approach in cancer treatment. The translatability of this technology for other diseases treatment makes this a highly relevant and promising approach.

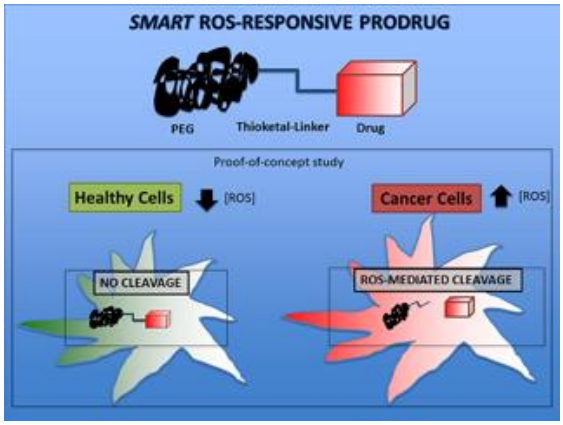

Keywords: ROS stimulus, ROS-responsive conjugate, TK-technology, cancer treatment applicability

1. Introduction

Drug delivery systems (DDS) aiming to improve the solubility and bioavailability of poorly water-soluble drugs have been broadly developed [171]. Amongst them, polymer-drug conjugates or prodrugs were demonstrated to be a straightforward strategy to increase the solubility and selectivity of certain drugs, enhancing their effectivity as well as reducing their adverse effects [172]. The potential of this approach is incremented by the possibility of further selective engineering of the prodrug by incorporating a cleavable linker between the polymer and drug, which can be enzymatically hydrolyzed inside cells or be responsive to a stimulus, thus being more tailored to the pathological features of a

given disease [17]. Therefore, by carefully planning the design of the prodrug featured by the presence of a stimulus- responsive moiety, able to be activated within the stimulus event, the selective "smart" release of drugs at pathological sites can be obtained.

The great potential of this approach lies in the real possibility of creating novel approaches for curing diseases more selectively than through a "simple" drug administration, allowing a more efficacious and less toxic treatment.

In terms of pathologies, cancer constitutes one of the most lethal diseases of high worldwide incidence and difficulty to be cured [75,173]. The efficacy of current treatments is still limited by side effects, with chemotherapy as first-line therapy of choice against this disease [172,174], being well-known for the lack of selectivity as well as the hydrophobicity of the majority of chemotherapeutics [174].

Amongst the number of possible targets and features which could be exploited with the aim of creating a more selective and "smart" drug delivery, great attention was given to reactive oxygen species (ROS) such as hydrogen peroxide, hydroxyl radicals, singlet oxygen, superoxide, nitric oxide, nitroxyl and nitrogen dioxide, since their concentrations are increased in several diseases [86], e.g., inflammatory diseases, neurodegenerative diseases and cancer [45,175]. In cancer, it is estimated that the intracellular concentration of H_2O_2 can reach 10-100 μM, while in normal cells, the estimated H_2O_2 concentration is between 0.001 and 0.7 μM [74]. For instance, gliomas are characterized by enhanced oxidative stress, which is a feature that increases the resistance to chemotherapy [176].

Thus, polymer prodrugs which respond to a ROS stimulus may confer selectivity in cancer therapy with the activated delivery of drugs in such target sites [177]. Currently, several ROS-responsive polymer platforms based on poly (propylene sulfide), selenium/tellurium, polyoxalate, poly(proline), boronic ester, and thioketal (TK) are being investigated [109]. Their ROS responsive mechanisms rely on either a transition from hydrophobic to hydrophilic states or a cleavage reaction of the polymer platforms [96]. TK is a subclass of thioether group, which is cleaved to thiol-containing groups upon the exposure to ROS [115]. *In vitro* studies on TK ROS-responsiveness to several ROS types [178] (i.e., H_2O_2, hydroxyl radical and superoxide) showed the ability of the TK moiety to be cleaved by the most relevant ROS that are encountered in pathological conditions. Most importantly, the byproducts originated from their cleavage are rapidly cleared from the circulation [121,148]. Therefore, they constitute good candidates as moieties for the design of "smart" ROS responsive polymers.

Another limitation of current chemotherapeutics is based on the low water solubility that strongly hampers the administration and bioavailability of drugs. One of the most exploited approaches to overcome this limitation consists of the use of poly(ethylene glycol) (PEG), a synthetic water-soluble polymer, FDA approved for its use in pharmaceutical formulations [179]. The conjugation of PEG with either biotherapeutic drugs or small molecules, known as PEGylation, was demonstrated to improve drug solubility and stability and to prolong the circulation time of drugs, reducing their renal clearance [79,180]. Accordingly, by combining TK linkers and PEG conjugation, administrable and selective prodrugs may be produced for the delivery of antitumor drugs in cancer treatment.

Therefore, in this study, we decided to use a fluorescent dye (NIR fluorescent dye, Cy5-NH_2) to be conjugated to PEG and TK in order to give proof-of-concept of the technology's feasibility and success in selective ROS-mediated cleavage. Using *in vitro* validation of Cy5 ability to be selectively released in response to cancer pathological conditions (glioblastoma cells and neuroblastoma cells), we investigated the potential of TK-technology to be used in cancer treatment.

2. Materials and Methods

2.1. Materials

Methoxy-polyethylene glycol amine (mPEG-NH_2, Mw 5000 Da) and mPEG propionic acid (Mw 5000 Da) were purchased from JenKem Technology and Sigma-Aldrich, respectively. N-hydroxy succinimide (NHS) and N-(3-dimethylaminopropyl)-N-ethylcarbodiimide hydrochloride (EDC. HCl) were provided by Sigma-Aldrich and used directly. All the solvents used, 3-Mercaptopropionic acid (3-MPA), dichloromethane (DCM), dimethylformamide (DMF), acetone, hydrogen peroxide (H_2O_2) and hexane, were of analytical grade and used without further purification. A Milli-Q water system (Millipore, Bedford, MA, USA), supplied with distilled water, provided high-purity water (18 V). F12-K and trypsin (TrypLE Select Enzyme (1X)) were purchased from Gibco. DMEM High Glucose, fetal bovine serum (FBS), and penicillin–streptomycin was purchased from Sigma-Aldrich. CellROX™ Green Reagent was purchased from Thermo Fisher Scientific. The primary antibodies were purchased from Cell Signaling

Technology (Rab5 (C8B1), Rabbit mAb), Thermo Fisher Scientific (EEA1, Rabbit mAb), and Abcam (Clathrin heavy chain, Rabbit pAb). Secondary Alexa Fluor conjugated antibodies were purchased from Life Technologies.

2.2. Synthesis

2.2.1. ROS-cleavable thioketal containing linker (TK-C.L.) synthesis

The synthesis of ROS-cleavable thioketal linker (Scheme 1A) was performed according to previous works without further modifications [30,143,144]. Briefly, a mixture of 3-MPA (49.1 mmol) and anhydrous acetone (98.2 mmol) was saturated in dry hydrogen chloride atmosphere and stirred at room temperature for 4 hours. After that, the reaction was quenched by placing the mixture on an ice-salt mixture until the crystallization was complete. The crystals were filtered by vacuum, washed gently with hexane and cold water, and finally dried in vacuum. The product was fully characterized by ^{1}H NMR and ESI-MS.

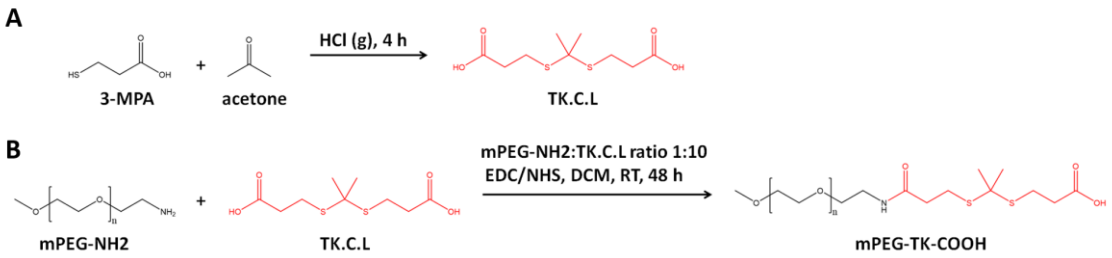

Scheme 1: Syntheses Scheme. A. Synthesis of TK-C.L. **B.** Synthesis of ROS-responsive polymer mPEG-TK-COOH.

2.2.2. ROS-responsive mPEG-TK-COOH polymer synthesis

mPEG-TK-COOH synthesis was performed according to Li et al. with some modifications[143] and is shown in Scheme 1B. Briefly, mPEG-NH_2 (0.1 mmol), TK-C.L. (1 mmol), EDC. HCl (1.2 mmol) and NHS (1.2 mmol) were well dissolved in DCM (5 mL) and stirred at room temperature for 48 h. The reaction was stopped at 48 h; the solvent was removed by rotary evaporation and the product precipitated by co-solvent

precipitation in DCM and diethyl ether. After drying in vacuum, the product was dissolved in DMF and dialyzed against distilled water for 72 h by using an MWCO: 3500 Da dialysis membrane. After freeze-drying, the expected mPEG-TK-COOH was collected as a white powder. The derivatization yield was determined from ^{1}H-NMR characterization data and indirectly by quantifying non-reacted mPEG-NH_2 through Quantitative Ninhydrin Assay.

The determination of the derivatization yield through ^{1}H-NMR was achieved by integrating peak data at chemical shifts: 3.2 and 3.48 ppm, which correspond to protons of -CH_2 groups next to amine group (of un-reacted mPEG-NH_2) and amide bond (formed by the covalent conjugation between mPEG-NH_2 and TK-C.L.), respectively.

The determination of the derivatization yield by colorimetric assay with ninhydrin was performed by placing 100 μL of mPEG-TK-COOH solutions (2.5- 4 mg/mL) into the wells of a 96-well plate and 75 μL of ninhydrin colour reagent, respectively. Then, the plate was incubated at 80°C for 30 min. After incubation, the plate was cooled to room temperature, and 100 μL of stabilizing solution (50% v/v ethanol) was added to each well. Finally, the absorbance was measured at 570 nm through a Multiskan Microplate Reader (Spectrum Finstruments®). Different concentrations of mPEG-NH_2 in aqueous solution were used for the generation of a calibration curve from which the concentration of non-reacted mPEG-NH_2 on the sample and therefore its percentage, were calculated. Linearity was assumed in the range of 0.015–1.5 mg/mL (r_2 = 0.9989). mPEG-TK-COOH derivatization yield was achieved by subtracting 100% to % mPEG-NH_2.

2.2.3. Synthesis of ROS-responsive and non-ROS-responsive fluorescent conjugate: mPEG-TK-Cy5 and mPEG-Cy5

mPEG-TK-COOH (Scheme 3.2) or mPEG propionic acid (Scheme 3) (11.46 μmol) were activated with EDC.HCl (57.4 μmol) and NHS (57.3 μmol) in 1.5 mL of DCM for an hour. Then, Cy5-NH_2 (12.8 μmol) diluted in 0.5 mL of DCM was added to the mixture and stirred for 48 hours at room temperature. The product was precipitated by co-solvent precipitation in DCM/cold diethyl ether on ice-bath. Diethyl ether was removed by rotary evaporation, and after drying the precipitate in a vacuum desiccator, the product was dissolved in DMF and dialyzed (MWCO: 3500 Da) against the same solvent for 24 h and

against MilliQ water for 48 h, respectively. The conjugates were isolated by freeze-drying and kept in a desiccator.

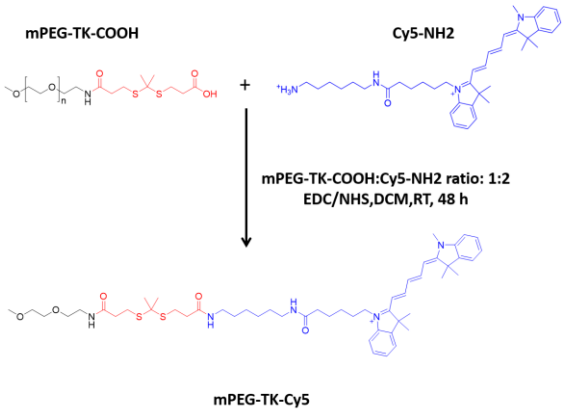

Scheme 2: Synthesis scheme of ROS-responsive polymer fluorescent conjugate, mPEG-TK-Cy5.

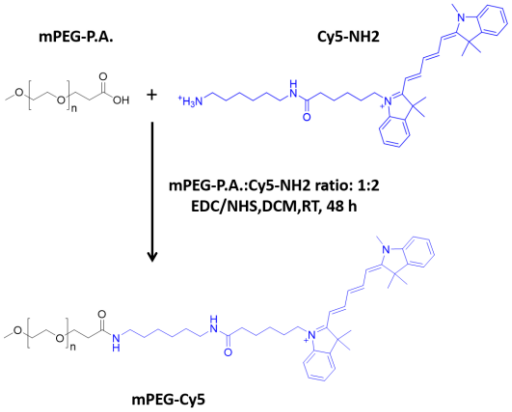

Scheme 3: Synthesis of non-ROS-responsive (control) polymer fluorescent conjugate, mPEG-Cy5.

2.2.4 Determination of mPEG-TK-Cy5 derivatization yield and Cy5-loading on mPEG-TK-Cy5 and mPEG-Cy5 fluorescent conjugates

The derivatization yield of mPEG-TK-Cy5 was indirectly determined by quantifying the non-reacted mPEG-TK-COOH on mPEG-TK-Cy5 sample through RP-HPLC. The RP-HPLC apparatus comprised a Model PU2089 pump provided with an injection valve with a 50 µL sample loop (7725i, Jasco), UV-Vis detector (UV1575, Jasco) and fluorescent detector (FP-2020 Plus, Jasco). UV-Vis detector and fluorescence detector were set to λ= 210 nm and λ_{exc}= 640 nm/ λ_{em}= 660 nm, respectively, and column temperature to 37°C.

The analysis was performed in gradient conditions with mobile phase A- Water 100%: TFA 0.1% and B- ACN 100%: TFA 0.1%, at a flow rate of 1 mL/min. The samples were injected on HC-C18 (250 mm x 4.60 mm, Agilent Technologies) and eluted following this gradient: 0-5 min, 70 % A; 5-20 min, 30 % A; 20-21, 30% A; 21-25 min, 70 % A and 25-30, 70% A. The Chromatographic peak areas of the samples were recorded and analyzed using a JASCO software (JascoBorwin 1.5). Un-reacted mPEG-TK-COOH content was calculated against a calibration curve performed with mPEG-TK-COOH polymer (linearity was assumed in the 0.3–9.5 mg/mL; r^2= 0.9956 range).

Cy5 content on mPEG-Cy5 and mPEG-TK-Cy5 conjugates was expressed as μg of Cy5 per mg of conjugate and was determined by measuring the fluorescence of conjugate solutions (1- 2.5 mg/mL) in methanol. The measurements were performed in a fluorometer (FP-8200, Jasco) with λ_{exc}= 620 nm and λ_{em}= 654 nm. Cy5 content on the conjugates was obtained against a calibration curve of Cy5-amine in methanol (linearity was assumed in the 0.103–1.03 mg/mL; r^2= 0.9903 range).

2.3 Characterization

2.3.1. Nuclear magnetic resonance (NMR)

TK-C.L. ^{1}H-NMR spectra were acquired on Avance400- Bruker spectrometer in $CDCl_3$ and d^6-DMSO solvents with TMS as an internal standard. On the other hand, mPEG-TK-COOH, mPEG-Cy5 and mPEG-TK-Cy5 ^{1}H-NMR spectra were obtained in Avance III 600 HD- Bruker in $CDCl_3$ (mPEG-TK-COOH) and d6-DMSO (mPEG-Cy5 and mPEG-TK-Cy5) solvents. The identification of all proton signals in mPEG-TK-COOH polymer was completed through the information collected by the following analysis: ^{1}H, ^{13}C, Homonuclear correlation spectroscopy (COSY), Heteronuclear single-quantum correlation spectroscopy (HSQC) and Heteronuclear multiple-bond correlation spectroscopy (HMBC) NMR.

2.3.2. MALDI-TOF/TOF mass spectrometry

mPEG-TK-COOH, mPEG-TK-Cy5, and mPEG-Cy5 mass spectra were acquired with Flex control- Ultraflex TOF/TOF, MALDI-TOF/TOF mass spectrometer). Briefly, the samples for MALDI-TOF analysis were prepared by mixing 2,5-DHB matrix in water/EtOH (9:1, v/v) and polymer or conjugate in water in a 1:1 v/v ratio. 1 μL of each sample was deposited onto the plate, and after drying, the plate was introduced into the instrument. The instrument was operated in positive charge and reflection mode, and each mass spectrum was acquired by averaging 80– 800 consecutive laser shots.

2.4. ROS- responsive validation studies of mPEG-TK-COOH and mPEG-TK-Cy5 in ROS- simulated conditions

2.4.1. ROS-mediated TK cleavage from mPEG-TK-COOH polymer in ROS-simulated conditions

This procedure was exploited in order to assess the ability of TK to be cleaved under ROS-simulated conditions and it was adapted and modified from Yue et al. [30]. mPEG-TK-COOH (10.82 μmol of thioketal groups) was incubated in water with either 100 μM, 1 mM, 100 mM or 400 mM H_2O_2 and 3.2 μM $CuCl_2$ at 37°C for 48 h. Once the incubation was completed, the polymer was dialyzed (dialysis membrane MWCO: 3500 Da) overnight against MilliQ water. The polymer inside the dialysis bag was finally freeze-dried and analyzed through ^{1}H NMR (400 MHz, $CDCl_3$).

2.4.2. mPEG-TK-Cy5 ROS-responsiveness in ROS-simulated conditions

mPEG-TK-Cy5 or mPEG-Cy5 (2 mg) were incubated in a mixture containing 400 mM H_2O_2 and 3.2 μM $CuCl_2$ in DMF/H_2O (5.4:4.6, v/v) at 37°C. This protocol was adapted and modified from Yue et al. [30] and Li et al. [143,144]. At selected times: 2, 6, 24, and 48 hours, samples aliquots of 50 μL were injected on RP-HPLC. The RP-HPLC system used in these studies is described in section 2.2.4.

2.5. *In vitro* studies of mPEG-TK-Cy5 on cells

2.5.1. Cell culture

C6 Rat Glioblastoma cells (ATCC) were cultured in F-12k culture medium with 20% FBS and 1% penicillin/streptomycin. DI TNC1 Rat Astrocyte cells (ATCC) were cultured in DMEM High Glucose medium with 10% FBS and 1% penicillin/streptomycin. SH SY5Y Neuroblastoma cells (Sigma Aldrich) were cultured in Ham's F12: EMEM (1:1) with 2mM Glutamine, 1% Non-Essential Amino Acids (NEAA) and 15% FBS. All cell lines were kept at 37°C under a humidified atmosphere containing 5% CO_2.

2.5.2. Comparative *in vitro* studies of mPEG-TK-Cy5 on C6, DI TNC1 and SH SY5Y cells

C6, DI TNC1 and SH SY5Y cells were seeded (100.000 cells/mL) on poly-L-lysine (0.1 mg/mL; Sigma-Aldrich) coated glass coverslips in a 24 well plate and incubated at 37°C until 80% confluence was reached. Subsequently, the medium was replaced, and 0.9 µg/mL of mPEG-Cy5 or mPEG-TK-Cy5 were added to the corresponding wells and incubated for 24 h. Before cell fixation, the cells were incubated with CellROX™ Green Reagent (5 µM) for 30 min. Then, the cells were rinsed with 1X PBS and fixed with 4% paraformaldehyde solution (PFA) in 1X PBS. Cell nuclei were counterstained with DAPI and coverslips subsequently mounted using Vecta Mount (Vector Laboratories, USA). The cells were observed using a confocal laser-scanning microscope (Zeiss LSM710). CellROX fluorescence of confocal images of C6, DI TNC1 and SH SY5Y cells treated with either of the conjugates was quantified using ImageJ (National Institutes of Health), by measuring at least 20 cells per condition and cell line.

2.5.3. mPEG-TK-Cy5 *in vitro* Cy5 release studies on C6 and SH SY5Y cells

Cells were seeded (1x 10^5 cells/mL) on poly-L-lysine (0.1 mg/mL; Sigma-Aldrich) coated glass coverslips in a 24- well plate and incubated at 37°C for 24 hours. The cells were

then incubated for 72 hours with either mPEG-Cy5 or mPEG-TK-Cy5 at equivalent Cy5 concentrations of 0.9 and 4.5 μg/mL, respectively. After the incubation period, cells were fixed with 4% PFA at RT for 15 minutes and processed for immunocytochemistry. After washing with three times with 1X PBS containing 0.2% Triton X-100 at RT, blocking was performed with a blocking solution (BS: 10% FBS in 1X PBS) for 1 h at RT. Subsequently, samples were incubated with primary antibody in BS at RT for 2 h. After washing three times with 1X PBS, incubation with Alexa488 secondary antibody dissolved in BS for 1 h was followed. After washing three times with 1X PBS, Cell nuclei were counterstained with DAPI and coverslips subsequently mounted using Vecta Mount (Vector Laboratories, USA). The cells were observed using a confocal laser scanning microscope (Zeiss LSM710). Confocal images were subsequently analyzed by Image J and Image- Pro 10, through applying a software tool that permits to plot the fluorescence intensity along a line segment traced in a region of interest. In order to evaluate cytoplasmic Cy5 intensity, a line segment was traced through the cytoplasm of selected cells, obtaining a plot of fluorescence distribution along the line.

2.6. Statistics

Statistical analysis was performed with Prisma version 5. All data are shown as mean of at least three experiments ± SD if not indicated otherwise. For comparisons, unpaired t-tests or one/two-way ANOVA with Bonferroni post-hoc test for pairwise comparison were performed. Statistically significant differences are indicated in the figures as follows: *$p<0.05$, **$p\leq0.01$ and ***$p\leq0.001$.

3. Results

3.1. Synthesis and characterization of TK-C.L. and mPEG-TK-COOH

TK-C.L. was obtained with a yield of 25% (Scheme 1A). The generation of by-products that were successfully eliminated during the purification process accounts for this low yield. Characterization was obtained by ^{1}H NMR, showing ^{1}H signals with chemical

shifts: 2.75 (t, 4H); 2.51 (t, 4H); 1.54 (s, 6H) in d6-DMSO and 2.932 (t, 4H), 2.702 (t, 4H) and 1.623 (s, 6H) in deuterated dichloromethane, respectively (Figure S1A and B). Thus, TK-C.L. was properly characterized, confirming the obtention of the correct chemical structure, in agreement to those reported previously in d^6-DMSO [30]. In addition, we confirmed the molecular weight to be 252.04 g/mol, which corresponds precisely to the theoretical molecular weight of TK-C.L. (252.35 g/mol) (Figure S1C).

The synthesis of ROS-responsive mPEG-TK-COOH polymer (Scheme 1B), successfully led to the intended product in very high yield (78.16 %). Furthermore, the derivatization yield obtained, measured by two different approaches (Ninhydrin assay and ^{1}H NMR), was about 84%. The full characterization of the product was achieved by NMR analysis, as ^{1}H, ^{13}C, Homonuclear correlation spectroscopy (COSY), Heteronuclear single-quantum correlation spectroscopy (HSQC) and Heteronuclear multiple-bond correlation spectroscopy (HMBC) NMR (Figure 8). The intense peaks at 3.66 ppm and 3.44 ppm correspond to protons of -CH_2O and -CH_3O groups of the mPEG polymer, respectively. The peak at 3.48 ppm corresponds to protons of –CH_2 group located next to the amide bond formed between mPEG-NH_2 and TK-C.L. This signal was shifted respective to the signal of protons from the –CH_2 group on mPEG-NH_2, which was found to be 3.2 ppm (Figure S2). This confirms the formation of covalent bonds between mPEG-NH_2 and TK-C.L. The peak at 1.6 ppm corresponds to the chemical shift of protons of –CH_3 groups of TK-C.L, in accordance with ^{1}H NMR data previously reported by Li et al. [143,144], describing a similar chemical shift of these protons in d^6-DMSO at 1.52 ppm. The mPEG-TK-COOH molecular weight calculated by MALDI-TOF was 5275.95 g/mol, which is very close to the theoretical molecular weight expected for this polymer (5234.3 g/mol).

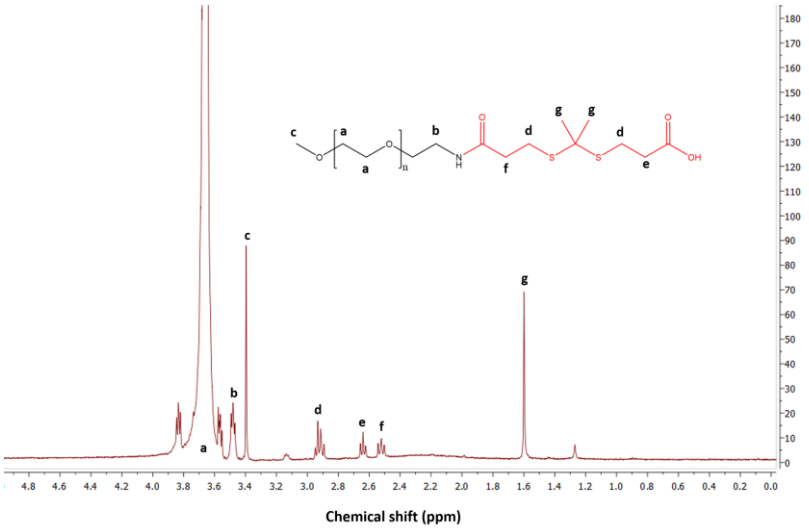

Figure 8: ^{1}H NMR characterization of mPEG-TK-COOH in $CDCl_3$. The chemical shifts of protons from the groups on the polymer are identified by letters.

3.1.2. mPEG-TK-COOH responsiveness to ROS

To assess the ability of mPEG-TK-COOH to respond to ROS, the polymer was incubated in water containing different concentrations of H_2O_2 (100 µM, 1 mM, 100 mM, and 400 mM) and $CuCl_2$ (3.2 µM), for 48 h at 37°C. These reagents produce hydroxyl radicals by reduction of H_2O_2 catalyzed by the conversion of Cu^{++} to Cu^{+++} to hydroxyl radical by a Fenton- like reaction [181]. The purified polymers obtained at the end of incubation were analyzed using ^{1}H-NMR, showing that the chemical shift at 1.58 ppm, corresponding to protons of TK $–CH_3$ groups, was decreased with increasing concentrations of H_2O_2 (100 µM- 100 mM) and no longer detected at 400 mM of H_2O_2 (Figure 9). This confirms that mPEG-TK-COOH responded to hydroxyl radicals by TK moiety cleavage under these experimental conditions. Acetone, which is a byproduct originated from Thioketal ROS-triggered cleavage, can also be detected as a broad peak at a chemical shift of ~ 2.0 ppm on 100 mM and 400 mM H_2O_2 spectra (Figure 9). This result is also in line with the findings of Yue et al. [30], who established TK bond cleavage from TL-CPT (TK-C.L. conjugated to the anticancer drug Camptothecin), due to the disappearance of the $–CH_3$ group proton signal (δ= 1.47- 1.54 ppm) with detection of acetone (δ= 2.2 ppm). Similarly, Xim and Shia [178] demonstrated the ROS responsiveness of TK moiety on

poly (amino thioketal) (PATK) polymers by the time- related disappearance of the -CH_3 group proton signal from TK (δ= 1.62 ppm).

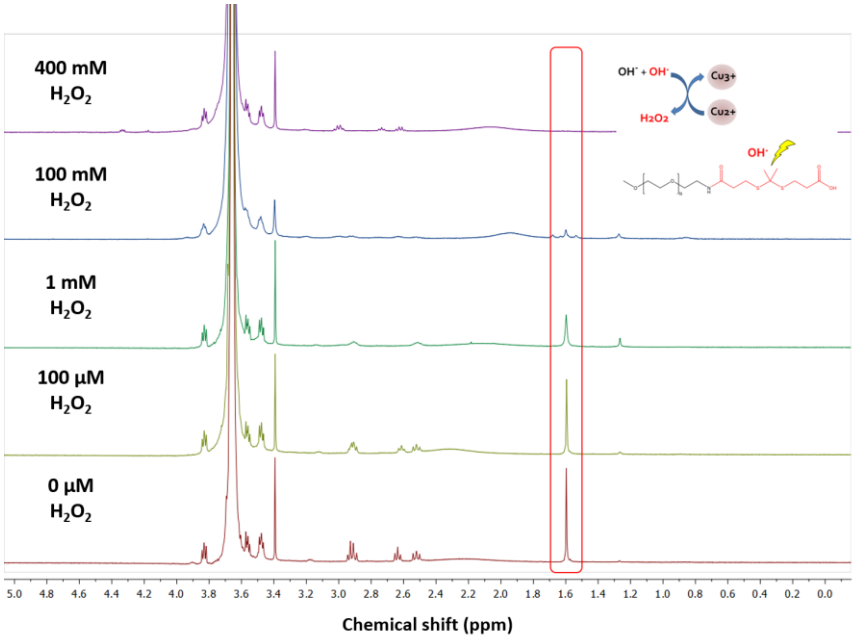

Figure 9: mPEG-TK-COOH ^{1}H NMR spectra after 48 h- incubation in ROS-simulated conditions at 0 µM, 100 µM, 1mM, 100 mM and 400 mM H_2O_2 concentration. The scheme on the upper right displays the Fenton-like reaction which accounts for hydroxyl radical generation, as well as the cleavage site on mPEG-TK-COOH polymer. The red rectangle depicted in the spectra indicates the chemical shift of methyl protons of TK moiety at 1.58 ppm, which decreased upon H_2O_2- concentration dependent ROS- triggered cleavage.

3.2.1. mPEG-TK-Cy5 and mPEG-Cy5 synthesis and characterization

Both fluorescent conjugates (mPEG-TK-Cy5 and control mPEG- Cy5) (Scheme 2 and 3, respectively) were synthesized with product yields over 90% (93 and 96%, respectively), with mPEG-TK-Cy5 derivatization yield around 30%. The Cy5 content of mPEG-TK-Cy5 and mPEG-Cy5 conjugates was 9.3 ± 3.1 µg/mg and 4.5 ± 1.4 µg/mg, respectively.

The characterization of either of the conjugates was performed by ^{1}H NMR (Figure S3) and MALDI-TOF. Chemical shifts in the range of 7.15 to 7.7 ppm, which correspond to proton signals from the aromatic groups of Cy5, have been identified in both spectra: mPEG-Cy5 and mPEG-TK-Cy5 (Figure S3A and B). In addition, the characteristic

chemical shift of TK -CH_3 protons can be observed in mPEG-TK-Cy5 (Figure S3A). The mean molecular weight of mPEG-TK-Cy5 and mPEG-Cy5 calculated through MALDI-TOF was 5851.4 g/mol and 5519.2, respectively. Both molecular weights are close to the theoretical molecular weights expected for either of the conjugates: 5871.66 g/mol and 5634.7 g/mol.

3.2.2. Cy5 release from mPEG-TK-Cy5 in ROS-simulated conditions

Studies on the selective Cy5 release from mPEG-TK-Cy5 upon ROS stimuli were performed by incubating mPEG-TK-Cy5 or mPEG-Cy5 in ROS-simulated conditions (DMF/H_2O (5.4:4.6) v/v with 400 mM H_2O_2 and 3.2 μM $CuCl_2$) as well as in control conditions (DMF/H_2O (5.4:4.6) v/v without H_2O_2 and $CuCl_2$) at physiological temperature (37°C). At different times, aliquots of either of the conjugates' samples were retrieved and analyzed by RP-HPLC.

Considering mPEG-TK-Cy5, the results after incubation in ROS-simulated conditions (Figure 10A) clearly evidence a time-dependent decrease of the mPEG-TK-Cy5 peak (r.t. at 19 min) with the concomitant increase of a peak that corresponds to Cy5 released (r.t. at 18 min) detected by both fluorescence and UV-vis. At 2 and 6 hours of incubation, the percentage of Cy5 release was 20.9% and 62.7%, respectively. At 24 hours of incubation, a plateau of the Cy5 release was reached with 98.2% of Cy5 released. When the same mPEG-TK-Cy5 conjugate was incubated in control conditions, the conjugates' peak remained unmodified (Figure S4), clearly confirming that this conjugate undergoes TK cleavage only in the presence of ROS.

Considering the non-ROS-responsive mPEG-Cy5 conjugate exposed to simulated ROS conditions, only the peak corresponding to mPEG-Cy5 (r.t.18 min) was observed (Figure 10C).

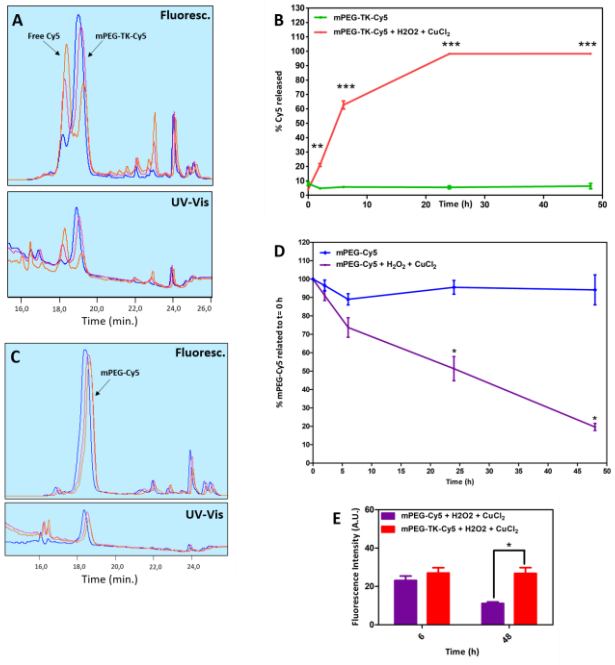

Figure 10: RP-HPLC studies of mPEG-TK-Cy5 and mPEG-Cy5 responsiveness to ROS. All data are shown as mean ± SD. **A.** Overlapped chromatograms of mPEG-TK-Cy5 injected samples at incubation times: 0 h (blue line), 2 h (pink line) and 6 h (orange line) in ROS simulated medium. **B.** Cy5 release curve from mPEG-TK-Cy5 with time with and without ROS. **C.** Overlapped chromatograms of mPEG-Cy5 injected samples at incubation times: 0 h (blue line), 2 h (pink line) and 6 h (orange line) in ROS simulated medium. Incubation times with significant differences with respect to the control group are indicated by asterisks (**p≤0.01 and ***p≤0.001). These statistical results were achieved by applying unpaired t-test. **D.** mPEG-Cy5 intensity percentage related to initial (t= 0 h) up to 48 h of incubation in ROS simulated conditions and in medium without ROS (control). Incubation times with significant differences with respect to the control group are indicated by asterisks (*p≤0.05). These statistical results were achieved by applying unpaired t-test. **E.** Total fluorescence of mPEG-TK-Cy5 and mPEG-Cy5 incubated in ROS simulated conditions, measured by fluorometer. The significant difference in conjugates fluorescence intensity is indicated by an asterisk (*p≤0.05) in the graph, and it was determined by two-way ANOVA with Bonferroni post hoc test.

Nevertheless, although Cy5 was not released from this conjugate due to the absence of the ROS-cleavable linker, conjugate fluorescence intensity decreased with time upon ROS exposure. To closer investigate this, curves of the percentage of mPEG-Cy5 intensity related to the initial (t= 0 h) of samples incubated in ROS simulated and control conditions (solvent mix without Fenton- like reagents), respectively, were plotted (Figure 10D). A significant difference between these samples was found at 24 and 48 hours of incubation (Figure 10D). This result was then confirmed by measuring fluorescence intensity in a fluorometer at 6 and 48 hours of incubation (Figure 10E). Regarding the

total fluorescence intensity of the mPEG-TK-Cy5 samples, which comprises mPEG-TK-Cy5 and released Cy5 fluorescence (Figure 10E), the fluorescence did not vary throughout the experiment. In addition, the total mPEG-TK-Cy5 fluorescence intensity at 48 hours of incubation was significantly higher than the total mPEG-Cy5 fluorescence intensity. Taken together, these results suggest that, while Cy5 from mPEG-Cy5 was quenched by ROS, TK linkages on mPEG-TK-Cy5 can be acting as ROS scavengers, preventing Cy5 from being quenched.

3.2.3. Comparative *In vitro* studies of mPEG-TK-Cy5 in C6 and DI TNC1 cells

To evaluate the selective release of Cy5 in cancer cells versus healthy cells, we incubated C6 glioblastoma (tumor) cells and DI TNC1 astrocyte (control) cells for 24 h with mPEG-TK-Cy5 or mPEG-Cy5. Previous work reported that ROS is essential for rat C6 glioma cells to grow [182,183]. As astrocytes can be the cells of origin for glioblastomas [184], we used a rat DI TNC1 astrocyte cell line as a control that exhibits several characteristic features of astrocytes, retaining a type 1 astrocyte phenotype [185,186]. Thus, this astrocyte cell line constitutes an appropriate control of normal astrocytes for comparative studies. In order to confirm that the ROS levels on C6 cells are higher than on DI TNC1 cells, a dye whose fluorescence is enhanced in ROS producing cells, CellROX^{TM} green reagent, was used in these studies. Figure 4 depicts the confocal images obtained after the incubation of the conjugates in either of the cell lines. The CellROX signals on Figure 11A-D were quantified using ImageJ, confirming that CellROX fluorescence of cells incubated with either mPEG-Cy5 or mPEG-TK-Cy5, was significantly higher in C6 cells than in DI TNC1 cells (Figure S5).

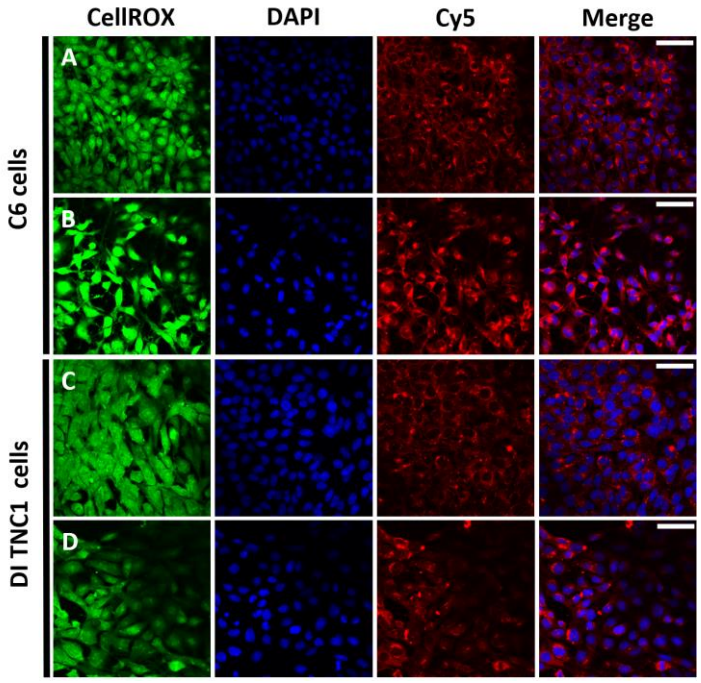

Figure 11: Confocal images of C6 and DI TNC1 cells incubated with either mPEG-Cy5 or mPEG-TK-Cy5 at equivalent Cy5 concentrations of 0.9 µg/mL for 24 h. A. mPEG-Cy5 incubated C6 cells. **B.** mPEG-TK-Cy5 incubated C6 cells. **C.** mPEG-Cy5 incubated DI TNC1 cells. **D.** mPEG-TK-Cy5 incubated DI TNC1 cells. The vertical panels show the different channels (dyes) of every confocal image. With channels as following: 488 nm (CellROX), 405 nm (DAPI) and 633 nm (Cy5). Merge results from the superposition of DAPI and Cy5 channels. Scale bar = 50 µm.

Regarding the intracellular distribution of mPEG-Cy5, a cluster distribution of the Cy5 signal can be observed in both C6 and DI TNC1 cells (Figure 11A and C), which indicates that mPEG-Cy5 is possibly inside endo/lysosomal vesicles. In the case of mPEG-TK-Cy5 incubated C6 cells, we could observe Cy5 signal in the cytoplasm, which is no longer vesicular distributed (Figure 11B), suggesting that Cy5 was released from mPEG-TK-Cy5 inside the endo/lysosomes and diffused into the cytosol of these cells. However, in the case of astrocytes incubated with mPEG-TK-Cy5, the Cy5 signal is also distributed in clusters, similar to mPEG-Cy5, meaning that Cy5 was not released from mPEG-TK-Cy5 in these cells. This demonstrates the selectivity of Cy5 release in an environment with high levels of ROS, such as found in glioblastoma cell cultures, in comparison to an environment with a low level of ROS, such as found in astrocytes cells.

To validate the obtained result that Cy5 release is primarily dependent on the presence of ROS, and thus occurs in other tumor cell lines with similar levels of ROS, we repeated the experiments using the neuroblastoma SH SY5Y cell line. Cultivated SH SY5Y cells

show comparable levels of ROS to C6 cells (Figure S6A). As Before, cells were incubated with mPEG-TK-Cy5 or mPEG-Cy5 for 24 h. Intriguingly, ROS levels measured by CellROX signal intensity significantly decreased in mPEG-TK-Cy5 treated cells ($p = 0.045$, *t*-test), confirming that the TK linkage on mPEG-TK-Cy5 can act as ROS scavenger (Figure S6B). More importantly, we confirmed a significantly different distribution of Cy5 signals between cells treated with mPEG-TK-Cy5 and mPEG-Cy5 (Figure S6C). Similar to C6 cells, several vesicle-like signals were found in mPEG-Cy5 treated cells. However, the Cy5 signal was more diffuse and significantly ($p = 0.0003$, *t*-test) less clustered in cells treated with mPEG-TK-Cy5 (Figure S6C).

3.2.4. *In vitro* Cy5 release from mPEG-TK-Cy5 on C6 cells

In order to confirm the results obtained by incubating C6 and SH SY5Y cells with mPEG-TK-Cy5 for 24 h, where we suggested that in these cells, Cy5 was released from this conjugate in ROS level dependent fashion, we performed a complementary experiment using C6 cells and testing two different equivalent concentrations of Cy5 with an extended incubation time (72 h). Again, non-ROS-responsive mPEG-Cy5 was also included in these studies, as control. Glioblastoma cells were incubated for 72 hours with either of the conjugates at equivalent Cy5 concentrations of 0.9 and 4.5 μg/mL, respectively. Confocal microscopy studies showed that both conjugates were internalized by cells. In mPEG-Cy5 incubated cells, a cluster-distribution of the red signal, corresponding to Cy5, can be observed at any of the equivalent Cy5 concentrations assayed (Figure 12A, a and b). These clusters correspond to mPEG-Cy5 that was endocytosed by cells.

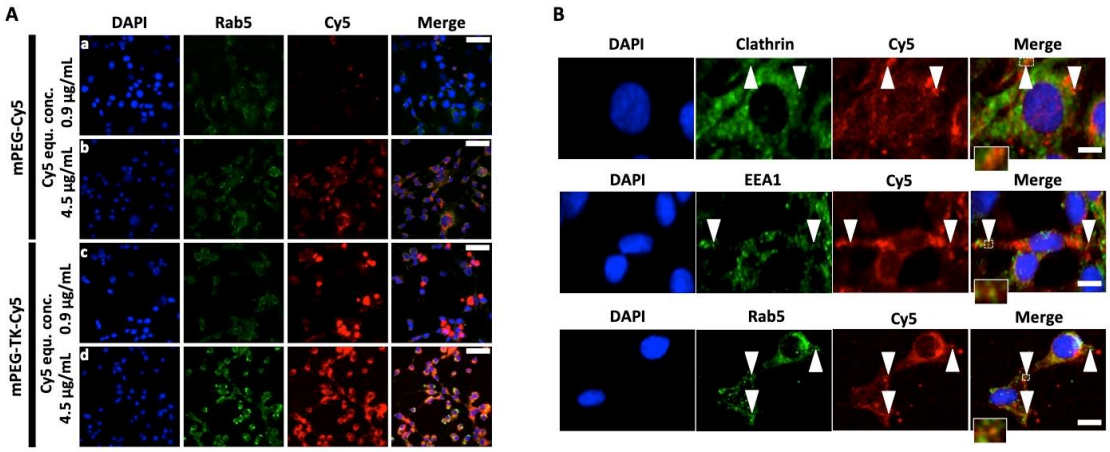

Figure 12: Confocal images of representative C6 cells incubated with either mPEG-Cy5 or mPEG-TK-Cy5. A. C6 cells incubated with either mPEG-Cy5 or mPEG-TK-Cy5 at equivalent Cy5 concentrations of 0.9 and 4.5 µg/mL, respectively for 72 h. **a)** mPEG-Cy5 incubated at an equivalent Cy5 concentration of 0.9 µg/mL. **b)** mPEG-Cy5 incubated at an equivalent Cy5 concentration of 4.5 µg/mL. **c)** mPEG-TK-Cy5 incubated at an equivalent Cy5 concentration of 0.9 µg/mL. **d)** mPEG-TK-Cy5 at an equivalent Cy5 concentration of 4.5 µg/mL. The vertical panels show the different channels (dyes) of every confocal image. With channels as following: 405 nm (DAPI), 488 nm (Rab5), and 633 nm (Cy5). Merge results from the superposition of all the channels. Scale bar: 50 µm. **B.** C6 cells incubated with mPEG-Cy5 for 24 h. The vertical panels show the different channels with 405 nm (DAPI), 488 nm (Clathrin, EEA1, or Rab5), and 633 nm (Cy5) as well as all channels merged. Arrows indicate co-localizing signals of Clathrin, EEA1, or Rab5 with Cy5. Scale bar: 10 µm (Clathrin), 15 µm (EEA1 and Rab5).

On the other hand, in the case of mPEG-TK-Cy5 incubated cells (Figure 12A, c and d), Cy5 was released from the conjugates as almost all the fluorescence signal is no longer cluster-distributed. Thus, this confirms that Cy5 from mPEG-TK-Cy5 conjugates was first released and subsequently diffused into the cytoplasm. The differences on Cy5 fluorescence localization inside cells were clearly visible at the higher Cy5 equivalent concentration (4.5 µg/mL) (Figure 12A, b and d). While Cy5 from mPEG-Cy5 was clustered inside endocytic vesicles, the Cy5 signal from mPEG-TK-Cy5 was mainly dispersed through the cytoplasm. These results further confirm that Cy5, triggered by ROS in glioblastoma cells, was detached from mPEG-TK-Cy5 with subsequent diffusion into the cytoplasm. Endocytosed mPEG-Cy5 shows very limited co-localization with clathrin, the early endosome marker EEA1, and the endosome associated protein Rab5 (Figure 12B) hinting at clathrin-dependent endocytosis as one way of cellular uptake. However, other mechanisms of uptake such as pinocytosis seem to have a major contribution to the internalization of mPEG-Cy5 and mPEG-TK-Cy5.

In mPEG-Cy5 incubated cells, Cy5 was not detached through ROS. The line profile analysis that was performed for the cytoplasm of selected cells on each confocal image shows that Cy5 fluorescence levels of mPEG-TK-Cy5 incubated cells do not vary along the cytoplasm at any of the Cy5 equivalent concentrations (Figure 13C and D). On the contrary, the line profile analysis of mPEG-Cy5 incubated cells reveals red fluorescence peaks alternated by valleys with background red fluorescence at both Cy5 equivalent concentrations (Figure 13A and B). The peaks can be well correlated to mPEG-Cy5 inside vesicles while the valley regions are associated with cytoplasm without Cy5, being in accordance with the cluster endo/lysosome distribution of red fluorescence observed inside these cells.

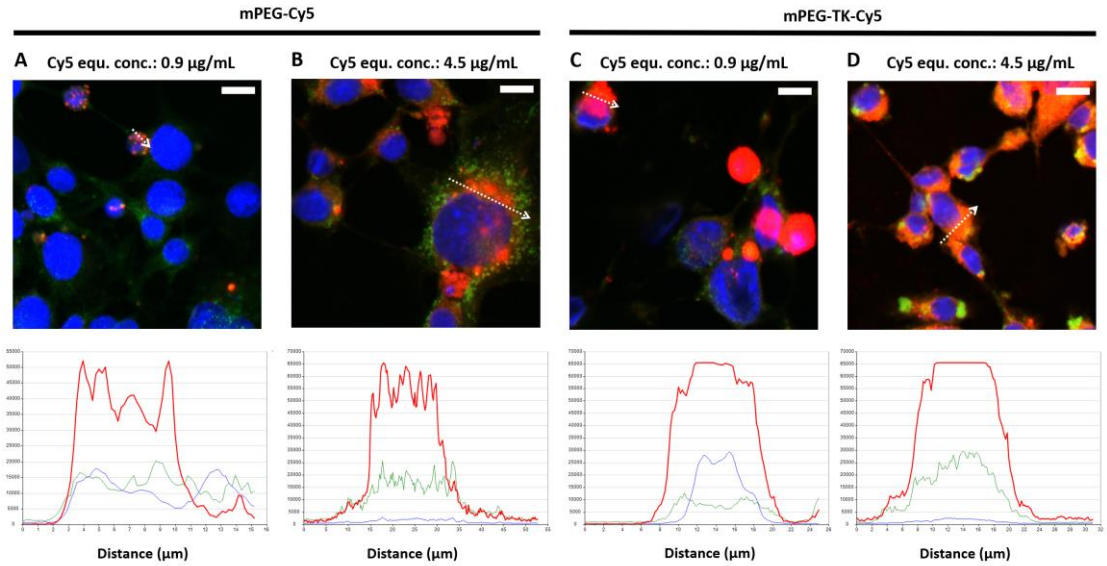

Figure 13: Line profile of selected cell cytoplasm on C6 glioblastoma cells from confocal images. Upper panel: confocal images with regions depicting the selected cell of each of the evaluated conditions. Down panel: Line profile fluorescence plots originated from the selected cells. **A-B:** mPEG-Cy5 at equivalent Cy5 concentrations of 0.9 and 4.5 µg/mL. **C-D:** mPEG-TK-Cy5 at equivalent Cy5 concentrations of 0.9 and 4.5 µg/mL. Scale bar: 10 µm

4. Discussion

In this study, we were able to synthesize and completely characterize ROS-responsive mPEG-TK-COOH. To validate the usefulness of this polymer as a polymer platform to obtain ROS-responsive polymer conjugates for cancer treatment, we conjugated this

polymer to the NIR functionalized fluorophore, Cy5-NH_2. The obtained fluorescent conjugate, mPEG-TK-Cy5, was then employed to conduct ROS-responsive studies in ROS- simulated conditions as well as *in vitro,* on either astrocyte or glioblastoma cell lines, and neuroblastoma cells. We confirmed that the fluorescent dye was released from mPEG-TK-Cy5 polymer conjugates in a time-dependent manner, while in the case of non-ROS-responsive control mPEG-Cy5, no release and therefore no cleavage of Cy5 was achieved. Moreover, we were also able to show another role of TK above the "smart" cleavage in the presence of ROS, which is a protection against ROS, clearly evidenced by the ability of TK in decreasing fluorescence quenching of Cy5 induced by ROS. Other ROS-responsive moieties have been shown to act as ROS scavengers in the literature, being used as antioxidants alone or in combination with antioxidant drugs [85,187]. Poole et al., for instance, incubated H_2O_2 exposed 3T3 fibroblasts with Curcumin (Cur) loaded Poly (propylene sulfide) (PPS) microparticles. They observed that blank PPS and Cur-PPS were both protective against H_2O_2- induced cytotoxicity to a similar extent. This demonstrated that blank microparticles exhibited scavenger capacity and therefore suggested that PPS and curcumin might be acting synergistically in preventing ROS-induced cell death [59]. Nevertheless, to our knowledge, this is the first work that shows a protective role against quenching using a fluorescent dye which is attached directly to a TK moiety. We hypothesize that in the case of a drug that is similarly attached to a polymer utilizing TK, the drug would be protected from ROS, preserving its stability.

In vitro results obtained from glioblastoma, neuroblastoma and astrocytes cells were also in line with the results obtained in simulated ROS conditions. mPEG-TK-Cy5 was selectively released in C6 and SH SY5Y cells, which produce high levels of ROS, in contrast to the results obtained by testing mPEG-TK-Cy5 on a "healthy" astrocyte cell line (DI TNC1 cells) featured by lower ROS levels. Liu et al., who developed an ROS-responsive amphiphilic dendrimer for the specific delivery of siRNA in cancer cells, also comparatively measured the ROS levels (through CellROX® orange reagent) in tumor and non-tumor cell lines, confirming higher ROS levels in tumor cells (MCF-7 and PC-3) in comparison to non-tumor cells (HEK and CHO). In addition, the gene silencing of ROS-responsive siRNA amphiphilic dendrimer nanocomplex was considerably observed only in the High-ROS cells, MCF-7 and PC-3 [127].

On the other hand, apart from the selective release of Cy5, we found that the CellROX signal was reduced on mPEG-TK-Cy5 treated SH SY5Y cells, confirming the ROS-

scavenging property of TK moiety as in the case of other ROS-responsive moieties [59,85,187].

Further studies performed with mPEG-TK-Cy5 on C6 cells showed that Cy5 was released from the conjugate, while on the contrary, mPEG-Cy5 incubated cells did not show to be able of releasing Cy5. As mentioned before, Cy5 fluorescence in the case of mPEG-Cy5 incubated cells came from endocytic vesicles while in the case of mPEG-TK-Cy5 incubated cells, this fluorescence came mainly from the cytoplasm. In addition, Cy5 fluorescence intensity of mPEG-Cy5 incubated on C6 cells was found to be lower in comparison to mPEG-TK-Cy5 incubated cells at any of the equivalent Cy5 concentrations assayed. As the structure of both polymer conjugates is almost the same, except for the presence or absence of the TK moiety, these differences in Cy5 fluorescence cannot be attributed to a difference in cell uptake. However, the difference might be attributed to self-quenching of Cy5 molecules from mPEG-Cy5 inside endocytosed vesicles. This phenomenon of self-quenching has been recently described to occur in fluorophores which are attached to molecules when they are densely packed into subcellular compartments [188]. Wang et al., who develop ditelluride- containing poly(ether-urethane) NPs for the encapsulation of DOX, reported a similar result. They observed that DOX was quenched inside the endocytosed NPs and most importantly, they correlated the DOX detectable fluorescence in cells to the quantity of DOX released from the NPs [87].

5. Conclusion

To confirm the ability of drugs to be released upon a ROS stimulus, polymeric conjugates were successfully synthesized and characterized based on the use of TK-technology. By employing the fluorescent dye Cy5-NH_2, we validated the ROS responsive release of Cy5 from an mPEG-TK-Cy5 conjugate in ROS-simulated conditions, also describing a protective role of TK, which acts as a “suicide” molecule in the case of ROS undesired actions (i.e., quenching of fluorescence). Motivated by the possible use of this ROS responsive polymer for application in cancer therapy, we assayed mPEG-TK-Cy5 using glioblastoma and neuroblastoma cells and demonstrated that Cy5 can be released upon ROS physiological concentrations in cancer cells. In addition, mPEG-TK-Cy5 in

astrocyte cells, as control, did not show to release Cy5. This confirms the selectivity of the Cy5 release in a "pathological" condition (tumor cells) in contrast to a "healthy" condition (astrocyte cells). We conclude that, due to their ability to selectively deliver drugs upon ROS stimulus while maintaining drug stability, the application of TK-technology in the design of conjugates constitutes a promising approach for future therapeutics against cancer. Furthermore, taking into consideration that high ROS levels are present in other pathologies than cancer as well, e.g., immunological, cardiovascular and neurodegenerative diseases, the TK-technology can also be applied in the design of conjugates against these diseases.

3.3. Annex 1: Supplementary figures.

A

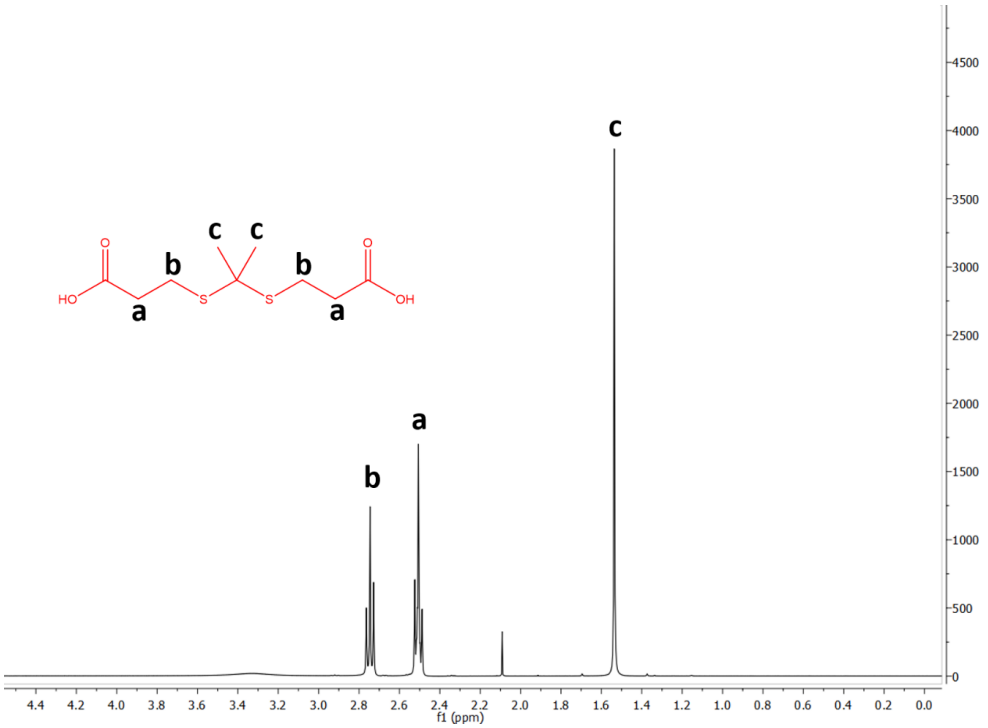

B

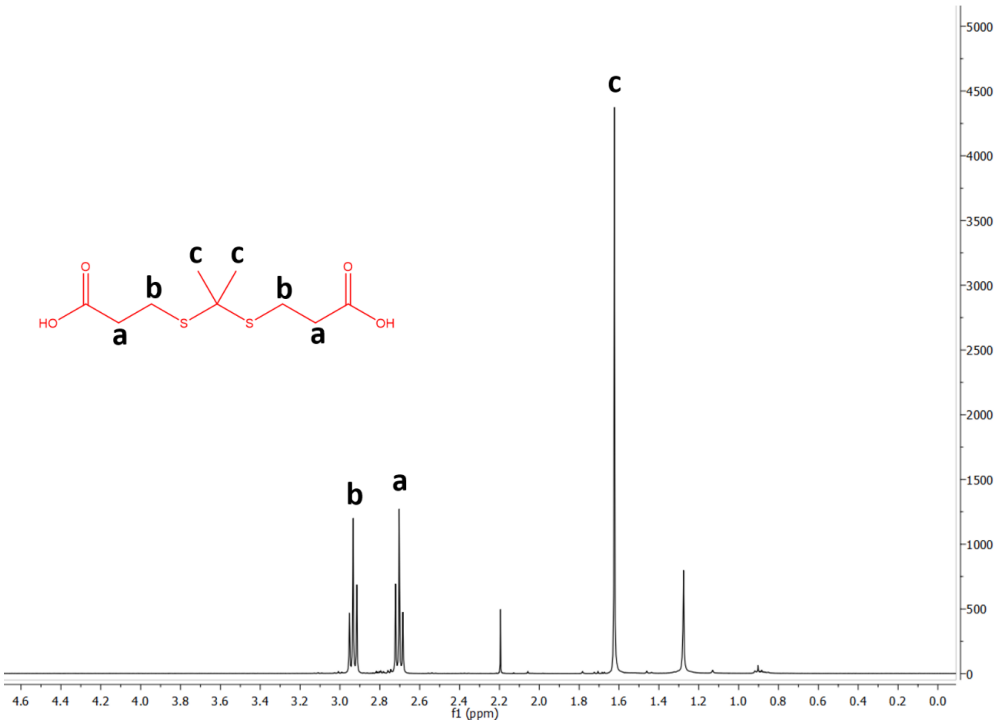

C

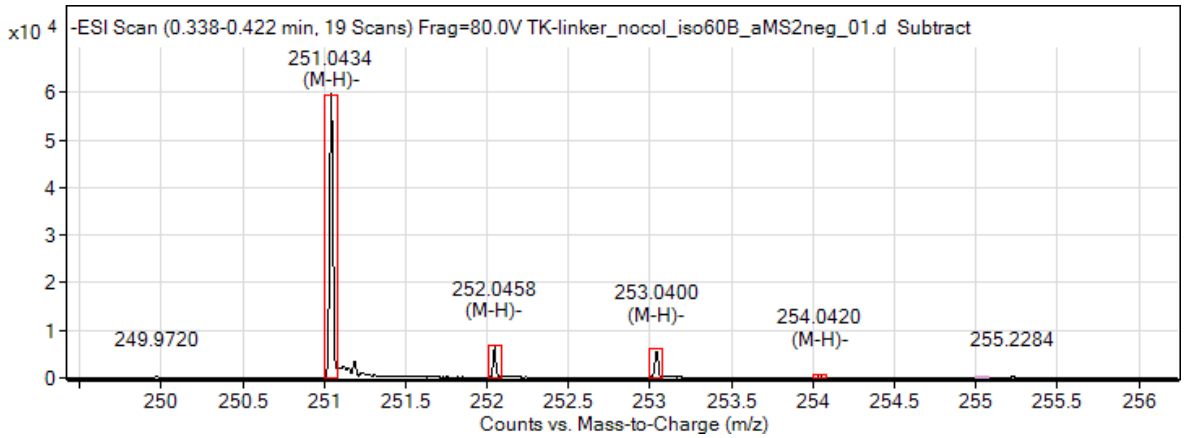

Figure S1. Characterization of TK-C.L. by ^{1}H NMR, 400 MHz. and ESI-MS. A. ^{1}H NMR spectrum of TK-C.L. in d_6-DMSO. **B.** ^{1}H NMR spectrum of TK-C.L. in $CDCl_3$. **C.** ESI (-) MS spectrum depicting [M-H]- ion peaks of TK-C.L. sample dissolved in ACN.

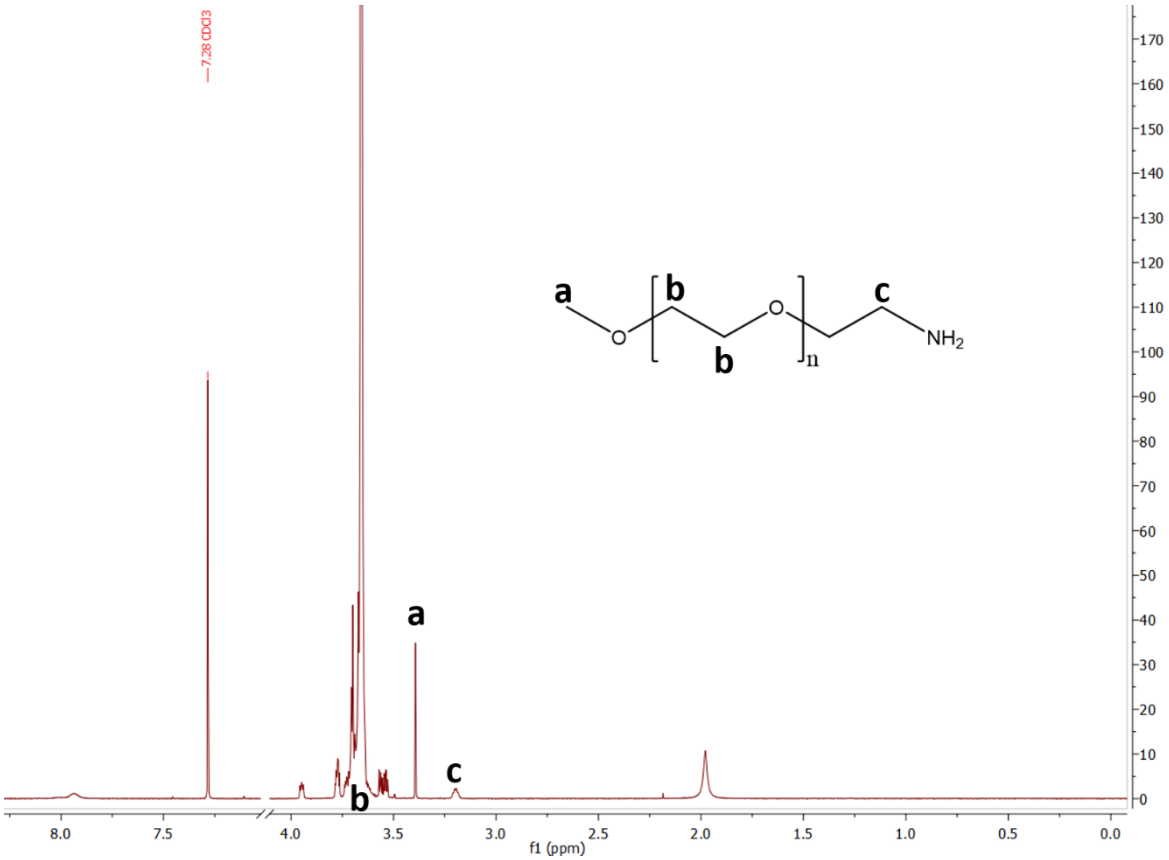

Figure S2. ^{1}H NMR spectrum of mPEG-TK-NH$_2$.

A

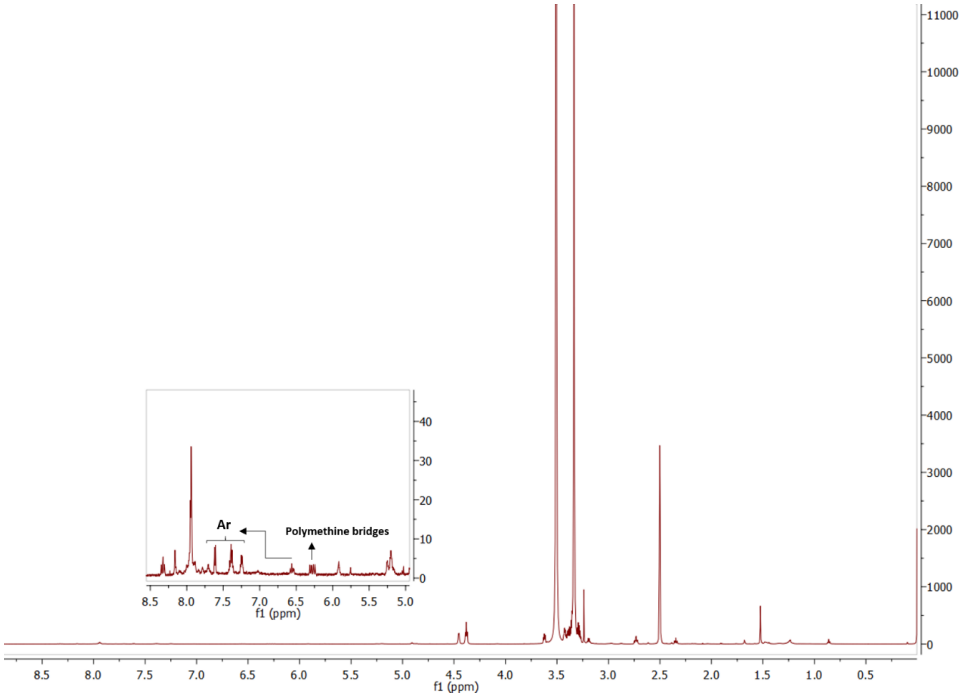

B

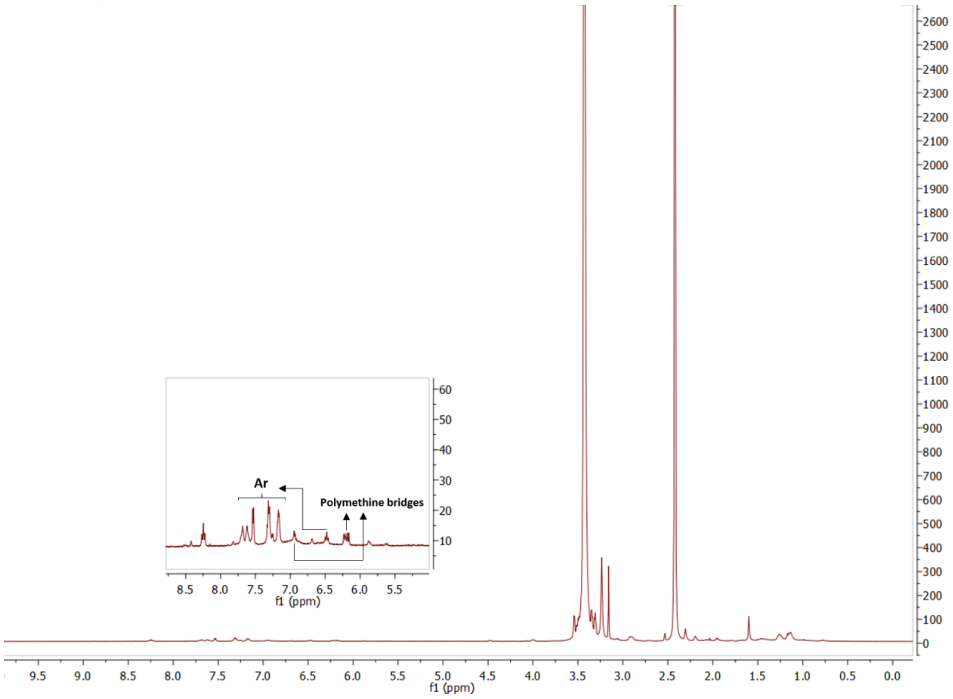

Figure S3. ^{1}H NMR spectra of A. mPEG-TK-Cy5 and B. mPEG-Cy5 in d_6-DMSO. The region of the spectra with the most relevant chemical shift of Cy5 portion is magnified and the protons from aromatic groups and polymethine bridges indicated.

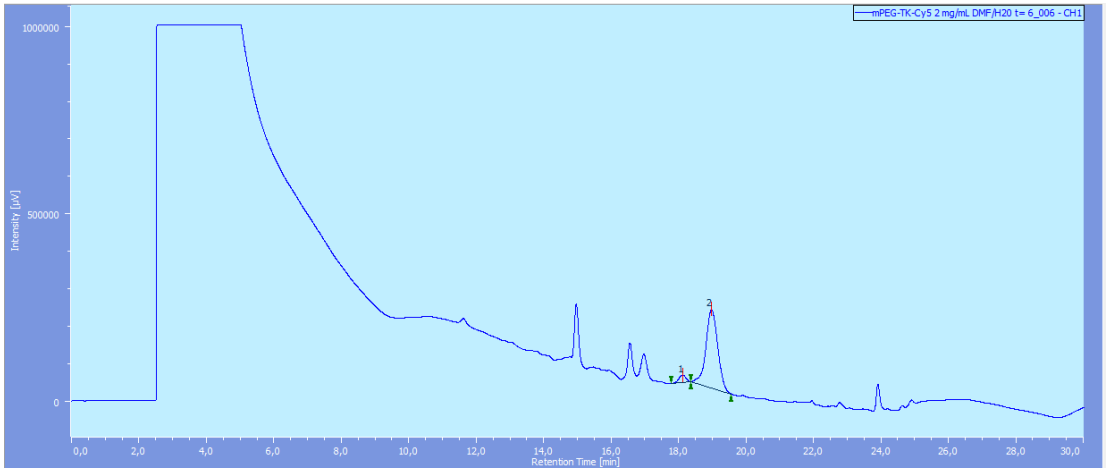

Figure S4. RP-HPLC chromatograms of mPEG-TK-Cy5 incubated in non-ROS-simulated conditions (Control) for 6 h. Peak 1: Cy5 released. Peak 2: mPEG-TK-Cy5. The depicted chromatogram was obtained using the UV-Vis detector.

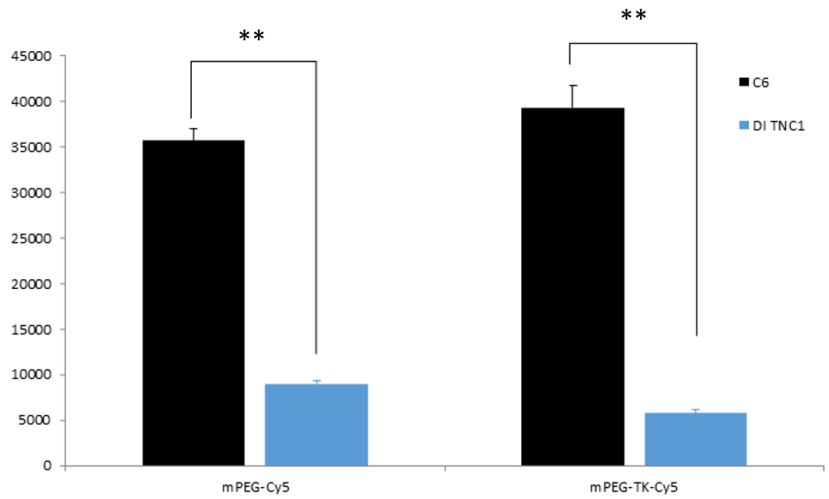

Figure S5. Quantification of CellROX fluorescence intensity of C6 and DI TNC1 incubated with either mPEG-Cy5 or mPEG-TK-Cy5 for 24 h. Fluorescence intensity is shown in Absolute Fluorescent Units (AFU). The significant difference on CellROX fluorescence intensity, is indicated by asterisks (**$p \leq 0.01$) in the graph and it was determined by one-way ANOVA with Bonferroni post hoc test.

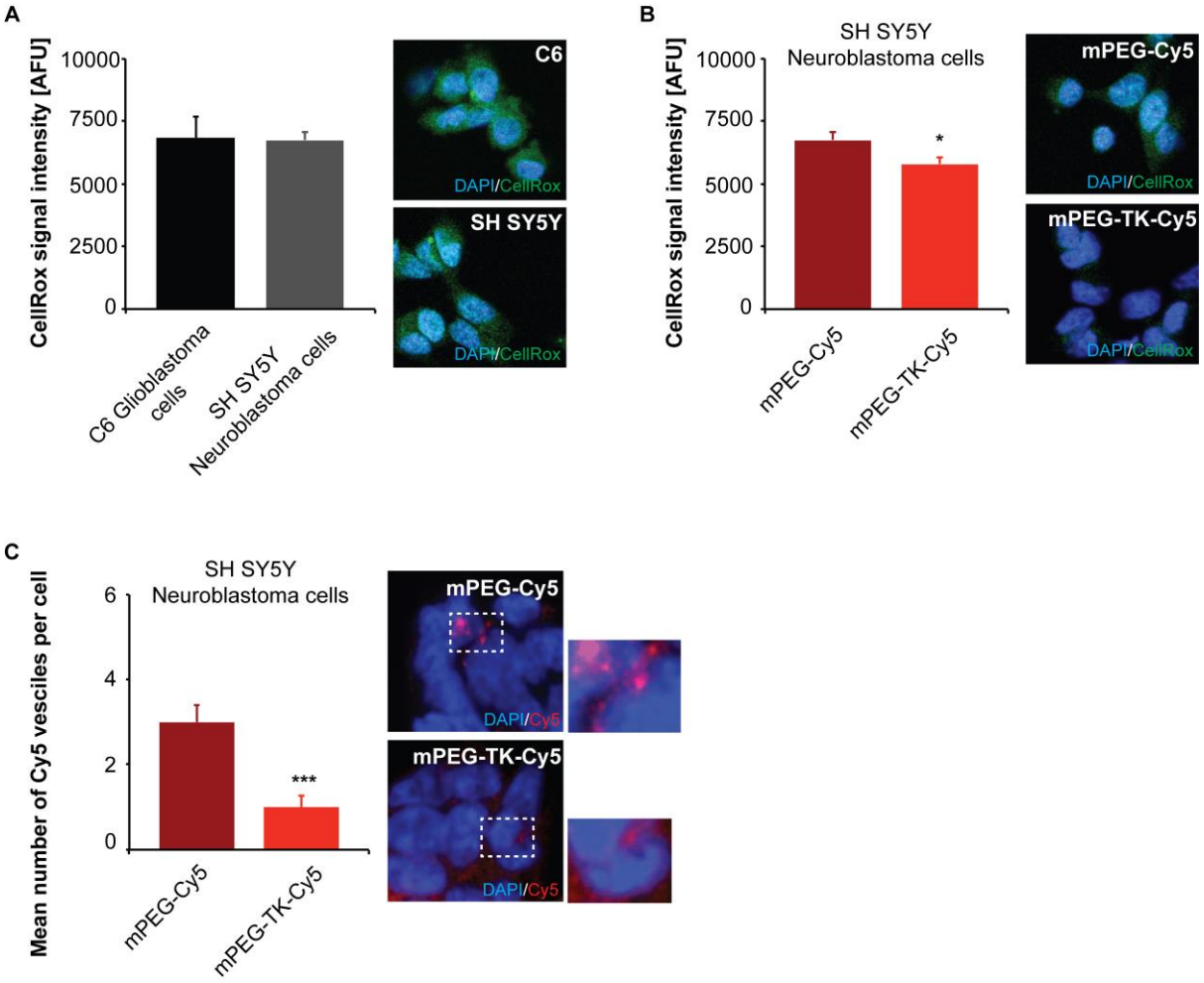

Figure S6. Confocal images of representative C6 and SH SY5Y cells. A. C6 and SH SY5Y cells were incubated with CellROX reagent. Fluorescence intensity is shown in Absolute Fluorescent Units (AFU) for n = 50 cells from at least 5 different optic fields of view per cell line. Exemplary images (right panel) show cell with CellROX and DAPI staining. **B.** SH SY5Y cells were incubated with either mPEG-Cy5 or mPEG-TK-Cy5 at equivalent Cy5 concentrations of 0.9 and 4.5 µg/mL, respectively. CellROX reagent fluorescence intensity is shown in AFU for n = 50 cells from at least 5 different optic fields of view per cell line. Exemplary images (right panel) show cell with CellROX and DAPI staining. **C.** SH SY5Y cells were incubated with either mPEG-Cy5 or mPEG-TK-Cy5 at equivalent Cy5 concentrations of 0.9 and 4.5 µg/mL, respectively. The mean number of Cy5 positive clusters per cell is shown for n = 50 cells from at least 5 different optic fields of view per cell line. Exemplary images (right panel) show cell with Cy5 and DAPI signals. **A-C.** Results are shown as mean ± SEM.

Chapter 4:

TK-based ROS-responsive cytotoxic prodrug for GBM treatment

4.1. Background and chapter aim

Among all cancer types, GBM is one of the most lethal and difficult to treat, being the high mortality rate of this cancer related to its resistance to therapy and tumor recurrence. Since the standard of care of GBM patients consisting of concomitant chemo- and radiotherapy cannot cure this disease, with a survival prolongation of a few months, the outcome of more effective therapeutics is required.

The current tendency in cancer therapy is to create more personalized nanomedicines that consider the biology of tumors, such as stimuli responsive DDS. Considering that GBM cell growth is enhanced by the presence of ROS, the use of ROS-responsive DDS along with cytotoxic drugs could improve the effectivity of chemotherapy in GBM.

Therefore, the aim of this chapter is to develop a TK-based prodrug for GBM therapy by means of the covalent link of the alkylating chemotherapeutic drug Melphalan (MPH) to mPEG by means of TK linkage, and evaluate its *in vitro* cytotoxicity on rat and human GBM (C6, U87MG and U251MG) cells and normal rat astrocyte (DI TNC1) cells, as well as explore the combinatorial effect of prodrug treatment and IR.

4.2. Results

"Synthesis, characterization, and *in vitro* studies of a ROS-responsive mPEG-TK-MPH prodrug for Glioblastoma", to be submitted.

Abstract:

Glioblastoma (GBM) is the most frequent and aggressive primary tumor of the brain, and accounts for a life expectancy in patients diagnosed with this disease of only 15 months. Therefore, more effective therapies against this malignancy are urgently needed. Since several diseases, including cancer, are featured by high levels of ROS, being these ROS a possible GBM hallmark to target or benefit from; the attachment of drugs to ROS-responsive molecules can be exploited aiming for a selective drug release. In this work, we designed a new ROS-responsive prodrug with Melphalan (MPH), obtained by linking this drug to methoxy polyethylene glycol (mPEG) through a ROS-cleavable group Thioketal (TK). These ROS-responsive prodrug molecules can undergo self-assembly in

water into micelles. The *in vitro* cytotoxicity of this ROS-responsive prodrug was assayed on different GBM cell lines and "healthy" astrocyte cells and compared with its non-ROS responsive counterpart, we could observe that the cytotoxicity of ROS-responsive prodrug on GBM cells expressing high levels of ROS was higher than the non-ROS-responsive prodrug. Furthermore, neither of the prodrugs were cytotoxic on astrocytes, thus demonstrating a safety profile. On the other hand, the combination treatment with this ROS-responsive prodrug and X-ray irradiation on human GBM cells resulted in an increase in cytotoxicity. Hence, these results represent a starting point for a rationale design of innovative and tailored ROS-responsive prodrugs.

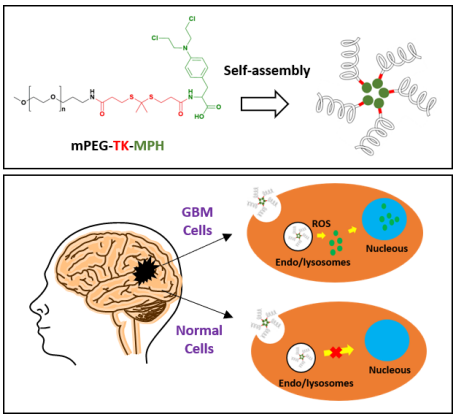

Keywords: ROS, TK-technology, ROS-responsive prodrug, Melphalan, GBM

1. Introduction

Cancer represents one of the most lethal diseases worldwide [75]. In high-income countries, the number of cancer deaths currently doubled the deaths caused by cardiovascular disease (CVD) [192]. Among all deadly types of cancer, brain cancer is one of the most difficult to treat and cure [193]. In particular glioblastoma (GBM), which is a malignant grade IV astrocytic tumor [189], is the most frequent and aggressive primary brain tumor with the poorest prognosis [193–197] and median survival of only 15 months [190]. Due to the ability of GBM cells to migrate to other brain regions, GBM recurrence, which takes place within 6-12 months after diagnosis [194,195,193] as a secondary tumor, is the main reason that accounts for this lethality [198].

The standard GBM therapy consists of tumor surgery followed by a concomitant radio- and chemotherapy with Temozolomide (TMZ) [189,190], an anticancer drug that is one of the few chemotherapeutic agents with an acceptable blood- brain barrier (BBB)

penetration (20% of the injected dose) . Nevertheless, this standard therapy only increases the survival for 2.5 months [189]. This is probably due to the aggressiveness of recurrent tumors as well as to the antitumoral drug resistance frequently observed [191]. On the other hand, as chemotherapeutic agents affect dividing cells, their selectivity is low [74], with frequent oral administrations [15] leading to decreases in patients' compliance and increase in drug resistance [6]. Hence, the design of new therapies against GBM that prolongs survival and achieves the cure are strongly needed.

Drug Delivery Systems (DDS) that improve the residence time in circulation, solubility and targetability of chemotherapeutic drugs have been applied to some marketed products. Abraxane®, Doxil®, Onivyde®, and Zoladex® are examples of DDS that are already approved for their clinical use in cancer treatment [6,199,200].

Nowadays, cancer therapy strategies are aiming to be more personalized due to the presence of tumor heterogeneity among cancer patients [201]. Thus, it is necessary to develop more precise nanomedicines that take into consideration the tumor biology in order to create more suitable DDS for the treatment of cancer [199]. In this regard, a DDS with the possibility to sense the tumor environment for a more selective drug release [202] holds great promise when it comes to advance the development of "Smart" DDS.

In order to produce disease selective DDS, with the possibility to release drugs in a given pathological condition, "Smart" DDS that respond to a specific stimulus such as pH, enzymes, glucose, GSH, and ROS, are currently being designed for their application against several diseases, including cancer [5,6], and demonstrated to improve treatment efficacy [125].

Oxidative stress, which is produced by a disequilibrium between ROS generation and detoxification [176], is a common feature of cancer cells, and it is promoted by high demanding metabolism, oncogenic stimulation, and mitochondrial dysfunction [203]. Considering that the continuous production of ROS by GBM cells is necessary for these cells to grow [182,144], the design of DDS that trigger the release of drugs upon ROS stimulus, known as ROS-responsive DDS, could improve the effectivity of chemotherapeutic agents in GBM. Currently, there is a growing number of research articles in which ROS-responsive chemical groups are used to prepare polymer prodrugs in cancer therapy [7,73,204]. The most used ROS- responsive chemical groups developed until recently are the following: polypropylene sulfide, selenium and tellurium, polyoxalate, poly(proline), phenyl boronic ester and thioketal (TK). Among them, phenyl boronic ester, and more recently TK, have been used as linkers for the synthesis of not

only ROS-responsive polymers to produce ROS-responsive reservoirs, but also for the design of prodrugs for cancer application.

Apart from Temozolomide (TMZ), carmustine, and lomustine are the most widely used drugs for GBM treatment [205]. Nevertheless, lomustin shows a brain/plasma ratio of 20% in rats, which is lower compared to TMZ, with 22–41%. Regarding carmustine, its passage through the BBB is lower with higher CNS toxicity [206]. Bevacizumab is used in patients that do not respond to TMZ, but its poor BBB crossing leads to to high concentrations being administered and, consequently, to adverse effects [207].

Amongst anticancer drugs, also Melphalan (MPH), an alkylating molecule, currently used for the treatment of myeloma, ovarian cancer, breast cancer, neuroblastoma, regionally advanced malignant melanoma, and localized soft tissue carcinoma [208,209], has been incorporated in some GBM treatment regimes [210,211] and like TMZ, crosses the BBB and goes inside cells [209]. Nevertheless, its poor water solubility (0.1 μg/mL, 25°C) [208] and non- tumor selectivity represents an important drawback of its use.

To overcome chemical-physical limitations (as poor solubility) and to increase locoregional and site-specific activity, several strategies have been exploited. To improve the solubility of chemotherapeutic agents, the conjugation of polyethylene glycol (PEG) to chemotherapeutic drugs, known as PEGylation, has a long history, aiming to increase circulation time and safety [179], with already established strategies present in clinical setting to extend the residence time in blood circulation with proven safety in humans [212]. An advantage of administrating PEGylated cytotoxic drugs instead of the free drugs is the possibility of by-passing drug efflux, mediated by P-glycoproteins (P-gps), which are one of main reasons for the limited efficacy of chemotherapeutic drugs in GBM, being responsible for efflux events of cytotoxic drugs from the cancer cells [213] and even at the BBB level. This was confirmed for several anticancer drugs (e.g., TMZ [49]). Moreover, PEGylation can also promote the circulation time of drugs by 5-100-fold [214]. This is particularly needed in the case of MPH, with a circulation half-life of only 75 minutes [215]. However, this favorable feature cannot be assessed evidently with *in vitro* experiments but could be relevant in an *in vivo* setting.

Creating a prodrug which is activated as a consequence of a pathological stimulus to improve locoregional and site-specific delivery could be an intelligent approach that has been widely reviewed [216–218] and also investigated for GBM treatment [217]. The insertion of a linker between PEG and a drug that responds to a pathologic stimulus may improve the selectivity as well as the effectivity of the drug [17]. TK linkers are

biocompatible linkers which are degraded to thiol-containing groups upon exposure to the most relevant ROS (hydroxyl radical, H_2O_2 and superoxide) [29,30]. They have been recently used in the design of ROS-responsive DDS for the delivery of drugs, siRNA, and DNA in cancer and inflammatory diseases. To our knowledge, TK- based ROS-responsive DDS for the treatment of GBM have not been previously developed [193,219]. Moreover, few examples on the use of ROS- responsive delivery systems for GBM treatment are reported in the literature, such as, phenyl boronic ester groups (as ROS-responsive unit) and angiopep-2 peptide (BBB- targeting ligand), for the delivery of siRNA to silence PLK1 and VEGFR2 [219].

Previously, proof-of-concept studies with ROS- responsive mPEG-TK conjugate with a fluorescent model drug (Cy5), demonstrated a stimulus-responsive release of this dye only in brain cancer cells (C6 rat GBM cells) and not in healthy brain cells (rat astrocytes) [130]. Based on these results, in this study, we propose to exploit mPEG-TK-COOH polymer, to produce a ROS-responsive antitumor prodrug with Melphalan (MPH), namely mPEG-TK-MPH, for the selective MPH release in GBM cells.

To that end, a physical-chemical characterization was performed as well as *in vitro* cytotoxicity studies, also exploring the potential of synergistic effects between the ROS-responsive mPEG-TK-MPH prodrug and X-ray irradiation on rat and human GBM cells in combinatory treatment regimens (chemotherapy and radiotherapy) which could induce the production of ROS [220].

2. Materials and Methods

2.1. Materials

Methoxy-polyethylene glycol amine (mPEG-NH2, Mw 5.000 Da) and mPEG propionic acid (Mw 5.000 Da) were purchased from JenKem Technology and Sigma-Aldrich, respectively. N-hydroxy succinimide (NHS) and N-(3-dimethylaminopropyl) -N-ethyl carbodiimide hydrochloride (EDC. HCl) were obtained from Sigma-Aldrich and used directly. All the solvents used, 3-Mercaptopropionic acid (3-MPA), dichloromethane (DCM), dimethylformamide (DMF), acetone, hydrogen peroxide (H_2O_2), hexane and methanol were of analytical grade and used without further purification. Melphalan was purchased from Fisher Scientific. Ultrapure water, which was used for all the experiments, was provided by a Milli-Q water system (Millipore, Bedford, MA, USA).

F12-K and trypsin (TrypLE Select Enzyme (1X)) were purchased from Gibco. Fetal bovine serum (FBS) and penicillin-streptomycin were purchased from Sigma-Aldrich. DPBS and DMEM High Glucose were purchased from Lonza (Verviers, Belgium) and Sigma-Aldrich. An oxidative fluorescent dye, Dihydroethidium (DHE) was purchased from Sigma-Aldrich.

2.2. Synthesis

2.2.1. Synthesis of Thioketal containing linker (TK- C.L.) and ROS-responsive mPEG-TK-COOH polymer

The synthesis of TK- C.L. and mPEG-TK-COOH polymer was performed according to our previous article, without modifications [130]. For the synthesis of TK.C.L., a mixture of 3-MPA (49.1 mmol) and anhydrous acetone (98.2 mmol) was stirred for 4 h in HCl (g) atmosphere. The reaction was stopped by placing the mixture on an ice salt bath, and the product was obtained after several washes with hexane and cold water. The product was then characterized by ^{1}H NMR and ESI-MS (Figure S7A). For the synthesis of mPEG-TK-COOH polymer, the following compounds were dissolved in DCM and stirred for 48 h at ambient temperature: mPEG-NH_2 5.000 Da (0.1 mmol), TK-C.L. (1 mmol), EDC. HCl (1.2 mmol) and NHS (1.2 mmol). The product was precipitated with diethyl ether, and after solvent elimination, it was dissolved in minimal DMF volume and purified by dialysis (MWCO: 3.500 Da) against MilliQ water for 72 h. After dialysis, the product inside the dialysis bag was freeze-dried, and the white powder obtained, characterized by ^{1}H NMR (Figure S7B) and MALDI-TOF.

2.2.2. Synthesis of ROS- responsive mPEG-TK-MPH and non-ROS responsive mPEG-MPH (control) prodrugs

Terminal carboxylic acid group on mPEG-TK-COOH or mPEG propionic acid (used as control) polymers (6 μmol), were activated with EDC.HCl (60 μmol) and NHS (60 μmol) for 1.5 h in DMF/DMSO (1:1 v/v) solvent mix. Right after the activation, the reaction started with the addition of MPH (30 μmol) to the mixture and left to stirring up to 48 h at 35°C (Scheme 4A-B). The reaction was stopped, and the mix dialyzed (MWCO: 3.500 Da) against methanol for 48 h and finally against Milli Q water for an additional 24- h

period. At the end of the purification process, the prodrugs were freeze-dried and kept in a desiccator until use. The prodrugs were characterized by ^{1}H NMR and MALDI-TOF.

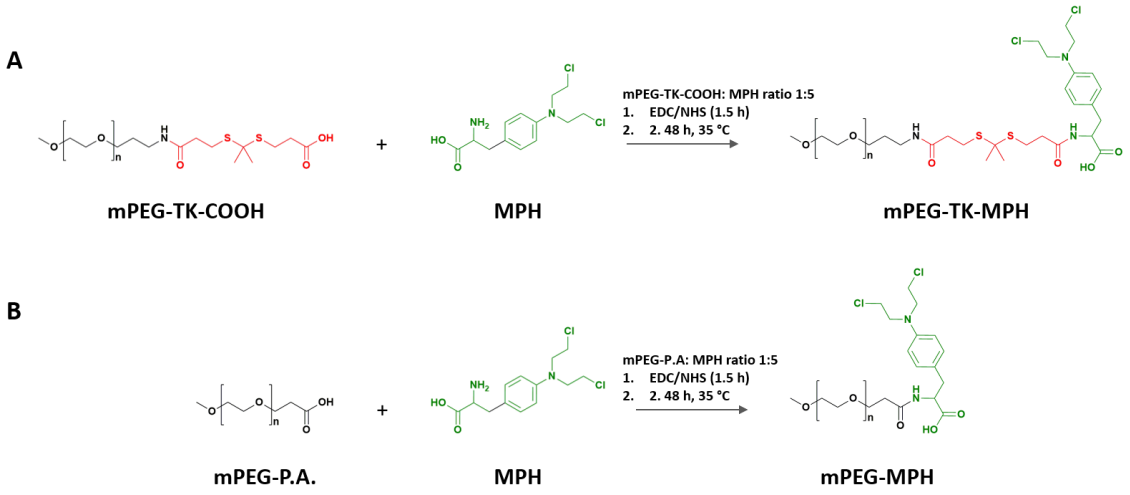

Scheme 4. Synthesis of prodrug with MPH. **A.** mPEG-TK-MPH. **B.** mPEG-MPH prodrug synthesis.

2.2.3. Prodrug self-assembly in water

Either mPEG-TK-MPH or mPEG-MPH prodrugs suspensions in MilliQ water were prepared (0,1 mg/mL- 10 mg/mL concentration range). Briefly, 10 mg of either of the prodrugs or their respective precursor polymers (mPEG-TK-COOH and mPEG-P.A., respectively), was suspended in 1 mL of MilliQ water. Then, different prodrug or polymer suspension concentrations were prepared by serial dilutions in MilliQ water for further study self-assembly ability using photon correlation spectroscopy (PCS) and AFM measurements.

2.3. Characterization

2.3.1. ^{1}H NMR, ESI-MS, and MALDI-TOF

^{1}H NMR spectra of TK-C.L. and mPEG-TK-COOH polymer were acquired on Avance400- Bruker spectrometer in CDCl3. In the case of mPEG-TK-MPH and mPEG-MPH prodrugs, the ^{1}H NMR spectra were also acquired on Avance400- Bruker

spectrometer in CD3OD. For all ^{1}H NMR spectra, tetramethylsilane (TMS) was used as an internal standard. The identification of all proton signals in mPEG-TK-MPH and mPEG-MPH was completed after 1D and 2D (COSY) ^{1}H NMR analyses.

TK-C.L. mass spectra were acquired with Q-TOF Accurate-Mass G6520A - Agilent Technologies, from which an ESI-MS spectrum in negative mode was obtained. Mass spectra of mPEG-TK-COOH, mPEG-TK-MPH, and mPEG-MPH were acquired with a Bruker Ultraflex TOF/TOF, MALDI-TOF/TOF mass spectrometer.

2.3.2. Size and morphology of self-assembled prodrugs

The mean particle size (Z-average) and the polydispersity index (PDI) of self-assembled prodrug micelles at different prodrug concentrations (10 – 0.01 mg/mL range) were determined through PCS using a Zetasizer Nano ZS (Malvern, UK; Laser 4 mW He–Ne, 633 nm, Laser attenuator Automatic, transmission 100–0.0003%, Detector Avalanche photodiode, Q.E. > 50% at 633 nm) at room temperature. A 10 mg/mL suspension of either of the prodrugs in Milli-Q water was prepared and directly measured. Then, serial dilutions from these prodrug suspensions were prepared and immediately measured after vortex mixing. All measurements were carried out by triplicates.

Atomic force microscopy (AFM) was used to resolve the morphology of self-assembled prodrugs. A selected sample of mPEG-TK-MPH suspended at a concentration of 0.7 mg/mL, was selected to be observed through Atomic Force Microscope (Park Instruments, Sunnyvale, CA, USA), at about 20 °C operating in air and in Non-Contact (NC) mode using a commercial silicon tip-cantilever (high resolution noncontact "GOLDEN" Silicon Canti-levers NSG-11, NT-MDT, tip diameter 5–10 nm; Zelenograd, Moscow, Russia) with stiffness about 40 Nm-1 and a resonance frequency around 150 kHz. Briefly, mPEG-TK-MPH dispersed in water at a selected concentration of 0.7 mg/mL, was deposited onto mica surface on a freshly cleaved mica disk (1 cm x 1 cm); 2 min after the deposition, the water excess was removed using blotting paper. The AFM topographical image, representing the amplitude of the vibrations of the cantilever, was obtained with a scan rate of 1 Hz and processed using a ProScan Data Acquisition software.

2.4. MPH content on mPEG-TK-MPH and mPEG-MPH prodrugs

MPH content on the prodrugs was expressed as μg of MPH per mg of prodrug and was determined by measuring the absorbance of prodrugs solutions in methanol. The measurement was performed in a spectrophotometer at ʎ= 300 nm (the maximum absorbance wavelength we obtained with MPH and MPH prodrugs). The MPH content of either of the prodrugs was obtained against a calibration curve of pure MPH in methanol (linearity was assumed in the 11.58- 74.25 μg/mL: r^2= 0.998950 range).

2.5. *In vitro* studies of mPEG-TK-MPH and mPEG-MPH on astrocytes (control) cells and GBM cells

2.5.1. Cell culture

All cell lines were from ATCC (American Type Culture Collection). C6 Rat Glioblastoma cells were cultured in F-12 k medium supplemented with 20% FBS and 1% penicillin/streptomycin. DI TNC1 Rat Astrocyte cells and human GBM cells (U87MG and U251MG cells) were cultured in DMEM High Glucose medium supplemented with 10% FBS and 1% penicillin/streptomycin. All cell lines were maintained in a humidified incubator at 37°C and 5% CO_2.

2.5.2. Determination of the levels of ROS in rat GBM and astrocytes cells

C6 and DI TNC1 cells were seeded (100.000 cells/mL) on 24 well plates containing poly-L-lysine (0.1 mg/mL; Sigma-Aldrich) coated glass coverslips and incubated at 37°C until 80% confluence was reached. Then, the cells were rinsed with 1X PBS and fixed with 4% paraformaldehyde solution (PFA) in 1X PBS. Cell nuclei were counterstained with DAPI, and coverslips subsequently mounted using Vecta Mount (Vector Laboratories, USA). The cells were observed using a confocal laser-scanning microscope (Zeiss LSM710). CellROX fluorescence of confocal images of C6 and DI TNC1 cells was quantified using ImageJ (National Institutes of Health), by measuring at least 20 cells per condition and cell line.

2.5.3. Cytotoxicity studies of ROS-responsive and non-ROS-responsive prodrugs on C6 GBM and DI TNC1 astrocytes cells

The cytotoxicity of mPEG-TK-MPH and mPEG-MPH prodrugs on C6 cells was evaluated by acquiring Cell Index vs. Time data in real-time, using the xCELLigence RTCA MP instrument (ACEA Biosciences). The experiments were carried out on 16 well E-Plates (ACEA Biosciences), which were coated with poly-l-lysine (PLL). After coating, plates were seeded with C6 or DI TNC1 cells (2 x 10^4 cells/mL) and put into xCELLigence RTCA MP instrument station, where Cell index vs. Time curves were recorded. After 24 h of cell seeding, the plates were removed from the instrument, the culture medium was renewed, and cells treated with mPEG-TK-MPH and mPEG-MPH prodrugs at an equivalent concentration of MPH of 11 μM. Cells were also treated with free MPH and mPEG-TK-COOH (control). Immediately after the addition of the compounds, the plates were put back into XCELLigence station, and the Cell index was measured every 5 minutes up to 48 h. At the end of the experiment, the data were analyzed using the RTCA Data Analysis Software 1.0. The cell index of all treated groups and control groups were normalized to 1 at the time point where the treatment started; Normalized Cell Index vs. Time curves were considered for data analysis.

2.5.4. Determination of the levels of ROS in human GBM cells

U87 MG and U251 MG cells were grown on glass slides (Ibidi, Martinsried, Germany) at a density of 5 x 104 cells/mL. After 48 h of incubation, the cells were washed with PBS and immediately incubated with DHE fluorescent dye in PBS (5 μM) for 30 minutes at 37°C. Cells were then washed with PBS and fixed with PFA (4%) for 15 minutes. The cells were washed with PBS and kept at 4 °C until analysis. The cells were observed using a confocal microscope (Zeiss LSM700), and the images obtained were analyzed by Image J. The quantification was performed by measuring the fluorescence of 10 ROI per image in triplicates. Channels used: DAPI (405 nm) and Ethidium homodimer (EthD (555 nm).

2.5.5. Cytotoxicity studies of ROS-responsive and non-ROS-responsive prodrugs on human GBM cells

U87 MG and U251 MG cells were seeded on 96 well plates at a density of 5 x 104 cells/mL and kept in an incubator at 37°C for 24 h. The medium was replaced, and cells were treated with mPEG-TK-MPH and mPEG-MPH prodrugs, at equivalent concentrations of MPH (concentration range: 10 μM-1000 μM) as well as free MPH. After 48 h of treatment, the medium was removed, washed with DPBS and then Resazurin in culture medium (44 μM) was added and incubated for 3 hours at 37°C. Finally, the fluorescence was measured on a plate reader (CLARIOstar) at λ_{exc}= 545 nm/ λ_{em}= 600 nm.

2.5.6. Influence of X-ray irradiation on ROS-responsive and non-ROS-responsive prodrugs cytotoxicity on human GBM cells

U87 MG and U251 MG were seeded in 96 well plates at a density of 5 x 104 cells/mL. After 24 h of incubation, the cells were irradiated with X-ray (Edimex Faxitron) for 2.66 min to reach a dose of 4 Gy. Immediately after being irradiated, cells were treated with free MPH (1000 μM), mPEG-TK-MPH, and mPEG-MPH prodrugs at an equivalent concentration of 1000 μM. After 24 h, a second irradiation round of 2.66 min (4 Gy dose) was applied to the cell plates. Finally, at the end of the experiment (48 h counted from the first irradiation dose),
the viability of cells was indirectly measured again by the resazurin method. The protocol described in section 2.5.5. was followed for the measurement of the resazurin fluorescence of the cells.

2.7. Statistics

All data are shown as the mean of at least three experiments ± SD. GraphPad Prism 5 was used for statistical analyses. For pairwise comparisons, unpaired t-test, one-way and two-way ANOVA with Bonferroni post-hoc test was performed.

3. Results and discussion

3.1. mPEG-TK-MPH and mPEG-MPH synthesis and characterization

Both prodrugs (mPEG-TK-MPH and control mPEG- MPH) (Scheme 4A and B) were obtained as a pale-yellow powder, with product yields over 90% (94 and 93%, respectively). The absence of free MPH, and thus the purity of both prodrugs was confirmed by RP-HPLC (data not shown). The MPH content on mPEG-TK-MPH and mPEG-MPH prodrugs was 56.3 ± 1.1 μg/mg and 63.6 ± 4.9 μg/mg, respectively.

^{1}H NMR spectra of either of the prodrugs show the presence of chemical shifts ascribed to protons appertaining to the benzenic group of MPH (6.69 and 7.09 ppm) (Figure 14A, B and Figure S8). In addition, the chemical shift ascribed to TK proton methyl groups (1.58 ppm) in the mPEG-TK-MPH spectrum can be observed. The mean molecular weight of mPEG-TK-MPH and mPEG-MPH prodrugs, obtained by MALDI TOF, were 5374.8 and 5300.7 g/mol, respectively, right-shifted in the spectra with respect to the MW of their starting polymers: mPEG-TK-COOH (5233.1 g/mol) and mPEG-P.A. (5168.5 g/mol). The characterization results confirmed the covalent conjugation of MPH to both mPEG polymers (mPEG-TK-COOH and mPEG-PA).

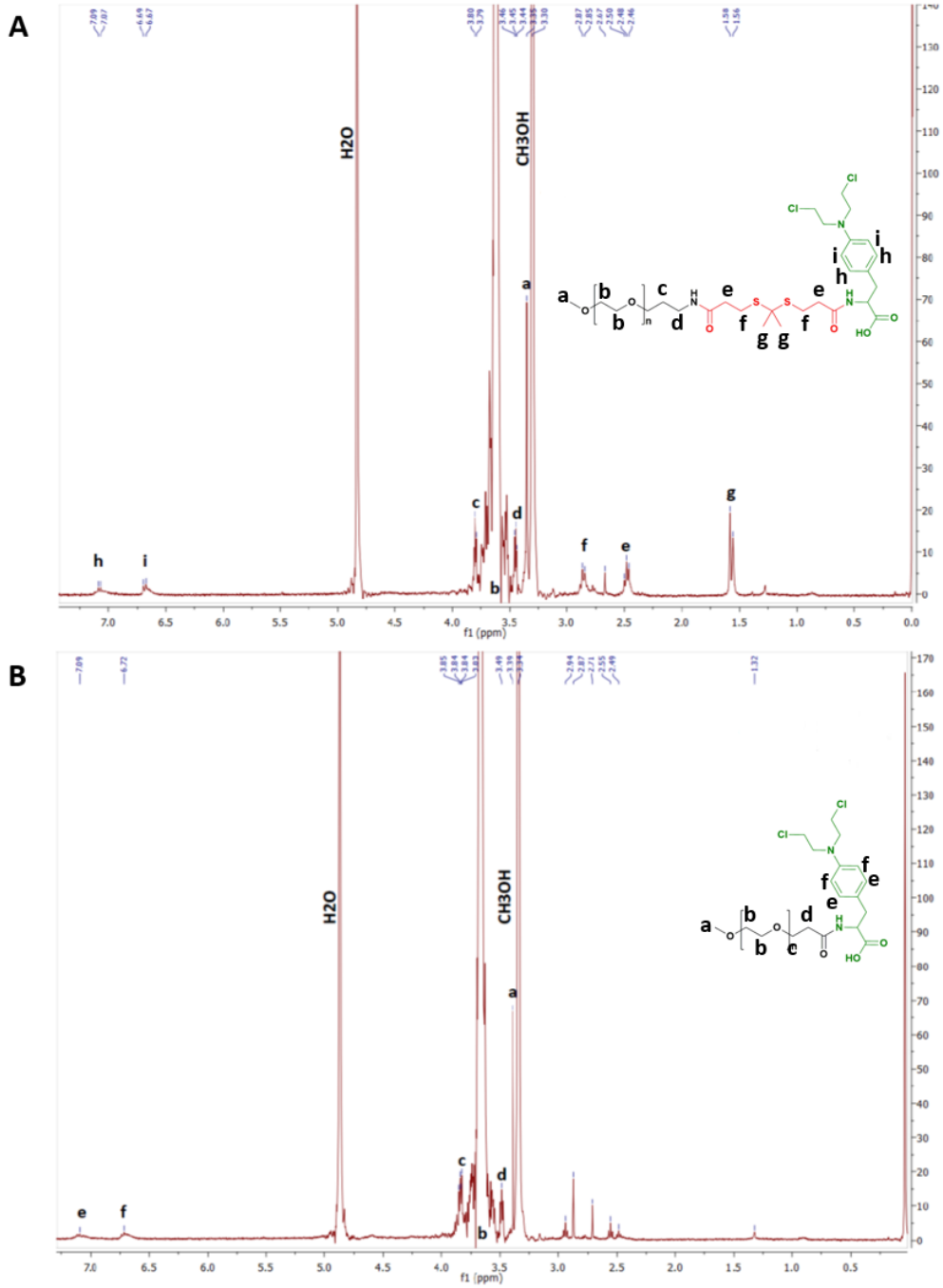

Figure 14. ^{1}H NMR spectra in CD_3CD. A. mPEG-TK-MPH and **B.** mPEG-MPH.

3.2. Size and morphology of self-assembled mPEG-TK-MPH and mPEG-MPH prodrug micelles

Since mPEG-TK-MPH and mPEG-MPH prodrugs have a hydrophilic portion (mPEG) covalently linked to a hydrophobic molecule (MPH), they might self-assemble in aqueous solution. This possibility was evaluated by PCS and AFM. A study of size variation and poly-dispersibility as a function of prodrug aqueous concentration was therefore

performed in milliQ water at a concentration range of 0.1 mg/ml-10 mg/ml (Figure 15A). At any concentration, from 10 mg/mL to 0.1 mg/mL, the mean size of mPEG-TK-MPH self-assembly micelles ranged from 260 to 300 nm.

On the contrary, PDI values, indicating the homogeneity of the samples, were different; under 0.25 mg/mL, PDI values were extremely high demonstrating a non-homogenous particle distribution, while from 0.25 to 10 mg/mL, all PDI values were acceptably low. The lowest PDI values (0.111), indicating the highest homogeneity of the sample, was recorded at 0.7 mg/mL.

A

	mPEG-TK-MPH		mPEG-MPH	
Concentration (mg/ml)	Size	PDI	Size	PDI
10	313.1 ± 2.5	0.133 ± 0.014	275.0 ± 0.5	0.119 ± 0.034
7	291.1 ± 6.5	0.171 ± 0.031	259.6 ± 2.7	0.107 ± 0.025
5	274.3 ± 6.5	0.130 ± 0.05	254.0 ± 2.4	0.113 ± 0.037
2,5	265.0 ± 7.3	0.150 ± 0.086	244.6 ± 6.8	0.121 ± 0.049
1	285.3 ± 12.1	0.191 ± 0.007	239.2 ± 2.8	0.153 ± 0.019
0.7	284.6 ± 8.9	0.111 ± 0.089	244.3 ± 4.4	0.172 ± 0.004
0.25	292.1 ± 3.7	0.190 ± 0.110	294.6 ± 12.9	0.218 ± 0.113
0.1	289.4 ± 13.5	0.266 ± 0.03	247.4 ± 14.3	0.264 ± 0.031

B

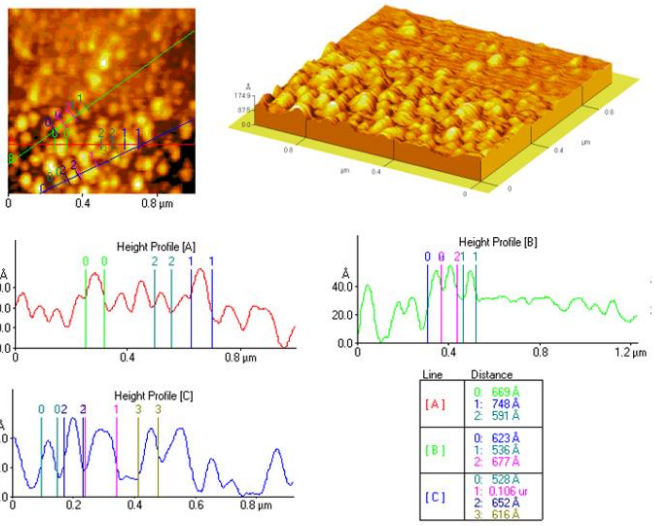

Figure 15. A. Mean size and PDI of prodrug micelles at different prodrug concentrations. **B.** Representative AFM image and height profile of mPEG-TK-MPH dispersed in water at a concentration of 0.7 mg/mL.

mPEG-TK-COOH did not show monodisperse compositions with high PDI values at any concentration range (Figure S9); this an expected result considering that due to its non-amphipathic nature, this polymer does not self-assemble. Since mPEG-TK-MPH suspended at the concentration of 0.7 mg/mL showed the lowest PDI index, we selected

this concentration to further characterized the morphology of self-assembled prodrugs through AFM. The analyzed sample of mPEG-TK-MPH, after suspension at 0.7 mg/mL, demonstrated to be coherent with spherical structures sizing around 100 nm (around 50-80 Ångström) that can be ascribed to prodrug micelles (Figure 15B).

The discrepancy in size among mean hydrodynamic size and the mean size obtained by AFM could be related to the fact that the effective hydrodynamic size includes the solvent surface layers of nanocarriers, which are no longer present in dried samples used for high-resolution microscopic techniques [221]. This result is in accordance with other research works in which particle size measured using PCS differed from that measured by TEM [204,222].

3.3. Cytotoxicity studies of mPEG-TK-MPH and mPEG-MPH on C6 GBM and DI TNC1 astrocyte cells

The selective *in vitro* effect on GBM cells over healthy cells of ROS-responsive mPEG-TK-MPH prodrug was evaluated on rat GBM cells (C6 cells) and "healthy" astrocytes cells (DI TNC1) from rat, respectively. The levels of ROS produced intrinsically by these cells were comparatively measured (data not shown), confirming that C6 cells produced significantly higher levels of ROS than DI TNC1 cells. This result is in agreement with our previous studies using these two cell lines [130].

In order to assay the cytotoxicity of MPH-based prodrugs on C6 and DI TNC1 cells, xCELLigence® RTCA DP instrumentation that uses gold-plated plates to measure cell attachment through electrical impedance, and thus cell viability, was employed [223]. C6 and DI TNC1 cell index curves were registered up to 72 h. Cell attachment and proliferation of untreated cells were recorded over 24 h. After 24 h, the plates were removed from the system to proceed with the addition of either free MPH, mPEG-TK-MPH, or mPEG-MPH into their corresponding wells. The ROS-responsive polymer without the drug (mPEG-TK-COOH) was also used at the same prodrug concentration in mg/mL, as control. Right after the addition of the different compounds, the plates were put back into the xCELLigence station, where the recording of cell proliferation was carried out up to 48 h. These studies were performed at a single MPH concentration of 11 μM since this concentration was reported to be the IC50 of MPH in C6 cells at 48 h of treatment [224].

When C6 GBM cells (Figure 16A) were treated with either mPEG-TK-MPH prodrug or free MPH, a significant cell growth inhibition in comparison to the control group was observed (Figure 16A). Furthermore, the cell growth of C6 cells treated with mPEG-TK-MPH was significantly inhibited in comparison to that of cells treated with mPEG-MPH. Since the level of ROS in endosomes is elevated, a ROS response can induce drug release and endosomal escape [125]. As we previously confirmed that Cy5 from mPEG-TK-Cy5 conjugate (which was obtained starting from the same ROS-responsive polymer, mPEG-TK-COOH) is endocytosed by C6 GBM cells, and then released inside these cells [130], we hypothesize a mechanism that justifies the higher cytotoxicity of mPEG-TK-MPH in comparison to mPEG-MPH. This mechanism can be explained as follows: after the endocytosis of self-assembled mPEG-TK-MPH micelles, the presence of ROS inside the endosomes can trigger the cleavage of TK bonds from the prodrugs with subsequent MPH release. Afterward, the released MPH can escape from the endosomes and then diffuse into the cell nucleus, where MPH finally will inhibit cell proliferation by inducing DNA inter-strand cross-links (ICL) [225,226].

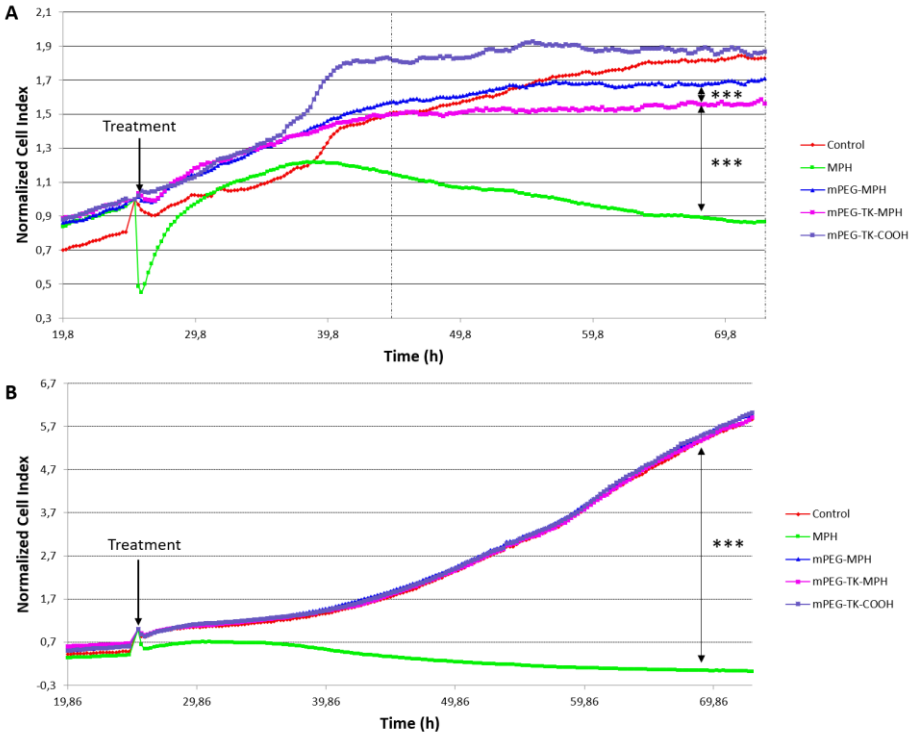

Figure 16. Normalized Cell Index curves of C6 (rat GBM cells) and DI TNC1 (Astrocyte cells). Both types of cells were treated with mPEG-TK-COOH (polymer control), free MPH (11 μM), mPEG-TK-MPH, and mPEG-MPH prodrugs at an equivalent MPH concentration (11 μM) for 48 h. **A.** C6 cells. Statistics: One-way ANOVA tests with Bonferroni post-test (*** $p \leq 0.001$). Between the dashed lines is indicated the

time period in which the differences between treatments are significant and are depicted in the graph. Time range: 19.5 h from the addition of the treatments, up to the end of the experiment (48 h). **B.** DI TNC1. The significant difference depicted in the graph was calculated considering the full time range from the addition of the different treatments to the end of the experiment (48 h).

Nevertheless, the cytotoxicity of the free drug was significantly higher in comparison to either of the prodrugs in cancer cells (Figure 16A), but also in healthy cells (Figure 16B). This may be because the passage of this drug into the cells is favored by L-type amino acid transporters (LATs) [225] such as L-type amino acid transporter 1 (LAT1), which transports neutral amino acids, including leucine. This transporter is present among other cells in glioma cells, including C6 [215,227–229], and can take MPH actively into cells [227]. In addition, taking into consideration its hydrophobic nature, passive transport of the free form of the drug cannot be excluded [225].

In contraposition, the prodrugs might be internalized by endocytosis, probably by fluid-phase endocytosis, as it was observed previously with mPEG-Cy5 conjugates [130]. As these prodrugs were not modified with a targeting ligand for GBM cells, the cell uptake might not be that high as it should be by receptor-mediated endocytosis [230] and, therefore, the activity of MPH is decreased. Apart from this aspect, since it was previously observed that TK cleavage depends on the amount of ROS, but also on the time exposed to ROS [130], the time needed to release MPH from the prodrug and/or micelle-like architecture could impact on release kinetics and, therefore, the speediness for induction of GBM cell death.

Regarding "healthy" DI TNC1 astrocyte cells, the prodrugs did not show to influence cell growth in these cells (Figure 3B), indicating the inability of triggering MPH drug release from mPEG-TK-MPH in cells with physiological levels of ROS, which are lower than in other glioma (C6) cancer cells [35]. On the other hand, control treatment with free MPH, led to a pronounced inhibition of cell growth in both cell lines. This could be ascribed to the expression of LAT1 transporters in all cells [231].

At the end of the experiment, concerning prodrugs administrations, Normalized Cell Index of free MPH treated cells was ~245-fold lower in healthy cells, describing a very low selectivity towards cancer versus healthy cells as described by several and frequent side-effects of free MPH [215,225]. Thus, merely looking at the Normalized Cell index ratio between mPEG-TK-MPH and free MPH at the end of the experiment in both types of cells (Figure 3A and B), we can conclude that mPEG-TK-MPH is very favorable in

terms of safety in the case of healthy cells and has a good selectivity in the case of cancer cells, with Normalized Cell index ratios at 48 h treatment of 5,9/0,02 = 295 and 1,6/0,9 = 1.8, respectively.

3.4. *In vitro* studies of mPEG-TK-MPH and mPEG-MPH prodrugs on human GBM cells

Apart from performing cytotoxicity studies with the prodrugs on rat GBM cells, we also performed *in vitro* studies using two human GBM cell lines: U87 MG and U251 MG, derived from grade IV GBM tumors. These cell lines are frequently used for *in vitro* drug screening previous to *in vivo* tests in animal models [232].

The intrinsic levels of ROS produced by these cells were indirectly measured by incubating the cells with DHE, a dye that can detect cytosolic superoxide, peroxynitrite and hydroxyl radical [233]. The results indicate a higher level of ROS in U251 MG in comparison to U87 MG cells (Figure 17).

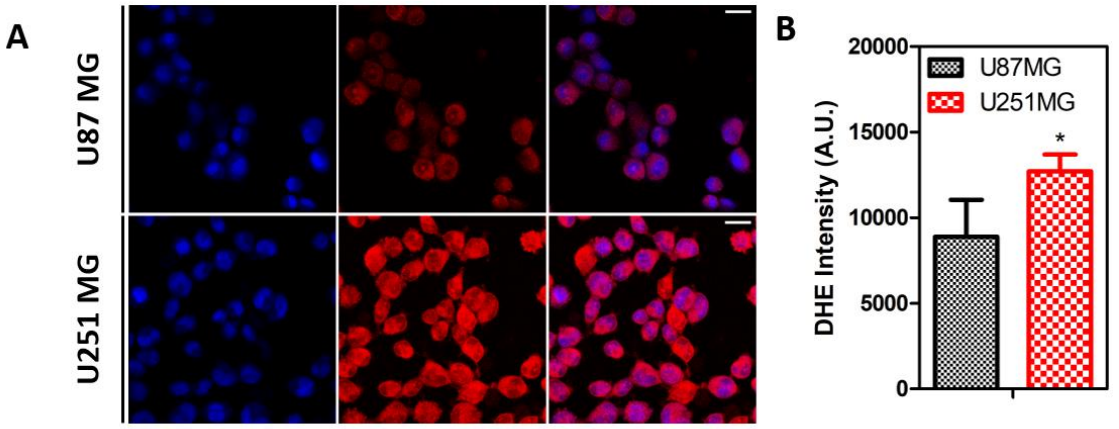

Figure 17. ROS levels on human GBM cells. Left: Representative images of U87MG and U251MG cells treated with DHE. Right: DHE intensity quantified on human GBM cells. Right: DHE intensity of human GBM exposed to H_2O_2 at different time intervals. Statistics: Unpaired t-test (*$p<0.05$).

Next, the cytotoxicity of mPEG-TK-MPH and mPEG-MPH prodrugs on these human GBM cells was assayed by treating the cells with different concentrations of free MPH or either of the prodrugs (at an equivalent concentration of MPH) for 48 h. Regarding U87 MG cells, neither the ROS-responsive mPEG-TK-MPH nor the non-ROS responsive mPEG-MPH prodrugs showed to be cytotoxic at the MPH concentration range and time

used in this experiment (Figure 18A). On the contrary, at 500 µM and 1000 µM equivalent concentrations of MPH, only mPEG-TK-MPH showed to be cytotoxic on U251 MG cells (Figure 18B) with a significant reduction on cell viability in comparison to the control prodrug mPEG-MPH.

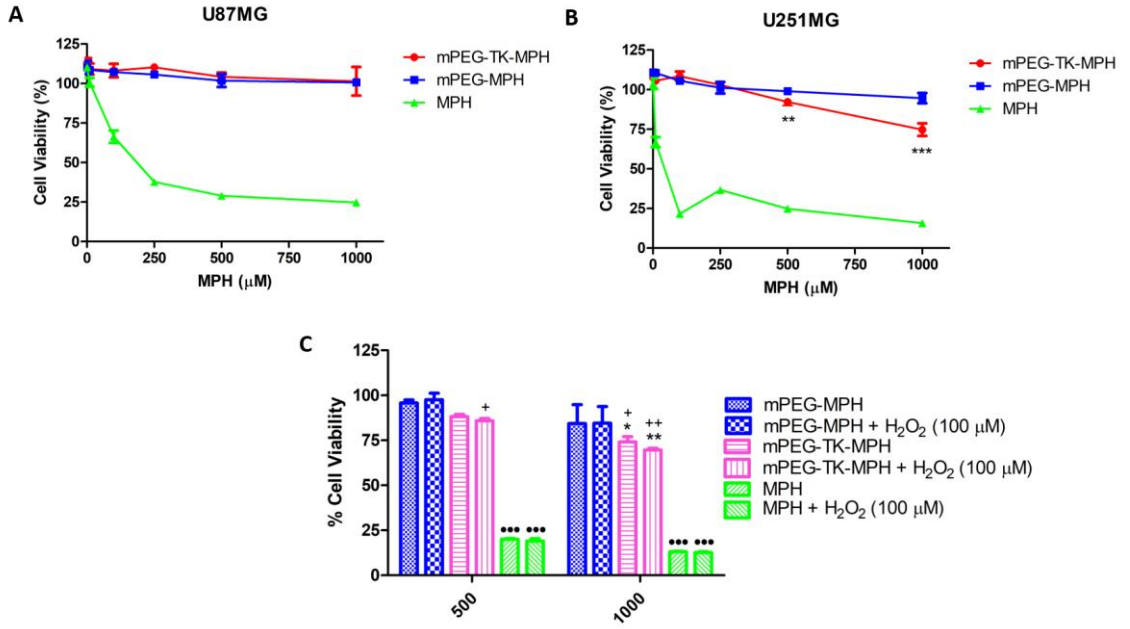

Figure 18. Cytotoxicity studies on human GBM cells. A. U87 MG cells treated with increasing concentration of either free MPH, mPEG-TK-MPH, or mPEG-MPH prodrugs at equivalent MPH concentrations for 48 h. **B.** U251 MG cells treated with increasing concentration of either free MPH, mPEG-TK-MPH, or mPEG-MPH prodrugs at equivalent MPH concentrations, for 48 h**.** Two-way ANOVA tests with Bonferroni post-test statistical analysis were performed. Comparisons: mPEG-MPH vs. mPEG-TK-MPH (** $p \leq 0.05$ and ** $p \leq 0.01$). **C.** Co-incubation of U251 MG cells treated with free MPH, mPEG-TK-MPH, or mPEG-MPH prodrugs, with H_2O_2 (100 µM). Two-way ANOVA tests with Bonferroni post-test statistical analysis were performed. Comparisons: mPEG-MPH vs. mPEG-TK-MPH and mPEG-TK-MPH + H_2O_2 (* $p<0.05$ and ** $p \leq 0.01$), mPEG-MPH + H_2O_2 vs. mPEG-TK-MPH and mPEG-TK-MPH + H_2O_2 (+ $p<0.05$and ++ $p \leq 0.01$), mPEG-MPH or mPEG-TK-MPH (w/ and w/o H_20_2) vs. MPH and MPH + H_2O_2 (‴ $p \leq 0.001$).

As it was observed for rat GBM cells, the cytotoxicity obtained with free MPH was significantly higher than the observed with either of the prodrugs (Figure 18A, B), with IC50s of 89 µM and 16 µM in U87 MG and U251 MG cells, respectively. This result could be related to the higher sensitivity of these kind of cells towards MPH due to overexpression of LAT1 transporter responsible for the active transport of MPH into cells in proliferating tumors, including U87 MG and U251 MG .

As higher levels of ROS were found in U251 MG in comparison to U87 MG, we hypothesize that the higher cytotoxicity of mPEG-TK-MPH in U251 MG might be related to the higher intrinsic intracellular levels of ROS produced by these cells.

An alternative explanation for the lower cytotoxicity of mPEG-TK-MPH in comparison with free MPH might be an insufficient TK cleavage by ROS. Therefore, to investigate if, by increasing the level of ROS, the cytotoxicity of ROS-responsive mPEG-TK-MPH can be increased, we used H_2O_2 as a ROS enhancer. We firstly tested different H_2O_2 concentration on either of these GBM cells in order to choose a non-toxic concentration (Figure S10) for the experiments. A non-toxic H_2O_2 concentration of 100 μM was used to measure the intracellular levels of ROS in U87 MG and U251 MG cells after different H_2O_2 incubation times (Figure S11). We could observe that the levels of ROS in U87MG cells treated with H_2O_2 at different times were not increased (Figure S11A). In contrast, the levels of ROS in U251 MG cells were particularly increased after 24 h incubation with H_2O_2, suggesting that H_2O_2 can be used to force the release of higher amounts of MPH in these cells. Therefore, next, we tested the effect of H_2O_2 on the cytotoxicity of mPEG-TK-MPH in U251 MG cells. Free MPH, mPEG-TK-MPH or mPEG-MPH, were co-incubated with 100 μM H_2O_2 for 48 h. Remarkably, at the equivalent MPH concentrations tested (500 μM and 1000 μM), we observed (Figure 18C) a more evident cytotoxic effect of mPEG-TK-MPH corresponding to a slight reduction of cell viability in H_2O_2 co-incubated cells, compared to not-forced conditions. This result, therefore, confirmed that when the intracellular concentration of ROS increases, the release of MPH from mPEG-TK-MPH and its cytotoxic activity improve.

3.5. Evaluation of the potential synergistic effect of X-ray irradiation on human GBM cells treated with mPEG-TK-MPH and mPEG-MPH prodrugs

mPEG-TK-MPH showed to be cytotoxic at concentrations higher than 500 μM. Since we notice an improved cytotoxicity of mPEG-TK-MPH prodrug after additional enhancement of ROS using H_2O_2, we hypothesize that the physiological levels of ROS in GBM cells might not be enough to induce TK linker cleavage from the ROS-responsive prodrug (mPEG-TK-MPH). Radiotherapy, defined as the use of ionizing radiation (IR) in therapy, was reported to be able to stimulate and increase mitochondrial-related ROS [234]. Given that the current clinical setting used for GBM treatment is based on concomitant chemotherapy and radiotherapy to improve patient survival [235], we

decided to explore the effect of combining ROS-responsive prodrug treatment with X-ray, a type of IR, on human GBM cells.

Notably, only a few studies report ROS-responsive DDS used in combination with a different type of IR (γ-ray). For instance, ROS-responsive Selenium-based micelles containing Doxorubicin demonstrated to have a synergistic antitumor effect on hepatocellular carcinoma cells at 5 Gy radiation dose [92]. This result could be explained due to a higher sensitivity of hepatocellular carcinoma cells in promoting ROS induction after irradiation. Similarly, tellurium-based micelles [94] demonstrated to respond to an even lower radiation dose (2 Gy).

As a consequence, we performed a protocol in which GBM cells received an overall X-ray dose of 8 Gy at 2 times (4 Gy as initial dose and 4 Gy after 24 h), which showed that irradiated U87 MG and U251 MG cells did not suffer from any cytotoxicity (Figure 19A and 19B).

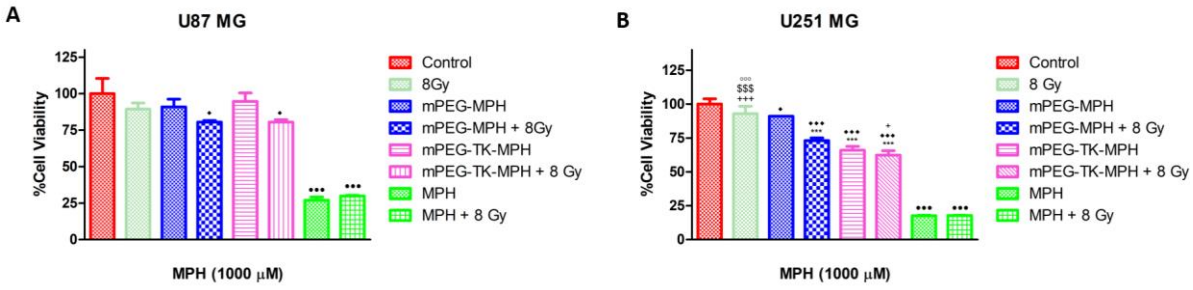

Figure 19. Influence of X-ray irradiation on human GBM cells treated with mPEG-TK-MPH and mPEG-MPH. A. U251 MG cells and **B.** U87 MG cells. Statistical comparisons performed by One-way ANOVA tests with Bonferroni post-test: Control vs. mPEG-MPH, mPEG-MPH+ 8Gy, mPEG-TK-MPH and mPEG-TK-MPH + 8Gy (♦ $p<0.05$ and ♦♦♦ $p\leq0.001$); mPEG-MPH vs. mPEG-MPH + 8 Gy, mPEG-TK-MPH and mPEG-TK-MPH + 8 Gy (*** $p\leq0.001$); mPEG-MPH + 8 Gy vs. 8 Gy, mPEG-TK-MPH and mPEG-TK-MPH + 8Gy (+ $p<0.05$ and +++ $p\leq0.001$), mPEG-TK-MPH vs. 8 Gy and mPEG-TK-MPH + 8 Gy ($$$ $p\leq0.001$); 8Gy vs. mPEG-TK-MPH + 8Gy (◦◦◦ $p\leq0.001$); MPH and MPH + 8 Gy vs. Control and all other treatments (‴ $p\leq0.001$).

Then, we assayed the cytotoxicity of mPEG-TK-MPH and mPEG-MPH at 1000 μM equivalent concentration of MPH (MPH concentration in which we observed the highest cytotoxicity of mPEG-TK-MPH on U251 MG cells) on irradiated human GBM cells.

Remarkably, viability tests showed an increase in cytotoxicity upon prodrug (mPEG-MPH and mPEG-TK-MPH) treatment and irradiation (Figure 19A and B) in comparison to control cells on both U87 MG and U251 MG cells.

It was reported that when the cytotoxic effect obtained by the combination of a chemotherapeutic drug and IR is higher than the predicted by the additive effect of single therapies, the chemotherapeutic drug can be classified as a radiosensitizer. Since many potent radiosensitizers are DNA-damaging agents [236], MPH might be acting as a radiosensitizer by increasing IR cytotoxicity. Thus, the higher cytotoxicity seen with mPEG-MPH and mPEG-TK-MPH on U87 MG and with mPEG-MPH on U251 MG irradiated cells, might be due to a synergistic effect with MPH that might be acting as a radiosensitizer.

On the other hand, in the case of free MPH treated cells, differences among irradiated and non-irradiated cells were not observed (Figure 6A and B). The high cytotoxicity of free MPH on any of the cell lines might explained why at the dose applied in these experiments, a synergistic effect was not evident.

It is likely that the ROS status of U87MG cells, even in the presence of beam radiations, does not reach the require amount to cleave thioketal group on mPEG-TK-MPH prodrug. In the case of U251 MG cells, the cytotoxicity of mPEG-TK-MPH treated, and irradiated cells was significantly higher in comparison to mPEG-MPH treated and irradiated cells (Figure 6B). Nevertheless, the slightly reduction on cell viability of mPEG-TK-MPH treated and irradiated cells in comparison to only mPEG-TK-MPH (without irradiation), was not significant. This result might indicate that at the X-ray dose received; the production of ROS was not enough to induce TK bond cleavage and MPH release from mPEG-TK-MPH to achieve higher cytotoxicity.

Thus, it seems likely that the radiation condition used was not capable to produce sufficient concentrations of ROS that trigger the release of active MPH. Possible instant or cumulative effect on ROS production could be obtained by using higher X-ray dose or X-ray dose regimen, respectively. In addition, it could be interesting to apply alternative IR therapy such as alpha and beta radiation, that might have a different impact on ROS production and therefore, on thioketal cleavage.

Since the locally administration of drugs has been investigated as it offers the possibility to bypass the BBB and blood brain tumor barrier (BBTB), concentrating higher amounts of drug in malignant tumors [237], it would be interesting to provide a locally sensitive strategy which would make it possible to have an activity in synergy with other actions including radiotherapy for the cleavage and drug activity. For the moment, pilot clinical studies using intravenous melphalan have not shown any significant impact [238]. Thus,

this new local opportunity through an activatable agent is interesting and merit to be further explored.

4. Conclusion

With this study, we demonstrated that ROS-sensitive mPEG-TK-MPH displayed a higher anticancer activity and cytotoxicity than the non-ROS sensitive prodrug mPEG-MPH in rat C6 and human U251 MG glioblastoma cells. Furthermore, we demonstrated a higher safety profile of ROS-sensitive mPEG-TK-MPH since it did not induce any cytotoxicity on healthy cells (DI TNC1 astrocyte cells). Therefore, due to their ability to specifically deliver drugs upon ROS stimulus with increased effectivity and selectivity for cancer over healthy cells, the application of TK-technology in the design of prodrugs could be considered as a promising approach for the development of future therapeutics against Glioblastoma.

In addition, we investigated the potential synergistic activity of X-ray radiation on human GBM cells, observing that both prodrugs were cytotoxic on U87MG cells, in which without irradiation, were not cytotoxic. On U251MG cells, both prodrugs also demonstrated to be cytotoxic, but, in the case of mPEG-TK-MPH, the cytotoxicity was comparable to non-irradiated mPEG-TK-MPH treated cells. Thus, the observed cytotoxicity effect was probably due to the irradiation but not to an additional cleavage of TK groups by X-ray generated ROS. Since in this work we could demonstrate that mPEG-TK-MPH respond to intracellular ROS in GBM cells, we are planning to investigate in situ the stimuli or local combinations capable of causing the expected MPH release and antitumor effect.

Despite the ROS-response technology of mPEG-TK-MPH demonstrated to work on GBM cells expressing high ROS levels, large improvements in terms of cytotoxicity could be realistically obtained in clinical translation. This study could be a starting point for a rationale design of innovative and tailored ROS-responsive prodrugs, capable not only of improving drug solubility and mediating selective ROS-triggered drug release, but also of increasing transport inside the cells of highly cytotoxic drugs with poor ability in cell permeation.

3.3. Annex 2: Supplementary figures

A.

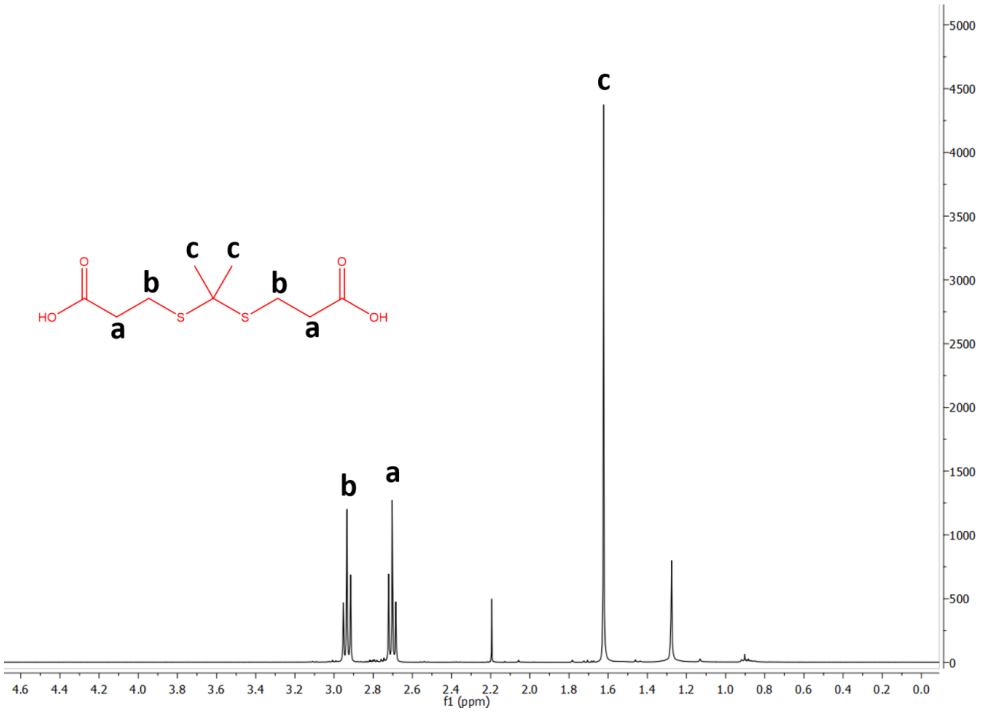

B.

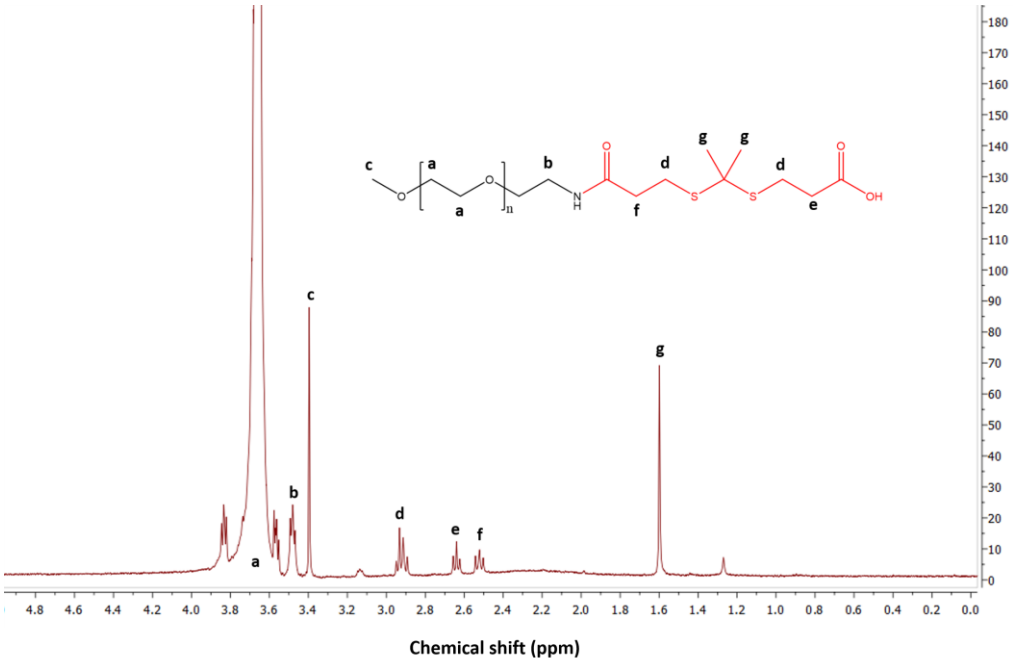

Figure S7. A. ^{1}H NMR spectra of TK-C.L. and **B.** mPEG-TK-COOH polymer.

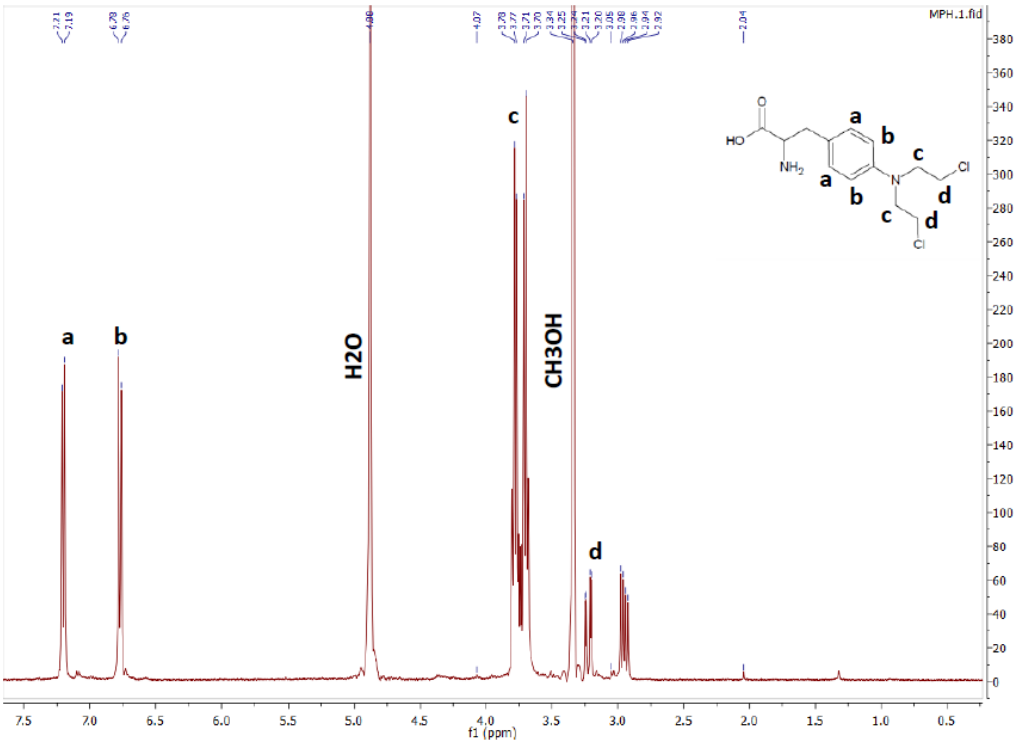

Figure S8. ^{1}H NMR MPH in CD_3CD.

	mPEG-TK-COOH		mPEG-P.A.	
Concentration (mg/ml)	**Size**	**PDI**	**Size**	**PDI**
10	305.2 ± 47.2	0.403 ± 0.044	183.7 ± 15.4	0.291 ± 0.030
7	390.75 ± 14.9	0.449 ± 0.054	153.7 ± 4.7	0.371 ± 0.043
5	385.05 ± 45.2	0.426 ± 0.025	158.1 ± 2.4	0.388 ± 0.002
2,5	259.0 ± 53.9	0.483 ± 0.009	227.05 ± 28.3	0.321 ± 0.0184
1	534.5 ± 316.0	0.508 ± 0.193	238.15 ± 6.1	0.353 ± 0.052
0.7	295.6 ± 14.6	0.353 ± 0.006	333.65 ± 12.5	0.335 ± 0.005
0.25	346.3 ± 69.6	0.857 ± 0.202	448.0 ± 53.0	0.418 ± 0.102
0.1	539.75 ± 113.6	0.702 ± 0.421	345.4 ± 24.4	0.282 ± 0.07

Figure S9. Mean size and PDI of mPEG-TK-COOH in water at 10-0.1 mg/mL range.

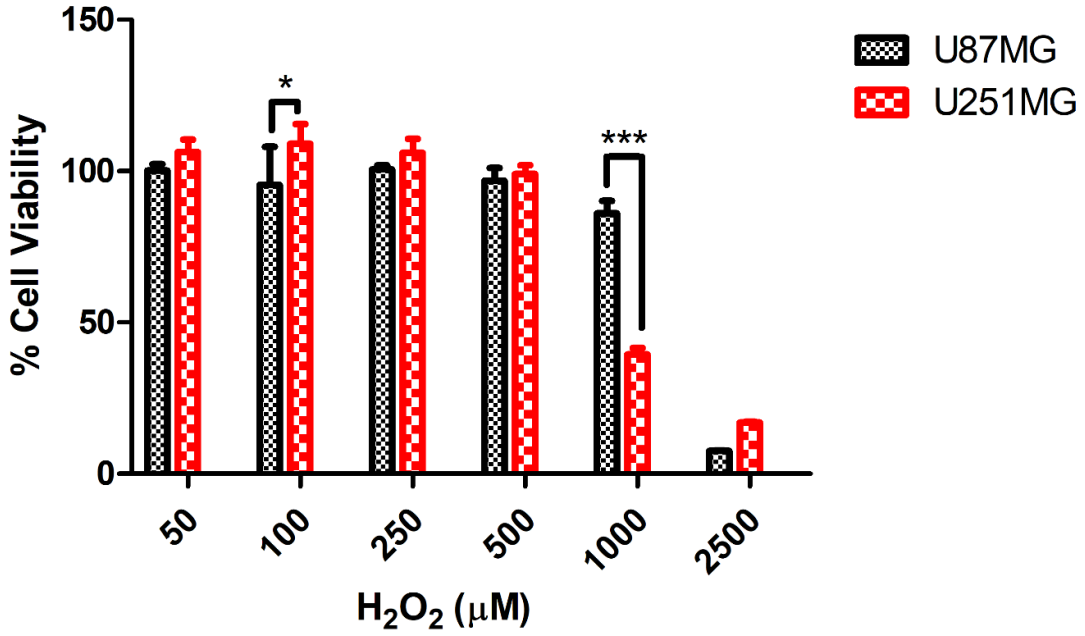

Figure S10: Cytotoxicity study performed by incubating U87 MG and U251 MG cells with increasing H_2O_2 concentrations. Two-way ANOVA, Bonferroni post test (*p<0.05, ***p<0.001). The H_2O_2 calculated IC 50 for U87MG and U251 MG cells were of 1252 and 783.6 µM, respectively.

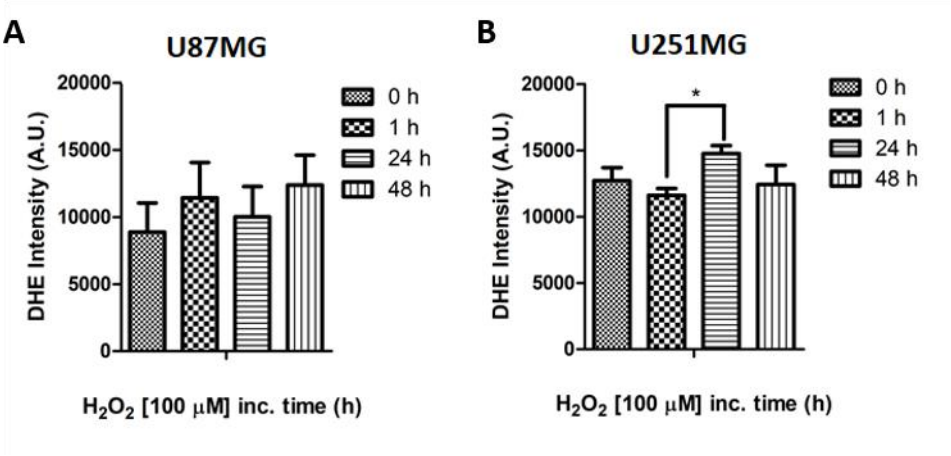

Figure S11: DHE intensity of human GBM exposed to H_2O_2 for different incubation times. A. U87MG and **B.** U251MG cells. One-way ANOVA, Bonferroni post-test (*p<0.05).

Chapter 5:

PLGA-TK-COOH: Synthesis, characterization and formulation of TK- based PLGA NPs

5.1. Background and chapter aim

Apart from PEG, PLGA is also a widely used synthetic polymer which is approved by the FDA and EMA for parenteral administration. Among all synthetic polymers, PLGA is the most used for pharmaceutical applications and among others DDS, it is used for the formulation of PLGA NPs. Generally, drugs are encapsulated into these NPs, but due to the availability of surface chemical groups, it is also possible to covalently attach drugs onto PLGA NPs surface.

The release of drugs from PLGA NPs generally occurs by sustained release. In certain cases, it is necessary to achieve faster drug release rates in the site of the disease. Thus, by means of stimuli responsive DDS that change their conformation or cleave upon a stimulus, such as ROS, drug release can be enhanced.

Accordingly, the objective of this chapter is, by means of applying TK-technology, to obtain ROS-responsive TK-based PLGA polymers for the preparation of ROS-responsive PLGA NPs (PLGA-TK-COOH polymer and PLGA-TK-PLGA co-polymer) aiming for delivering drugs to extra and intracellular sites of pathological brain in the future.

5.2. Introduction

Synthetic biodegradable and biocompatible polymers are being widely used in various applications including drug delivery [239], and in comparison to natural polymers, their higher stability and reproducibility make them suitable for pharmaceutical application [240]. Among these polymers, poly(lactide-co-glycolide) (PLGA), a co-polymer of poly(lactic acid) (PLA) and poly (glycolic acid) (PGA), approved by the FDA and EMA for parenteral administration in humans, is nowadays the most used synthetic polymer in the pharmaceutical field [241,242] (Figure 20).

They have been applied for the formulation of drug delivery carriers such as NPs and microparticles as well as scaffolds for tissue engineering, implants and medical devices [243]. The release of drugs from PLGA based formulations occurs by diffusion, erosion of PLGA polymers or by a combination of both [244].

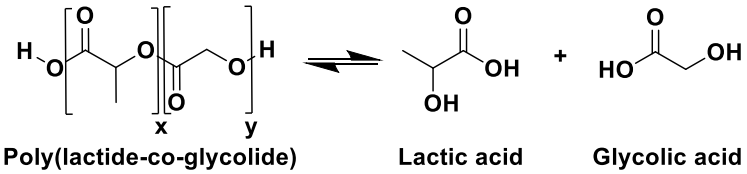

Figure 20: Structure of Poly(lactide-co-glycolide) and their constitutive monomers. Lactic acid and Glycolic acid monomers are also the degradation products of the polymer that are then metabolized by the body.

In more details, PLGA NPs are suitable for the encapsulation of a broad range of therapeutics of small and high molecular weights, and in contraposition with conventionally administered drugs, they can sustain drug release for longer periods of time and can also be functionalized onto their surface with targeting ligands, imaging agents, drugs, etc [245–247] due to the presence of carboxylic ends ready for conjugation and chemical reactions.

Despite their ability to prolong drug release, in some cases the drug release from these types of NPs is not desirable and in some cases difficult to be predicted: depending on the hydrophilicity of the drugs, it may happen that some encapsulated drugs could be distributed close or adsorbed onto the surface of the NPs, thus leading to a burst release. In order to resolve this possible limitation, amongst the different strategies, conjugation of drugs directly to the polymer backbone followed by a "triggered" cleavage of the yet formed chemical bonds, was proposed [248].

The conjugation of a ligand to PLGA polymer was commonly assisted by carbodiimide chemistry taking advantage of carboxyl groups on the polymer to link directly to a ligand as PEG block or a PEG-block with a ligand attached [249]. Therefore, the conjugation of peptides to PLGA polymers were often exploited by means of this carbodiimide chemistry, in which peptides containing a terminal amine group can be attached to the carboxylic acid group on PLGA. By exploiting this technology, peptide-engineered PLGA NPs obtained by Colzani and co-workers, were obtained by derivatizing PLGA polymers with two peptides (epidermal Growth Factor Receptor targeting agent and model peptide) obtaining functionalization yields higher than 80% [242]. In addition, our group has exploited this chemistry to functionalize PLGA polymers with a glycopeptide, H_2N-Gly-L-Phe-D-Thr-Gly-L-Phe-L-Leu-L-Ser(O-β-D-Glucose)-$CONH_2$) (g7), that target and enable NPs to cross the BBB without provoking any damage to the barrier [250].

Despite that, the limited types of functional groups available on PLGA NPs (only carvoxylic ends) may represent a drawback for covalent conjugation. In this regard the absorption onto PLGA of other molecules (as polymers and surfactants) featured by specific terminal groups (carboxyl, hydroxyl, amine) were exploited for ligand attachment and therefore to exploit different chemical reactivities [251]. Another approach is the introduction of functional groups to PLGA polymers [252] so that they harbor chemical functionalities other than carboxylic acid, improving the versatility in relation to the molecules that can be attached to them.

Interestingly, amine functionalized PLGA was recently employed to produce di-block co-polymers with PEG by means of TK diacid linker, in order to obtained ROS-responsive NPs encapsulating DOX for the treatment of oral cancer chemotherapy [143,144]. The authors confirmed ROS-responsiveness of these di-block co-polymers with PLGA and PEG, obtaining promising results for cancer application.

Since we are interested in designing ROS-responsive DDS for the treatment of brain diseases, we hypothesized to formulate TK-based PLGA NPs aiming for the delivery of therapeutics to extra and intracellular sites with ROS-featuring diseases, following two kind of approaches: a) by means of *attaching the drug to the surface of the NPs through TK linkages* or b) through the *encapsulation of an hydrophobic drug into PLGA NP made up from PLGA-TK-PLGA co-polymers.*

Therefore, in this chapter, the application of TK-technology for the synthesis of ROS-responsive PLGA-TK-COOH polymer, ROS-responsive co-polymer PLGA-TK-PLGA as well as the preparation of NPs from this polymer and co-polymer, respectively, will be shown and discussed.

5.3. Materials and Methods

5.3.1. Materials

PLGA-NH_2 (53:47, MW=15985 g/mol) was purchased from PolySciTech Division of AKINA, INC. and PLGA RG-503H, (50:50, MW=11000 g/mol) was purchased from Boehringer-Ingelheim, Ingelheim am Rhein, Germany. N-hydroxy succinimide (NHS) and N-(3-dimethylaminopropyl)-N-ethylcarbodiimide hydrochloride (EDC. HCl) were

provided by Sigma-Aldrich and used directly. All the solvents used: dichloromethane (DCM), methanol (MeOH), diethyl ether, chloroform, ethanol and acetone, were of analytical grade and used without further purification. A Milli-Q water system (Millipore, Bedford, MA, USA), supplied with distilled water, provided high-purity water (18 V). Fluorescamine reagent, Polyvinyl alcohol (PVA, MW=15000) and Pluronic F-68 (molecular weight of 8500–9000 Da) were purchased from Sigma-Aldrich (Milan, Italy).

5.3.2. Syntheses

5.3.2.1. ROS-responsive PLGA-TK-COOH polymer synthesis

The synthesis of ROS-responsive PLGA-TK-COOH polymer (Scheme 5) was performed by carbodiimide chemistry to form an amide bond among PLGA-NH_2 and TK-diacid containing linker (TK-C.L), whose synthesis was already described by our group [130]. Different molar ratios among EDC.HCl, NHS and TK-C.L. to PLGA-NH_2 as well as different reaction times, were assayed (Table 3). Briefly, TK-C.L. was first activated with EDC. HCl and NHS in 400 µL of DCM for 1.5 h. After activation, this mixture was added dropwise into a flask containing PLGA-NH_2 in 1 mL of DCM and stirred for 72 h or 48 h at room temperature. The product was precipitated from the mixture with a mix of cold diethyl ether: methanol 50/50 (v/v) and centrifuged at 5.700 rpm for 10 minutes. In order to eliminate unreacted reagents, the product was washed with the same precipitation mixture and centrifuged three times in the same conditions. After washing, the product was transferred to a pre-weighed evaporator glass and dried in vacuum desiccator, to finally calculate product yield (P.Y.%).

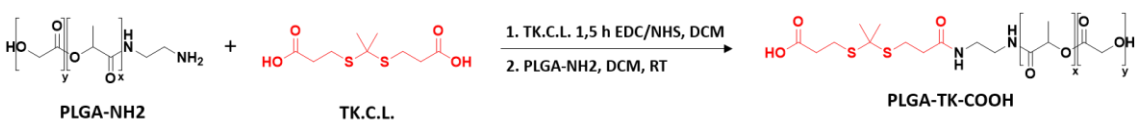

Scheme 5: Synthesis of ROS-responsive PLGA-TK-COOH polymer.

Synthesis	EDC.HCl/NHS: PLGA-NH_2 molar ratio	TK-C.L.: PLGA-NH_2 molar ratio	Synthesis time (h)
1	1:3,1	1:3	72
2	1:5,2	1:5	72
3	1:10,3	1:10	72
4	1:10,3	1:10	48

Table 3: Molar ratios used among reactants and PLGA-NH_2 polymer and reaction time.

5.3.2.2. Determination of PLGA-TK-COOH derivatization yield by means of Fluorescamine assay

In order to calculate the D.Y.% of PLGA-TK-COOH, a technique described by Eckstein and Dreyfuss in 1980 for the measurement of the concentration of primary amine groups of non- water-soluble polymers [253] was adopted. Our protocol was carried out by performing a calibration curve with PLGA-NH_2, starting from PLGA-NH_2 standard stock solutions (1.24 mg/mL and 1.43 mg/mL) in chloroform. The calibration curve was prepared by firstly adding growing volumes of either of the standard stock solutions (10, 20, 50, 75 and 100 µL) into separate 10 mL volumetric flasks. The second step was to add 200 µL of Fluorescamine stock solution (2×10^{-3} M) into the flasks, followed by the addition of 400 µL of Ethanol, 95% (v/v) and finally, chloroform up to reach 10 mL. Immediately after preparation, these standard solutions were measured in a fluorometer (FP-8200, Jasco) with λexc = 395 nm and λem = 485 nm. The same procedure was followed to measure PLGA-TK-COOH samples of 1 mg/mL in Chloroform by triplicates and PLGA RG-503H as control. The un-reacted content of PLGA-NH_2 in PLGA-TK-COOH samples was calculated against PLGA-NH_2 calibration curve (linearity was assumed in the range 1,24 - 18,54 µg/mL; r^2 = 0,9991), being the PLGA-TK-COOH derivatization yield calculated by subtracting 100 % to % PLGA-NH_2.

5.3.2.3. ROS-responsive PLGA-TK-PLGA co-polymer synthesis

The synthesis of PLGA-TK-PLGA co-polymer (Scheme 6) was carried out by covalent coupling of PLGA-NH_2 to PLGA-TK-COOH, at a molar ratio of 1:1.19. Briefly, PLGA-

TK-COOH polymer (6.2 µmol) was firstly mixed for 1.5 h with EDC.HCl (62 µmol) and NHS (62 µmol) in 2 mL of DCM. Then, PLGA-NH_2 (5.2 µmol) dissolved in 1 mL of DCM, was added to the mix and stirred for 48 h. The product was precipitated from the mixture in cold diethyl ether: methanol 50/50 (v/v) and centrifuged at 5.700 rpm for 10 minutes. In order to eliminate unreacted reagents, the product was washed with the same precipitation mixture and centrifuged three times in the same conditions. After washing, the product was transferred to a pre-weighed evaporator glass and dried in vacuum desiccator for further determination of product and derivatization yields.

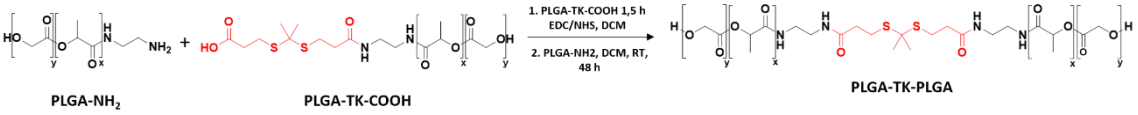

Scheme 6: Synthesis of ROS-responsive PLGA-TK-PLGA polymer.

5.3.3. Characterization

5.3.3.1. PLGA-TK-COOH polymer characterization by ^{1}H NMR

PLGA-TK-COOH polymer was characterized by ^{1}H NMR and 2D ^{1}H-^{1}H COSY spectra. PLGA-NH_2 and PLGA-TK-COOH polymers were measured in Avance III 600 HD-Bruker in $CDCl_3$ and analyzed by MNova software.

5.3.3.2. GPC characterization of PLGA-TK-COOH and PLGA-TK-PLGA

Number (Mn) and weight-average molecular weights (Mw) of PLGA-NH_2 and PLGA-TK-COOH were determined by a GPC system equipped with an Agilent 1260 Infinity GPC/SEC System, using a refractive index detector. Tetrahydrofluran (THF) was used as the eluent at a flow rate of 1 mL/min. Agilent GPC/SEC Software was used to calculate the molecular weight based on a universal calibration curve generated by a polystyrene standard of narrow molecular weight distribution (linearity assumed in 0.162- 6570 KDa; r^2= 0.996488 range).

5.3.4. Preparation of TK surface functionalized PLGA (TK-PLGA) NPs

TK-PLGA NPs were prepared by single emulsion/evaporation method and nanoprecipitation by using ionic and non-ionic surfactants PVA and F68, respectively.

5.3.4.1. TK-PLGA NPs prepared by single emulsion/solvent evaporation with PVA 1%

TK-functionalized PLGA NPs were prepared by using 10% of PLGA-TK-COOH and 90% of PLGA RG-503H. The protocol followed to prepare TK-PLGA NPs by single emulsion/solvent evaporation with PVA as surfactant was previously standardized by our group with some modifications [254]. Firstly, 45 mg of PLGA 503H and 5 mg of PLGA-TK-COOH, were weighted and dissolved in 1.5 mL of DCM. 6 mL of PVA 1% (w/v) solution in water was added to a round-bottom glass tube and placed on an ice bath for further sonication by means of a sonicator tip. As soon as the sonication started, the solution of PLGA in DCM was quickly added to the tube and sonicated at 55 watts, 60 seconds. The emulsion obtained was then placed in a Becker with subsequent magnetic stirring for about 3 hours to let DCM be evaporated. PLGA (control) NPs, made up from PLGA 503H, were also prepared. The excess of surfactant from the NPs was discarded by centrifugation (Beckmann) at 17000 rpm for 10 min at 4°C. The supernatant was then discarded, and the pellet resuspended in 4 mL of milliQ water. The size and Z Potential of the NPs were finally measured by photon correlation spectroscopy (PCS), using a Zetasizer Nano ZS (Malvern, UK; Laser 4 mW He–Ne, 633 nm, Laser attenuator Automatic, transmission 100–0.0003%, Detector Avalanche photodiode, Q.E. > 50% at 633 nm) at room temperature.

5.3.4.2. TK-PLGA NPs prepared by nanoprecipitation with PVA 1% (w/v)

TK-PLGA NPs were prepared by using 10 or 20% of PLGA-TK-COOH polymer and PLGA 503H. Briefly, 5 or 10 mg of PLGA-TK-COOH and 45 or 40 mg of PLGA 503H were weighted and dissolved in 4 mL of acetone and introduced goat by goat to a beaker containing 12,5 mL of PVA 1% while stirring. After 15 minutes, the acetone was discarded by vacuum rotary evaporation for about 1 h or up to confirm that the acetone was totally removed. NPs suspensions were then placed in centrifugation tubes and

centrifuged (Beckmann) at 16000 rpm for 10 minutes at 4°C. The pellet was finally dispersed in 4 mL of MilliQ water and the size and Z Potential of the formulated NPs measured by means of PCS. PLGA (control) NPs, were also prepared following the same procedure with 50 mg of PLGA 503H.

5.3.4.3. TK-PLGA NPs prepared by nanoprecipitation with F-68 3% (w/v)

The preparation of TK-PLGA NPs by nanoprecipitation was carried out following a previously standardized method with some modifications [255]. Briefly, 12,5 mL of Pluronic F-68 water solution (3% w/v), was added into a small beaker and placed on a magnetic stirrer at a high-speed stirring. Either PLGA 503H (control NPs) or PLGA 503H with PLGA-TK-COOH (10% or 20%) (Table 4) were well dissolved in 4 mL of acetone and then added dropwise into the surfactant solution. After 15 minutes of stirring, the mix was transferred to a round bottom flask for rotavapor in order to get rid of acetone. The NP suspensions were then transferred to a centrifuge tube, discarding the excess of surfactant by ultracentrifugation at 16.000 rpm (Beckman Ultracentrifuge) for 10 minutes at 4°C. The pellet obtained was dispersed in 4 mL of Milli-Q water and the size and Z Potential measured by PCS.

PLGA NP	PLGA 503H(mg)	PLGA-TK-COOH (mg)
PLGA (Control)	50	-
TK-PLGA 10%	45	5
TK-PLGA 20%	40	10

Table 4: Polymer composition used for TK-PLGA NP formulation by nanoprecipitation with Pluronic F-68.

5.3.4.4. Characterization of TK-PLGA NPs surface by ESCA

The presence of TK on the NPs surface was studied by electron spectroscopy for chemical analysis (ESCA) aiming for the detection of Sulfide (S) onto the surface of the NPs, exploiting a technique that was previously used to detect Nitrogen (N) to confirm peptide-

NP conjugates [33]. This analysis was performed on all the NPs which were prepared by single emulsion (PLGA (Control) NPs and TK-PLGA (10%) NPs) and nanoprecipitation (PLGA (Control) NPs, TK-PLGA (10%) NPs, TK-PLGA (20%) NPs) in PVA 1% (w/v). In addition, PLGA-TK-COOH polymer was also analyzed as control. The samples were placed onto aluminum slides and ESCA analysis was performed on an XRC 1000 X-ray source analysis system (Specs Surface Nano Analysis, Germany) and a Phoibos 150 hemispherical electron analyzer (Specs Surface Nano Analysis, Germany), using MgKα1,2 radiations. Spectra were recorded in fixed retardation ratio (FAT) mode with 40 eV pass energy. The pressure in the sample analysis chamber was around 10^{-9} mbar. Data were acquired and processed using the SpecsLab2 software.

5.3.5. PLGA-TK-PLGA NPs prepared by nanoprecipitation with Pluronic F-68 3% (w/v)

In order to prepare TK-based NPs from PLGA-TK-PLGA co-polymers, the method of nanoprecipitation with Pluronic F-68 3% (w/v), was applied. The protocol followed was the same as the used to prepare TK-surface functionalized PLGA NPs (section 5.2.4.3.), except for the polymer used (50 mg of PLGA-TK-PLGA co-polymer).

5.4. Results and discussion

5.4.1. Synthesis, determination of the derivatization yield and characterization of PLGA-TK-COOH polymer

For the synthesis of PLGA-TK-COOH, different molar ratios of crosslinking reagents (EDC/NHS) and TK-C.L. to PLGA-NH_2 and different reaction times, were tested (Table 4). High product yields (P.Y. %) as well as high derivatization yields (D.Y. %) were obtained for all the syntheses (Table 5). Among all the PLGA-TK-COOH polymer syntheses, syntheses 3 and 4, with TK-C.L. to PLGA-NH_2 molar ratio of 10:1 and reaction times of 72 and 48 h, respectively, showed the highest D.Y.% of almost 100%.

Syntheses	P.Y. (%)	D.Y. (%)
1	80,0 ± 0,1	87 ± 3,7
2	87,3 ± 3,2	93,6 ± 0,6
3	86,2 ± 1,6	98,1 ± 1,8
4	83,4 ± 0,8	96 ± 1,6

Table 5: PLGA-TK-COOH polymer syntheses (1-4) and yields (P.Y. and D.Y.) obtained.

Here we proposed the adaptation of a specific method for the quantification of primary amine groups, namely Fluorescamine method, to quantify un-reacted PLGA-NH_2 and determine PLGA-TK-COOH derivatization yield. It is worth to notice that, as far as we know, this methodology was never applied before on PLGA polymers. The use of Fluorescamine reagent, which is a non-fluorescent reagent that turns into highly fluorescent upon the reaction with primary amine groups, was described for the first time by Udenfriend et al., who used this reagent aiming for the detection of amino acids, peptides and proteins, demonstrating a sensitivity of detection in the picomolar concentration range [256]. Later on, the use of Fluorescamine to quantify primary amine groups on non-water soluble high molecular weight polymers was reported, demonstrating the design of a highly sensitive method in which low amine concentrations (even below to 10^{-6} M) could be detected, and being more accurate than other methods used with high MW polymers [253].

Thus, by applying this technique, we were able to determine the content of non-reacted PLGA-NH_2 by means of PLGA-NH_2 calibration curve, and subsequently the D.Y. (%) of PLGA-TK-COOH polymers. Most importantly, PLGA 503H, without amine groups, did not react with Fluorescamine, demonstrating reaction specificity to PLGA-NH_2. In addition, this technique can be applied for the determination of the derivatization yield of PLGA-drug conjugates made up from PLGA-NH_2 and drugs that do not have primary amine groups on their structure.

Regarding the characterization of PLGA-TK-COOH polymers, ^{1}H NMR analysis were performed on PLGA-NH_2 and PLGA-TK-COOH. The characteristic peaks form the chemical groups on LA (lactic acid) and GA (glycolic acid) blocks of PLGA can be

observed in both spectra (Figure 21A and B) at chemical shifts 5.15, 1.51 and 4.76 ppm. These chemical shifts are in accordance with those reported in the literature for the two PLGA structural units: the most intense signals of CH (5.1 ppm) and CH_3 (1.4 ppm) from lactic acid and CH_2 (4.8 ppm) from GA [257]. Nevertheless, the chemical shifts appertaining to TK.C.L. could not be identified and this might be due to the high difference of molecular weight between PLGA (~16 KDa) and the linker (0.252 KDa) that make difficult to detect ^{1}H NMR signals from the linker. In addition, the chemical shift that correspond to the methyl group on LA block (1.51 ppm) match with the chemical shift of TK linker methyl group (1.5 ppm) (Figure 8) [130].

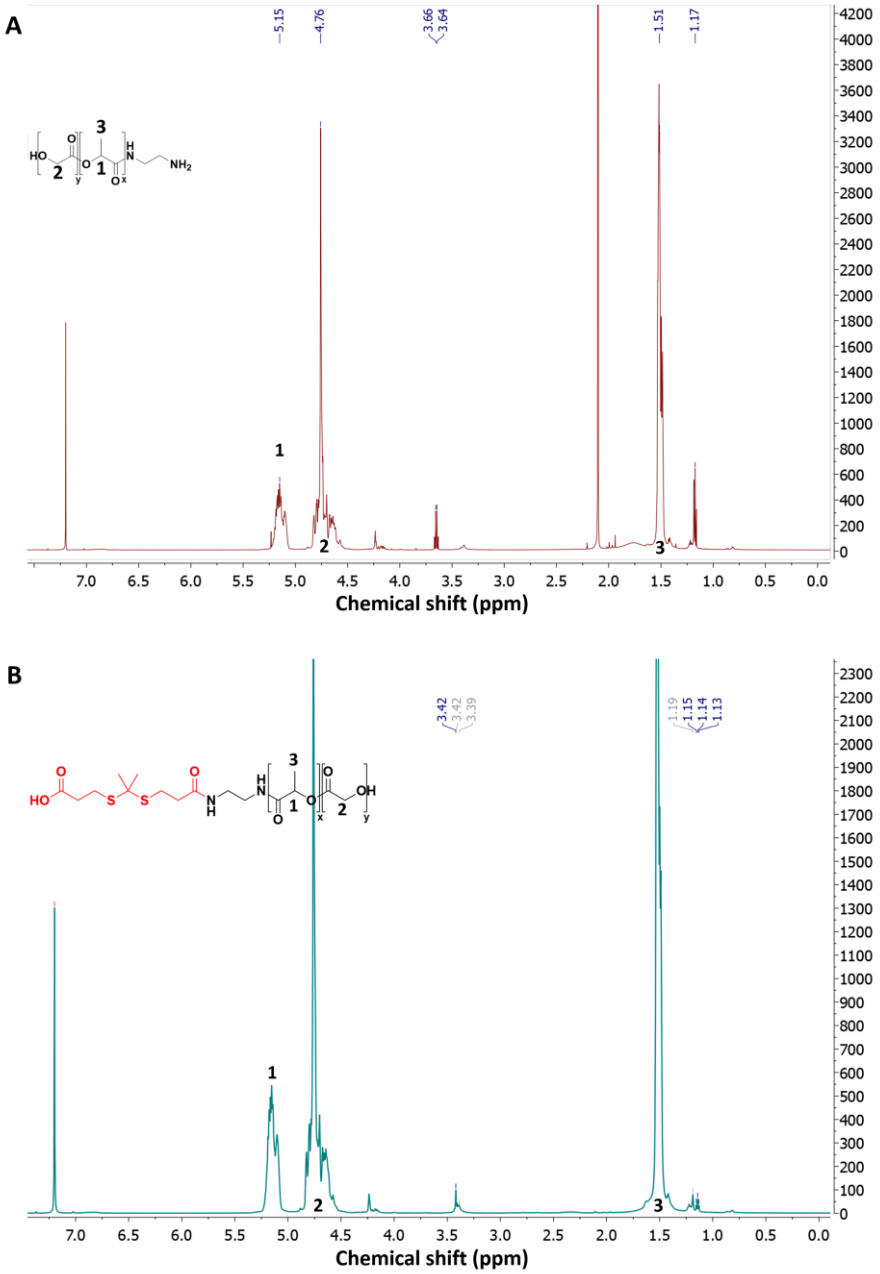

Figure 21: ^{1}H NMR spectra of PLGA-NH_2 (A) and PLGA-TK-COOH (B) polymers in $CDCl_3$.

In order to better characterized the conjugation of TK.C.L. to PLGA-NH_2, a 2D ^{1}H-^{1}H COSY spectra of both PLGA-NH_2 and PLGA-TK-COOH were performed (Figure 22). We could identify two signals on PLGA-TK-COOH spectrum at 3.41 ppm and 1.14 ppm that established ^{1}H-^{1}H interactions (corresponding to neighbor protons), that were shifted with respect to 3.67 ppm and 1.17 ppm neighbor protons on PLGA-NH_2 spectrum (Figure 22). These two new ^{1}H NMR signals (3.41 ppm and 1.14 ppm) on PLGA-TK-COOH spectrum correspond to the shifted quadruplet and triplet signals on PLGA-NH_2 spectrum

(3.67 and 1.17) (Figure 21A). Thus, these two shifts can be associated to the terminal CH_2 protons near the amide bond among PLGA-NH_2 to TK.C.L. confirming covalent conjugation.

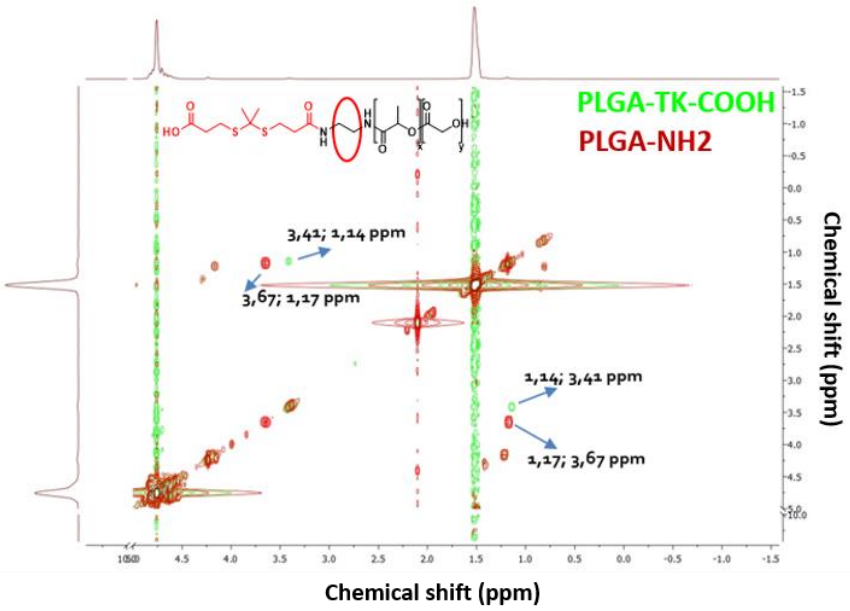

Figure 22: Superposed 2D ^{1}H-^{1}H COSY NMR spectra of PLGA-NH_2 and PLGA-TK-COOH polymers. The arrows indicate the ^{1}H-^{1}H chemical shifts observed on both spectra that differed from one another. Circled in red are shown the terminal -CH_2 groups on PLGA-TK-COOH with shifted ^{1}H-^{1}H interactions in relation to PLGA-NH_2.

In order to characterize the MW of PLGA-TK-COOH polymer, we firstly performed MALDI-TOF analyses by using MALDI matrices of sinapinic acid and (2- (4-hydroxyphenylazo) benzoic acid. Nevertheless, since the sample could not be ionized, the average molecular weight could not be obtained.

Thus, to complete the characterization of this polymer, we used a less sensitive method to calculate average MW by means of GPC/SEC chromatography, based on Polystyrene calibration curve. Both polymers, PLGA-NH_2 and PLGA-TK-COOH were analyzed by this technique, being the main results summarized in Figure 23 and Table 6. The calculated average MW of PLGA-NH_2 polymer was of 18097 g/mol, while the average MW of PLGA-TK-COOH was right-shifted with respect to that of the PLGA-NH_2, suggesting that a chemical bond between PLGA-NH_2 and TK-C.L. was obtained. On the other hand, a second peak (peak 2) with a low average MW of 218 g/mol, was identified and due to its MW is close to that of TK.C.L. (252,4 g/mol), this result suggests that this

second peak corresponds to TK-C.L. impurities. Thus, this result indicated that a deeper and more effective purification of PLGA-TK-COOH must be done.

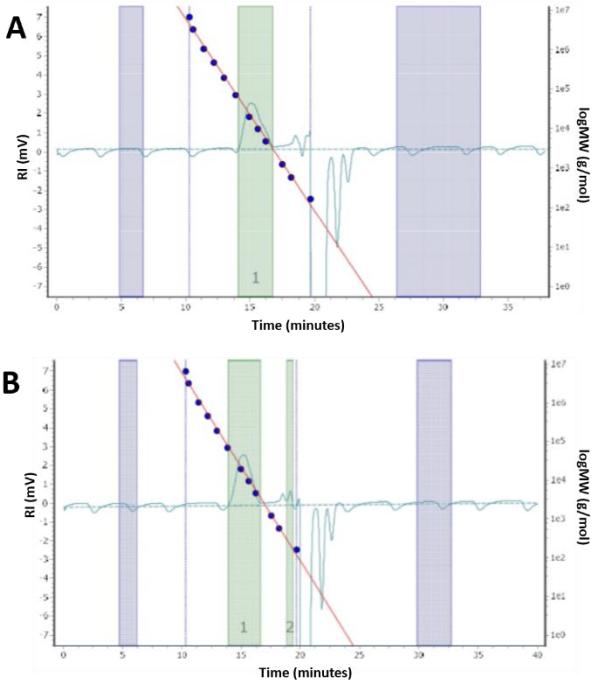

Figure 23: GPC/SEC chromatograms of PLGA-NH_2 and PLGA-TK-COOH detected by Refractive Index (RI). Overlapped to these chromatograms it is shown the calibration curve obtained with Polystyrene (PS) standards of different molecular weight. **A.** PLGA-NH_2 (Peak 1) and **B.** PLGA-TK-COOH (Peak 1).

Polymer	Peak	Max. RT (min)	Mn (g/mol)	Mw (g/mol)	PdI
PLGA-NH_2	1	15.05	12085	18097	1.497
PLGA-TK-COOH	1	15.23	13641	19457	1.426
	2	19.13	214	218	1.019

Table 6: GPC/SEC results obtained with PLGA-NH_2 and PLGA-TK-COOH polymers.

5.4.2. Synthesis and characterization of PLGA-TK-PLGA co-polymer

The synthesis of PLGA-TK-PLGA co-polymer was carried out by carbodiimide mediated PLGA-TK-COOH coupling to PLGA-NH_2, by using a slightly higher molar ratio of PLGA-TK-COOH to PLGA-NH_2. The product and derivatization yields obtained from the reaction were of 98% and 97.3%, respectively. The characterization of this co-polymer was carried out by GPC/SEC chromatography and the results obtained summarized in Table 7.

An average MW of 23.9 KDa, which was shifted respect to the average MW of the starting homopolymers: PLGA-TK-COOH (19.5 KDa) and PLGA-NH_2 (18.1 KDa), was calculated from the PS MW standard curve.

The average molecular weight obtained was higher than either PLGA-TK-COOH or PLGA-NH_2 and it might be indicating co-polymer formation. Nevertheless, the expected average weight would have been closer to the sum of the molecular weights of each polymer (~32.0 KDa), and it might be due to GPC columns separates the polymer molecules on the basis of their effective size in solution that depends on the size or hydrodynamic radius.

On the other hand, a second peak with and average molecular weight of 223 g/mol (Figure 24), can be associated to TK.C.L. as in the case of PLGA-TK-COOH.

Thus, additional studies will be made in order to further characterize the co-polymer, such as ^{1}H NMR by considering the integration values of the main peaks and analyzing the possible difference of the integration ratios.

Polymer	Peak	Max. RT (min)	Mn (g/mol)	Mw (g/mol)	PdI
PLGA-TK-PLGA	1	14.95	15885	23882	1.503
	2	19.10	220	223	1.014

Table 7: GPC/SEC results obtained with PLGA-TK-PLGA polymers.

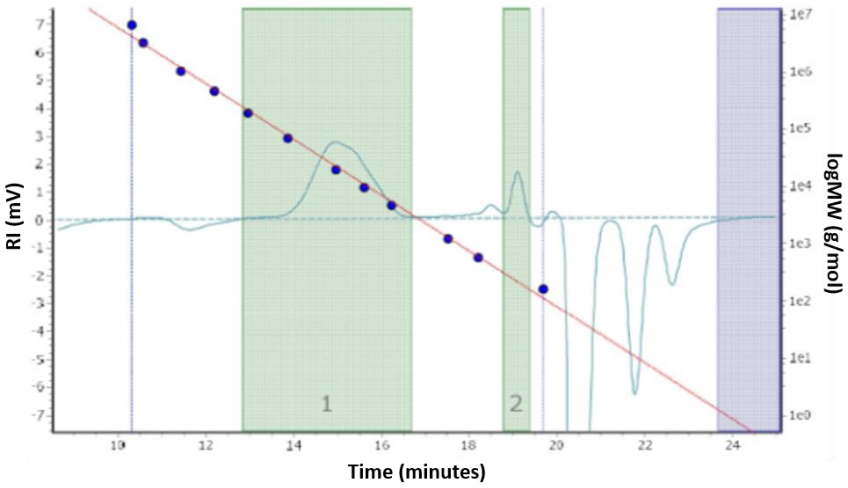

Figure 24: GPC/SEC chromatogram of PLGA-TK-PLGA detected by Refractive Index (RI). Overlapped to these chromatograms it is shown the calibration curve obtained with Polystyrene (PS) standards of different molecular weight. Peak 1: PLGA-TK-PLGA co-polymer, Peak 2: TK.C.L. impurity.

5.4.3. TK-PLGA NPs prepared by single emulsion and nanoprecipitation

With the aim of preparing TK-functionalized PLGA NPs for their potential application in the delivery of drugs to extracellular disease sites featured by ROS, these TK-PLGA NPs were prepared following the most common methods to prepare NPs starting from biodegradable polymers: single emulsion and nanoprecipitation [258], using as NP stabilizers, the anionic and non-anionic surfactants, Polyvinyl alcohol (PVA) and Pluronic F-68 [261], respectively (Figure 25), which were both approved by the FDA for their clinical use [246,260].

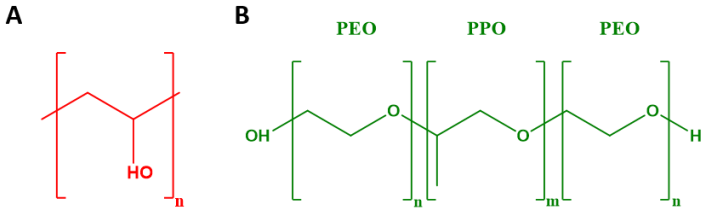

Figure 25: Chemical structures of surfactants used to prepare NPs. A. PVA and **B.** Pluronic F-68. This surfactant is a poloxamer comprised of a tri-block co-polymer formed by polypropylene oxide (PPO) and polyethylene oxide (PEO) [261].

Regarding TK-PLGA NPs prepared by single emulsion and nanoprecipitation with PVA 1% (w/v), form their PCS characterization in terms of mean size and surface charge, it could be observed (Table 8 A and B) that they did not vary in relation to their respective control NPs.

A

PLGA NP type	Size (nm)	PdI	Z Potential (mV)
PLGA (Control)	230.8±0.7	0.0965±0.019	-11±0.8
TK-PLGA 10%	220.4±2.2	0.0675±0.011	-18.7±0.212

B

PLGA NP type	Size (nm)	PdI	Z Potential (mV)
PLGA (Control)	160.6 ±2.3	0.049±0.003	-25.4±4.5
TK-PLGA 10%	164.4±0.141	0.046±0.031	-21.9±0.6
TK-PLGA 20%	162.3±2.5	0.039±0.053	-22±1

Table 8: TK-PLGA NPs prepared by using PVA 1 % (w/v). A. TK-PLGA NPs prepared by single emulsion. **B.** TK-PLGA NPs prepared by nanoprecipitation.

ESCA analysis, which is a method used for the identification of the atoms that are present on the surface of materials, can be used to analyze the atomic composition on the surface of NPs [262]. This method was already applied by our group to validate the surface functionalization of PLGA NPs with BBB-targeting peptide g7, by identifying the characteristic N signal associated with the peptide [254].

Since all the materials forming PLGA and TK-PLGA NPs have in common C, H and O atoms, but not S atoms, which are only present in TK group, the identification of S signal could be used as proof of TK surface accessibility.

In this regard, we analyzed the surface of TK-PLGA NPs prepared by single emulsion and nanoprecipitation methods with PVA 1%. Nevertheless, S was not detected in any of the TK-PLGA NPs formulated (Figure 26A). The presence of S signal could only be detected on PLGA-TK-COOH polymer, with an atom abundancy of 0.4% (Figure 26) probably indicating the presence of TK onto surface on NPs. Even if this intensity is very low and taking into consideration that NPs have been formulated starting from 10 or 20 % of this polymer, the percentage of sulfide if present on the surface of the nanoparticles should be of 0.04% and 0.08%, respectively, that are both below the sensitivity limit of this technique for sulfide (0.1%) [263].

Hence, in order to confirm availability of TK group onto the surface of the NPs, it would be necessary to perform additional studies such as Fourier transformed infrared spectroscopy (FTIR) and NMR [264].

A

Samples analysed	C (%)	O (%)	N (%)	S (%)
1-PLGA (Control) NPs	66.9	33.1	-	-
2-PLGA-TK (10%) NPs	34.1	65.9	-	-
3-PLGA (Control) NPs	67.9	32.1	-	-
4-PLGA-TK (10%) NPs	71.4	28.6	0.7	-
5-PLGA-TK (20%) NPs	68.3	31.7	-	-
6-PLGA-TK-COOH polymer	85	15	1.1	0.4

B

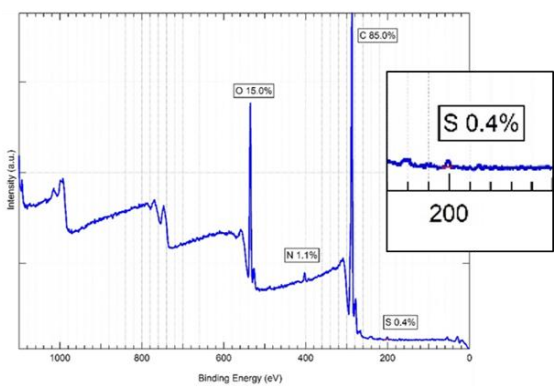

Figure 26: ESCA analysis. A. Chemical composition of PLGA NPs prepared by single emulsion (1-2) and nanoprecipitation (3-5) with PVA 1% (w/v) and PLGA-TK-COOH polymer (6). **B.** ESCA spectrum of PLGA-TK-COOH, in which the sulfide peak at 200 eV is magnified.

Regarding TK-PLGA NPs prepared by nanoprecipitation with Pluronic F-68, differences among the different formulations in terms of size and surface charge were not find, being of similar size and charge to control NPs (Table 9). As in the case of TK-based NPs prepared with PVA 1%, the possible accessibility of TK on NP surface needs for further evaluation by the same methodologies proposed for those prepared with PVA 1% (FTIR and NMR).

PLGA NP type	Size (nm)	PdI	Z Potential (mV)
PLGA (Control)	136.2 ± 1.3	0.135 ± 0.014	-36.3 ± 0.3
TK-PLGA 10%	141.8 ± 0.5	0.158 ± 0.004	-34 ± 1
TK-PLGA 20%	129.6 ± 0.2	0.128 ± 0.019	-36.7 ± 1

Table 9: TK-PLGA NPs prepared by nanoprecipitation with Pluronic F-68 3 % (w/v). The percentages between parenthesis refers to the percentage of PLGA-TK-COOH used in NP formulation.

5.4.4. Preparation of PLGA-TK-PLGA NPs by nanoprecipitation with Pluronic F-68 3 % (w/v)

Aiming for the formulation of ROS-responsive TK-based NPs for the encapsulation of drugs, PLGA-TK-PLGA co-polymer was used to formulate TK-based NPs. The results in terms of NP average size and charge, demonstrated that TK-based PLGA NPs made up from PLGA-TK-PLGA co-polymer, could be formulated (Table 10). In addition, the size of PLGA-TK-PLGA NPs in comparison to PLGA control NPs, was slightly higher in diameter. This result can be associated to the higher molecular weight of the co-polymer (~32 KDa) in relation to PLGA (11.0 KDa) and PLGA-TK-COOH (~16 KDa), that might influence in the physicochemical properties of the NPs obtained. Remarkably, homogeneity index remains at more than good values and even ameliorates in the case of PLGA-TK-PLGA formulation.

PLGA NP type	Size	PdI	Z Potential (mV)
PLGA (Control)	140.8±0.212	0.151±0.011	-26.5±0.212
PLGA-TK-PLGA	184.6±6.5	0.081±0.044	-26.4±0.424

Table 10: PLGA-TK-PLGA NPs prepared by nanoprecipitation with surfactant F-68 3% (w/v).

5.5. Conclusion

In this chapter results we therefore report preliminary data based on the use of TK-diacid containing linker exploited to prepare PLGA-TK-COOH polymer, PLGA-TK-PLGA co-polymer and TK-based NPs from these polymers.

It is clear that it is possible to obtain ROS-responsive PLGA-TK-COOH polymers with high product and derivatization yields as well as we evidenced the exploitation of a well-known and reported method to quantify terminal amine groups, for the first time applied on non-soluble high molecular weight polymers with PLGA-NH_2 in order to determine the derivatization yield of PLGA-TK-COOH, being a valuable technique to characterize PLGA polymer modifications such as PLGA prodrugs.

By means of proper characterization data, we could confirm the suitability of these polymers to be used to formulate TK-functionalized NPs aiming for the selective drug release in response to ROS. Being preliminary data, it is obvious that deeper and focused studies are still to be performed, especially regarding the evaluation of TK disposition onto the surface of the nanoparticles, and secondly the accessibility of TK groups to respond to ROS.

We can conclude that TK-technology can be exploited to prepare prodrugs and co-polymers to obtain NPs that hold great promise to be employed for the delivery of drugs to extracellular or intracellular sites featured by high concentrations of ROS.

Chapter 6:

Conclusions and perspectives

6.1. Conclusions

Nowadays, several DDS aiming to improve the bioavailability and specificity of a great number of drugs were developed. The design of "Smart" DDS that release their payloads or attached drugs in response to a specific stimulus, offer the possibility to control drug release at the site of the disease and thus, can improve the effectivity of conventional DDS. In this regard, "Smart" DDS that respond to endogenous and exogenous stimuli (e.g. GSH, pH, ROS, light, magnetism, etc) were proposed. Since several pathologies share the common feature of producing high levels of ROS (e.g. inflammatory diseases and cancer), the exploitation of this stimulus for the design of ROS-responsive DDS was growing over the past 15 years [89]. Among different sensitive materials that respond to ROS, TK materials harbor attractive features: a) ability to respond to the most relevant ROS, b) biocompatibility and c) versatility to be attached to polymers and molecules by its incorporation in linkers, that turn them interesting for the design of ROS-responsive DDS.

Either synthetic or natural polymers, are being widely used to obtain ROS-responsive polymers and prodrugs, and due to their simplicity and biocompatibility, DDS made up from these polymers or prodrugs, can increase their chance of being translated into the clinic.

Therefore, this PhD thesis was centered on the use of synthetic, biodegradable and FDA approved polymers: PEG and PLGA as starting materials for the design of TK-based ROS-responsive polymers and ROS-responsive prodrugs, for the potential treatment of ROS featuring brain diseases, such as GBM and AD.

Chapter 3. TK-technology: Proof-of-concept studies

The first objective of this PhD thesis was to confirm the feasibility of the application of TK-materials to produce ROS-responsive polymers and conjugates, aiming for the potential design of prodrug for cancer therapy. In this regard, we firstly synthesized and characterized TK diacid C.L. and then proceed with its covalent conjugation to mPEG polymer. The following results were obtained:

- ***Production of ROS-responsive mPEG-TK-COOH polymer*** *with a high derivatization yield (84%) and purity.*
- ***Validation of the response of mPEG-TK-COOH to ROS,*** *which was concentration dependent, evidenced by the disappearance of TK methyl group signal on ^{1}H NMR spectrum.*

In order to validate the possible release of a drug from ROS-responsive prodrug, we performed proof-of-concept studies by preparing a fluorescent conjugate with Cy5 NIR dye, by means of conjugating Cy5 to mPEG-TK-COOH polymer through TK linkages. An alternative non-ROS-responsive conjugate without TK bonds was prepared for comparison purposes.

- ***Release of Cy5 from mPEG-TK-Cy5*** *is time-dependent, and in contraposition, no Cy5 release was detected in the case of mPEG-Cy5.*
- ***Protection of Cy5 fluorescence from ROS-mediated quenching by TK linkages:*** *obtained by measuring the total fluorescence of mPEG-TK-Cy5 and mPEG-Cy5 samples after 48 h of incubation in simulated ROS- conditions, in which we could observe that while the fluorescence of mPEG-Cy5 samples was decreased, the fluorescence of mPEG-TK-Cy5 samples was not modified with respect to initial.*

On the other hand, we also perform ***in vitro*** **studies on brain cancer cells and astrocytes** cells as control, in which we firstly measured the **intrinsic intracellular levels** of ROS comparatively in all cell lines.

- ***Increase in intracellular concentration of ROS in cancer cells****: either on GBM (C6) or neuroblastoma (SH SY5Y) cells, the intracellular concentrations of ROS were higher than in astrocytes cells.*
- ***Intracellular distribution and drug release in cancer cells:*** *we studied the intracellular distribution of both prodrugs on all the cell lines and found that Cy5 was only released in High-ROS cells: C6 and SH SY5Y, but not in astrocytes cells. Furthermore, the non-ROS responsive prodrug, did not show to release Cy5 on any of these cell lines. Thus, from these results we could confirm that Cy5 could only be released from mPEG-TK-Cy5 and not from mPEG-Cy5 inside cancer cells.*

Therefore, from this first part of the PhD thesis, it can be concluded that mPEG-TK-Cy5 conjugate, due to its ability to selectively deliver drugs upon ROS stimulus while maintaining

"drug" stability (prevention of ROS undesired actions as fluorescence quenching), the application of **TK-technology in the design of prodrugs, constitutes a promising approach for future therapeutics against cancer**. Furthermore, considering that both mPEG and TK-linker do not address potential safety issues, mPEG-TK-COOH offers **biocompatibility** and thus, applicability in terms of starting polymer to produce ROS-responsive prodrugs **for cancer therapy** as well as **other high ROS diseases**, such as **inflammatory and neurodegenerative diseases**.

Chapter 4. TK-based ROS-responsive cytotoxic prodrug for GBM treatment

The second objective of the PhD thesis was to prepare a TK-**based chemotherapeutic prodrug for GBM treatment.** In this regard we used the ROS-responsive polymer PEG-TK-COOH (which was properly obtained and validated within objective 1), for the design of an ROS-responsive prodrug with Melphalan, namely mPEG-TK-MPH. Like in objective 1, we also produced a non-ROS-responsive prodrug without TK linkages, namely mPEG-MPH, as control.

- ***Full chemical and technological characterization****: NMR spectroscopy and mean MW of prodrug were conducted.*
- ***Self-assembly micelles****: either mPEG-TK-MPH or mPEG-MPH can undergo self-assembling into micelles among 260-300 nm size, at a concentration range of 10 mg/mL to 0.1 mg/mL.*

We then performed ***in vitro*** **studies on mice GBM cell lines and Astrocyte as control** in which we studied real time mPEG-TK-MPH cytotoxicity in comparison to mPEG-MPH and free MPH at a concentration of 11 μM (IC50 reported in the literature for MPH on C6 cells).

- ***Selectivity:*** *cytotoxicity of mPEG-TK-MPH on C6 cells was significantly higher than with mPEG-MPH, while on astrocytes cells, any of the prodrugs showed to be cytotoxic on the cells, demonstrating to be selective towards C6.*

We also performed ***in vitro*** **assays on human GBM cells lines** (U87MG and U251MG), in which we firstly measured the intrinsic ROS levels produced by each type of cells and then assayed **prodrug cytotoxicity.**

- ***ROS levels on U251MG*** *were higher than those produced on U87MG cells.*

- ***Cytotoxicity****: at high equivalent MPH concentrations (500 and 1000 μM), mPEG-TK-MPH was only cytotoxic on High-ROS U251MG cells, with MPH displaying the highest cytotoxicity on both cell lines.*
- ***Effect of external induction of ROS****: The co-treatment with a non-toxic concentration of H_2O_2, demonstrated to improve the cytotoxicity of mPEG-TK-MPH on U251MG cells.*

In view of this last result, we finally evaluated if the **exposure of human GBM cells to IR (X-ray) could also induce the production of intracellular ROS** and thus, improve mPEG-TK-MPH cytotoxicity.

- *We could not observe an improvement of the cytotoxicity on U251MG irradiated and prodrug treated cells in comparison to the cells which were only treated with the prodrug, being the dose or the frequency used, not enough to induce additional TK cleavage.*

It can be concluded that TK-**technology worked with mPEG-TK-MPH on High-ROS cells (C6 and U251MG)**.

Despite the cleavage of TK linkages and MPH release was not high enough to observe higher antitumor efficacy *in vitro* in comparison to the free drug, **this prodrug showed to be selective towards GBM cells and improve MPH solubility**.

Thus, it is worth to perform *in situ* experiments in GBM mice models, consisting on the combination of this prodrug with external stimuli, searching for clinical applicability in localized GBM treatment. Thus, the work presented in this chapter, represent a starting point for a rationale design of innovative and tailored ROS-responsive prodrugs.

Chapter 5. PLGA-TK-COOH: Synthesis, characterization and formulation of TK-based PLGA NPs

In the third part of this PhD thesis, still at a preliminary level, the aim was to apply TK-technology on PLGA polymers, aiming for the future preparation of ROS-responsive PLGA NPs for the delivery of drugs to extra and intracellular compartments.
In this regard, we synthesized another type of polymeric ROS-responsive conjugate with poly-lactide-co-glycolide (PLGA), namely PLGA-TK-COOH, with the aim of creating ROS-responsive polymeric PLGA conjugates and ROS-responsive PLGA-NPs.

We reached some preliminary results as:

- ***Full chemical characterization of produced polymers***
- ***Set up of technological formulations***: *starting from different ratios of PLGA-TK-COOH and PLGA polymers, ROS-responsive TK-surface functionalized PLGA-NPs by single emulsion and nanoprecipitation techniques by means of anionic and neutral surfactant (PVA and F-68, respectively).*
- ***Co-polymer production and nanoparticles formulation:*** *PLGA-TK-COOH was also used to synthesize PLGA-TK-PLGA co-polymer, from which ROS-responsive PLGA-NPs were formulated by nanoprecipitation.*
- ***Full chemical-physical characterization of produced nanoparticles****: both types of PLGA-NPs were characterized in terms of their mean particle size and surface charge.*

We conclude the **TK feasibility to be used for the formulation of TK-based PLGA-NPs.** Nevertheless, validation studies regarding TK-NP-surface accessibility must be done among other studies, including the accessibility of TK-linkages to be cleaved by ROS.

6.2. Perspectives

In order to achieve high antitumor efficiency of ROS-responsive DDS in cancer therapy, it is generally necessary to enhance intracellular ROS production by means of combination with an external stimuli, such as light and ultrasound, or amplifiers of ROS (e.g., Lapa and α-TOS) [152,71]. Since radiotherapy is applied in almost a half of cancer patients [265], being a standard of care along with chemotherapy in GBM [266]; the use of X-ray in combination with ROS-responsive DDS against this disease, is very attractive. As far as we know, the use of TK-based DDS in combination with X-ray was not proposed before. Accordingly, one of the first perspectives of this work is to optimize the X-ray dose and irradiation frequency applied to human GBM cells, in order to achieve high intracellular ROS concentrations for an improved *in vitro* cytotoxicity of mPEG-TK-MPH on these cells. In addition, the potential benefit of combinatorial therapies with this

prodrug, will be studied in an in-situ model of localized GBM aiming for a possible clinical translation.

On the other hand, due to the starting ROS-responsive polymer used to obtain mPEG-TK-MPH (mPEG-TK-COOH), is made up from biocompatible components [212,123], another perspective is to extend the application of this polymer to other diseases featured by ROS. Thus, the following perspective will be to prepare ROS-responsive prodrugs starting from mPEG-TK-COOH polymer, for the treatment of High-ROS diseases such as inflammation and neurodegenerative diseases.

Concerning the use of TK-based PLGA NPs, before to move forward with either, drug attachment or encapsulation, the first perspective of this part of the thesis, will be to assess the accessibility of TK linkages to ROS in ROS-simulated conditions. As a second perspective, the combination of TK-based NPs with a a targeting ligand aiming for BBB-crossing, such as g7 peptide [52], is planned for AD application. Since our research group have reached promising results in terms of reducing Aβ aggregates in neurons treated with PLGA NPs loaded with anti- Aβ peptide (KLVFF) [255] or anti-amyloidogenic agent (curcumin) [254]; these drugs represent good candidates to be used with TK-based PLGA NPs.

Bibliography:

[1] Kim S, Seong K, Kim O, et al. Polyoxalate Nanoparticles as a Biodegradable and Biocompatible Drug Delivery Vehicle. Biomacromolecules. 2010;11:555–560.

[2] Reddy PD, Swarnalatha D. Recent Advances in Novel Drug Delivery Systems. :3.

[3] Shi J, Wang B, Wang L, et al. Fullerene (C60)-based tumor-targeting nanoparticles with "off-on" state for enhanced treatment of cancer. J. Controlled Release. 2016;235:245–258.

[4] Höcherl A, Jäger E, Jäger A, et al. One-pot synthesis of reactive oxygen species (ROS)-self-immolative polyoxalate prodrug nanoparticles for hormone dependent cancer therapy with minimized side effects. Polym. Chem. 2017;8:1999–2004.

[5] Kwon EJ, Lo JH, Bhatia SN. Smart nanosystems: Bio-inspired technologies that interact with the host environment. Proc. Natl. Acad. Sci. 2015;112:14460–14466.

[6] Liu D, Yang F, Xiong F, et al. The Smart Drug Delivery System and Its Clinical Potential. Theranostics. 2016;6:1306–1323.

[7] Yue C, Yang Y, Zhang C, et al. ROS-Responsive Mitochondria-Targeting Blended Nanoparticles: Chemo- and Photodynamic Synergistic Therapy for Lung Cancer with On-Demand Drug Release upon Irradiation with a Single Light Source. Theranostics. 2016;6:2352–2366.

[8] Wen J, Yang K, Xu Y, et al. Construction of A Triple-Stimuli-Responsive System Based on Cerium Oxide Coated Mesoporous Silica Nanoparticles. Sci. Rep. 2016;6:srep38931.

[9] Lee Y, Lee S, Lee DY, et al. Multistimuli-Responsive Bilirubin Nanoparticles for Anticancer Therapy. Angew. Chem. Int. Ed. 2016;55:10676–10680.

[10] Wang D, Jin Y, Zhu X, et al. Synthesis and applications of stimuli-responsive hyperbranched polymers. Prog. Polym. Sci. 2017;64:114–153.

[11] Tapeinos C, Pandit A. Physical, Chemical, and Biological Structures based on ROS-Sensitive Moieties that are Able to Respond to Oxidative Microenvironments. Adv. Mater. 2016;28:5553–5585.

[12] Li F, Lu J, Kong X, et al. Dynamic Nanoparticle Assemblies for Biomedical Applications. Adv. Mater. 2017;29:n/a-n/a.

[13] Karimi M, Ghasemi A, Zangabad PS, et al. Smart micro/nanoparticles in stimulus-responsive drug/gene delivery systems. Chem. Soc. Rev. 2016;45:1457–1501.

[14] Raza H. Dual Localization of Glutathione S-Transferase in the Cytosol and Mitochondria: Implications in Oxidative Stress, Toxicity and Disease. FEBS J. 2011;278:4243–4251.

[15] Alvarez-Lorenzo C, Concheiro A. Smart drug delivery systems: from fundamentals to the clinic. Chem. Commun. 2014;50:7743–7765.

[16] Zhang X, Zhang T, Ma X, et al. The Design and Synthesis of Dextran-Doxorubicin Prodrug-based pH-Sensitive Drug Delivery System for Improving Chemotherapy Efficacy. Asian J. Pharm. Sci. [Internet]. 2019 [cited 2020 Jan 4]; Available from: http://www.sciencedirect.com/science/article/pii/S1818087619308323.

[17] Chang M, Zhang F, Wei T, et al. Smart linkers in polymer–drug conjugates for tumor-targeted delivery. J. Drug Target. 2016;24:475–491.

[18] Ou K, Kang Y, Chen L, et al. H2O2-responsive nano-prodrug for podophyllotoxin delivery. Biomater. Sci. 2019;7:2491–2498.

[19] Binding of alpha5 monoclonal antibody to cell surface alpha5beta1 integrin modulates MMP-2 and MMP-7 activity in B16F10 melanoma cells. - Abstract - Europe PMC [Internet]. [cited 2020 Jan 3]. Available from: https://europepmc.org/article/med/14529092.

[20] Wu J, Chen J, Feng Y, et al. Tumor microenvironment as the "regulator" and "target" for gene therapy. J. Gene Med. 2019;21:e3088.

[21] Papadimitriou SA, Salinas Y, Resmini M. Smart Polymeric Nanoparticles as Emerging Tools for Imaging—The Parallel Evolution of Materials. Chem. – Eur. J. 2016;22:3612–3620.

[22] Du J, Lane LA, Nie S. Stimuli-responsive nanoparticles for targeting the tumor microenvironment. J. Controlled Release. 2015;219:205–214.

[23] Seidi F, Jenjob R, Crespy D. Designing Smart Polymer Conjugates for Controlled Release of Payloads. Chem. Rev. 2018;118:3965–4036.

[24] Raza A, Rasheed T, Nabeel F, et al. Endogenous and Exogenous Stimuli-Responsive Drug Delivery Systems for Programmed Site-Specific Release. Molecules [Internet]. 2019 [cited 2020 Jan 5];24. Available from: https://www.ncbi.nlm.nih.gov/pmc/articles/PMC6470858/.

[25] Liang J, Liu B. ROS-responsive drug delivery systems. Bioeng. Amp Transl. Med. 2016;1:239–251.

[26] El-Sawy HS, Al-Abd AM, Ahmed TA, et al. Stimuli-Responsive Nano-Architecture Drug-Delivery Systems to Solid Tumor Micromilieu: Past, Present, and Future Perspectives. ACS Nano. 2018;12:10636–10664.

[27] Mura S, Nicolas J, Couvreur P. Stimuli-responsive nanocarriers for drug delivery. Nat. Mater. 2013;12:991–1003.

[28] Chen Y, Li H, Deng Y, et al. Near-infrared light triggered drug delivery system for higher efficacy of combined chemo-photothermal treatment. Acta Biomater. 2017;51:374–392.

[29] Li B, Lin L, Lin H, et al. Photosensitized singlet oxygen generation and detection: Recent advances and future perspectives in cancer photodynamic therapy. J. Biophotonics. 2016;9:1314–1325.

[30] Yue C, Zhang C, Alfranca G, et al. Near-Infrared Light Triggered ROS-activated Theranostic Platform based on Ce6-CPT-UCNPs for Simultaneous Fluorescence Imaging and Chemo-Photodynamic Combined Therapy. Theranostics. 2016;6:456–469.

[31] Phua SZF, Xue C, Lim WQ, et al. Light-Responsive Prodrug-Based Supramolecular Nanosystems for Site-Specific Combination Therapy of Cancer. Chem. Mater. 2019;31:3349–3358.

[32] Yuan Y, Xu S, Zhang C-J, et al. Light-responsive AIE nanoparticles with cytosolic drug release to overcome drug resistance in cancer cells. Polym. Chem. 2016;7:3530–3539.

[33] Wan G-Y, Liu Y, Chen B-W, et al. Recent advances of sonodynamic therapy in cancer treatment. Cancer Biol. Med. 2016;13:325–338.

[34] Wu P, Dong W, Guo X, et al. ROS-Responsive Blended Nanoparticles: Cascade-Amplifying Synergistic Effects of Sonochemotherapy with On-demand Boosted Drug Release During SDT Process. Adv. Healthc. Mater. 2019;8:1900720.

[35] Oak M, Mandke R, Singh J. Smart polymers for peptide and protein parenteral sustained delivery. Drug Discov. Today Technol. 2012;9:e131–e140.

[36] Wang L, Fan F, Cao W, et al. Ultrasensitive ROS-Responsive Coassemblies of Tellurium-Containing Molecules and Phospholipids. ACS Appl. Mater. Interfaces. 2015;7:16054–16060.

[37] Noh J, Kwon B, Han E, et al. Amplification of oxidative stress by a dual stimuli-responsive hybrid drug enhances cancer cell death. Nat. Commun. 2015;6:ncomms7907.

[38] Kumari S, Badana AK, G MM, et al. Reactive Oxygen Species: A Key Constituent in Cancer Survival. Biomark. Insights. 2018;13:1177271918755391.

[39] Freitas M, Baldeiras I, Proença T, et al. Oxidative stress adaptation in aggressive prostate cancer may be counteracted by the reduction of glutathione reductase. FEBS Open Bio. 2012;2:119–128.

[40] Tang M, Zheng Q, Tirelli N, et al. Dual thermo/oxidation-responsive block copolymers with self-assembly behaviour and synergistic release. React. Funct. Polym. 2017;110:55–61.

[41] Tang M, Hu P, Zheng Q, et al. Polymeric micelles with dual thermal and reactive oxygen species (ROS)-responsiveness for inflammatory cancer cell delivery. J. Nanobiotechnology. 2017;15:39.

[42] Chen G, Deng H, Song X, et al. Reactive oxygen species-responsive polymeric nanoparticles for alleviating sepsis-induced acute liver injury in mice. Biomaterials. 2017;144:30–41.

[43] Bhattacharyya A, Chattopadhyay R, Mitra S, et al. Oxidative Stress: An Essential Factor in the Pathogenesis of Gastrointestinal Mucosal Diseases. Physiol. Rev. 2014;94:329.

[44] Jäger E, Höcherl A, Janoušková O, et al. Fluorescent boronate-based polymer nanoparticles with reactive oxygen species (ROS)-triggered cargo release for drug-delivery applications. Nanoscale. 2016;8:6958–6963.

[45] Wang X, Michaelis EK. Selective Neuronal Vulnerability to Oxidative Stress in the Brain. Front. Aging Neurosci. [Internet]. 2010 [cited 2018 Apr 19];2. Available from: https://www.ncbi.nlm.nih.gov/pmc/articles/PMC2874397/.

[46] Cheignon C, Tomas M, Bonnefont-Rousselot D, et al. Oxidative stress and the amyloid beta peptide in Alzheimer's disease. Redox Biol. 2018;14:450–464.

[47] Manoharan S, Guillemin GJ, Abiramasundari RS, et al. The Role of Reactive Oxygen Species in the Pathogenesis of Alzheimer’s Disease, Parkinson’s Disease, and Huntington’s Disease: A Mini Review. Oxid. Med. Cell. Longev. 2016;2016:e8590578.

[48] Bates GP, Dorsey R, Gusella JF, et al. Huntington disease. Nat. Rev. Dis. Primer. 2015;1:1–21.

[49] Yang J, Yang J, Liang SH, et al. Imaging hydrogen peroxide in Alzheimer's disease via cascade signal amplification. Sci. Rep. 2016;6:35613.

[50] Granzotto A, Zatta P. Resveratrol and Alzheimer's disease: message in a bottle on red wine and cognition. Front. Aging Neurosci. [Internet]. 2014 [cited 2017 Oct 9];6. Available from: https://www.frontiersin.org/articles/10.3389/fnagi.2014.00095/full.

[51] Feng Y, Wang X. Antioxidant Therapies for Alzheimer's Disease. Oxid. Med. Cell. Longev. [Internet]. 2012 [cited 2019 Oct 10];2012. Available from: https://www.ncbi.nlm.nih.gov/pmc/articles/PMC3410354/.

[52] Vilella A, Tosi G, Grabrucker AM, et al. Insight on the fate of CNS-targeted nanoparticles. Part I: Rab5-dependent cell-specific uptake and distribution. J. Control. Release Off. J. Control. Release Soc. 2014;174:195–201.

[53] Jiang X-C, Xiang J-J, Wu H-H, et al. Neural Stem Cells Transfected with Reactive Oxygen Species–Responsive Polyplexes for Effective Treatment of Ischemic Stroke. Adv. Mater. 2019;31:1807591.

[54] Lv W, Xu J, Wang X, et al. Bioengineered Boronic Ester Modified Dextran Polymer Nanoparticles as Reactive Oxygen Species Responsive Nanocarrier for Ischemic Stroke Treatment. ACS Nano. 2018;12:5417–5426.

[55] Martino G, Pluchino S. The therapeutic potential of neural stem cells. Nat. Rev. Neurosci. 2006;7:395–406.

[56] Feng S, Hu Y, Peng S, et al. Nanoparticles responsive to the inflammatory microenvironment for targeted treatment of arterial restenosis. Biomaterials. 2016;105:167–184.

[57] Dou Y, Chen Y, Zhang X, et al. Biomaterials. 2017;143:93–108.

[58] Lu X, Mestres G, Singh VP, et al. Selenium- and Tellurium-Based Antioxidants for Modulating Inflammation and Effects on Osteoblastic Activity. Antioxidants [Internet]. 2017 [cited 2019 Oct 10];6. Available from: https://www.ncbi.nlm.nih.gov/pmc/articles/PMC5384176/.

[59] Poole KM, Nelson CE, Joshi RV, et al. ROS-responsive microspheres for on demand antioxidant therapy in a model of diabetic peripheral arterial disease. Biomaterials. 2015;41:166–175.

[60] Yao Y, Zhang H, Wang Z, et al. Reactive oxygen species (ROS)-responsive biomaterials mediate tissue microenvironments and tissue regeneration. J. Mater. Chem. B. 2019;7:5019–5037.

[61] Xiao B, Merlin D. Oral colon-specific therapeutic approaches toward treatment of inflammatory bowel disease. Expert Opin. Drug Deliv. 2012;9:1393–1407.

[62] Wilson DS, Dalmasso G, Wang L, et al. Orally delivered thioketal-nanoparticles loaded with TNFα-siRNA target inflammation and inhibit gene expression in the intestines. Nat. Mater. 2010;9:923–928.

[63] Rezaie A, Parker RD, Abdollahi M. Oxidative Stress and Pathogenesis of Inflammatory Bowel Disease: An Epiphenomenon or the Cause? Dig. Dis. Sci. 2007;52:2015–2021.

[64] Voisin M-B, Leoni G, Woodfin A, et al. Neutrophil elastase plays a non-redundant role in remodeling the venular basement membrane and neutrophil diapedesis post-ischemia/reperfusion injury. J. Pathol. 2019;248:88–102.

[65] Chouchani ET, Pell VR, Gaude E, et al. Ischaemic accumulation of succinate controls reperfusion injury through mitochondrial ROS. Nature. 2014;515:431–435.

[66] Burgoyne JR, Oka S, Ale-Agha N, et al. Hydrogen peroxide sensing and signaling by protein kinases in the cardiovascular system. Antioxid. Redox Signal. 2013;18:1042–1052.

[67] Kang C, Gwon S, Song C, et al. Fibrin-Targeted and H2O2-Responsive Nanoparticles as a Theranostics for Thrombosed Vessels. ACS Nano. 2017;11:6194–6203.

[68] Jung E, Lee J, Jeong L, et al. Stimulus-activatable echogenic maltodextrin nanoparticles as nanotheranostic agents for peripheral arterial disease. Biomaterials. 2019;192:282–291.

[69] Ratemi E. 5 - pH-responsive polymers for drug delivery applications. In: Makhlouf ASH, Abu-Thabit NY, editors. Stimuli Responsive Polym. Nanocarriers Drug

Deliv. Appl. Vol. 1 [Internet]. Woodhead Publishing; 2018 [cited 2019 Mar 3]. p. 121–141. Available from: http://www.sciencedirect.com/science/article/pii/B9780081019979000059.

[70] Liu J, Huang Y, Kumar A, et al. pH-Sensitive nano-systems for drug delivery in cancer therapy. Biotechnol. Adv. 2014;32:693–710.

[71] Ye M, Han Y, Tang J, et al. A Tumor-Specific Cascade Amplification Drug Release Nanoparticle for Overcoming Multidrug Resistance in Cancers. Adv. Mater. :n/a-n/a.

[72] Cheng R, Feng F, Meng F, et al. Glutathione-responsive nano-vehicles as a promising platform for targeted intracellular drug and gene delivery. J. Control. Release Off. J. Control. Release Soc. 2011;152:2–12.

[73] Xu X, Saw PE, Tao W, et al. ROS-Responsive Polyprodrug Nanoparticles for Triggered Drug Delivery and Effective Cancer Therapy. Adv. Mater. Deerfield Beach Fla [Internet]. 2017 [cited 2019 Mar 3];29. Available from: https://www.ncbi.nlm.nih.gov/pmc/articles/PMC5681219/.

[74] Hagen H, Marzenell P, Jentzsch E, et al. Aminoferrocene-based prodrugs activated by reactive oxygen species. J. Med. Chem. 2012;55:924–934.

[75] Kim E-J, Bhuniya S, Lee H, et al. An Activatable Prodrug for the Treatment of Metastatic Tumors. J. Am. Chem. Soc. 2014;136:13888–13894.

[76] Song C-C, Du F-S, Li Z-C. Oxidation-responsive polymers for biomedical applications. J. Mater. Chem. B. 2014;2:3413–3426.

[77] Xu Q, He C, Xiao C, et al. Reactive Oxygen Species (ROS) Responsive Polymers for Biomedical Applications. Macromol. Biosci. 2016;16:635–646.

[78] Ye H, Zhou Y, Liu X, et al. Recent Advances on Reactive Oxygen Species-Responsive Delivery and Diagnosis System. Biomacromolecules. 2019;20:2441–2463.

[79] Hu P, Tirelli N. Scavenging ROS: Superoxide Dismutase/Catalase Mimetics by the Use of an Oxidation-Sensitive Nanocarrier/Enzyme Conjugate. Bioconjug. Chem. 2012;23:438–449.

[80] Joshi-Barr S, de Gracia Lux C, Mahmoud E, et al. Exploiting Oxidative Microenvironments in the Body as Triggers for Drug Delivery Systems. Antioxid. Redox Signal. 2013;21:730–754.

[81] Kim K, Lee C-S, Na K. Light-controlled reactive oxygen species (ROS)-producible polymeric micelles with simultaneous drug-release triggering and endo/lysosomal escape. Chem. Commun. 2016;52:2839–2842.

[82] Dai L, Yu Y, Luo Z, et al. Photosensitizer enhanced disassembly of amphiphilic micelle for ROS-response targeted tumor therapy in vivo. Biomaterials. 2016;104:1–17.

[83] Zhao C, Li Y, Shao L, et al. Reactive oxygen species-responsive theranostic nanoparticles for enhanced hypoxic tumor photodynamic therapy via synchronous HIF-1α inhibition and ATP depletion. Mater. Chem. Front. 2019;3:1793–1799.

[84] Gupta MK, Martin JR, Werfel TA, et al. Cell Protective, ABC Triblock Polymer-Based Thermoresponsive Hydrogels with ROS-Triggered Degradation and Drug Release. J. Am. Chem. Soc. 2014;136:14896–14902.

[85] Milcovich G, Contessotto P, Marsico G, et al. Synthetic/ECM-inspired hybrid platform for hollow microcarriers with ROS-triggered nanoporation hallmarks. Sci. Rep. 2017;7:13138.

[86] Gupta MK, Meyer TA, Nelson CE, et al. Poly(PS-b-DMA) micelles for reactive oxygen species triggered drug release. J. Controlled Release. 2012;162:591–598.

[87] Wang Y, Zhu L, Wang Y, et al. Ultrasensitive GSH-Responsive Ditelluride-Containing Poly(ether-urethane) Nanoparticles for Controlled Drug Release. ACS Appl. Mater. Interfaces. 2016;8:35106–35113.

[88] Ren H, Wu Y, Li Y, et al. Visible-Light-Induced Disruption of Diselenide-Containing Layer-by-Layer Films: Toward Combination of Chemotherapy and Photodynamic Therapy. Small. 2013;9:3981–3986.

[89] Yu L, Yang Y, Du F-S, et al. ROS-Responsive Chalcogen-Containing Polycarbonates for Photodynamic Therapy. Biomacromolecules. 2018;19:2182–2193.

[90] Cao W, Wang L, Xu H. Selenium/tellurium containing polymer materials in nanobiotechnology. Nano Today. 2015;10:717–736.

[91] Xia J, Li T, Lu C, et al. Selenium-Containing Polymers: Perspectives toward Diverse Applications in Both Adaptive and Biomedical Materials. Macromolecules. 2018;51:7435–7455.

[92] Ma N, Xu H, An L, et al. Radiation-Sensitive Diselenide Block Co-polymer Micellar Aggregates: Toward the Combination of Radiotherapy and Chemotherapy. Langmuir. 2011;27:5874–5878.

[93] Deepagan VG, Kwon S, You DG, et al. In situ diselenide-crosslinked polymeric micelles for ROS-mediated anticancer drug delivery. Biomaterials. 2016;103:56–66.

[94] Cao W, Gu Y, Li T, et al. Ultra-sensitive ROS-responsive tellurium-containing polymers. Chem. Commun. 2015;51:7069–7071.

[95] Feng C, Zhu D, Chen L, et al. Targeted Delivery of Chlorin e6 via Redox Sensitive Diselenide-Containing Micelles for Improved Photodynamic Therapy in Cluster of Differentiation 44-Overexpressing Breast Cancer. Front. Pharmacol. [Internet]. 2019 [cited 2020 Jan 6];10. Available from: https://www.frontiersin.org/articles/10.3389/fphar.2019.00369/full.

[96] Saravanakumar G, Kim J, Kim WJ. Reactive-Oxygen-Species-Responsive Drug Delivery Systems: Promises and Challenges. Adv. Sci. 2017;4:n/a-n/a.

[97] Tinggi U. Selenium: its role as antioxidant in human health. Environ. Health Prev. Med. 2008;13:102–108.

[98] Sandoval JM, Levêque P, Gallez B, et al. Tellurite-induced oxidative stress leads to cell death of murine hepatocarcinoma cells. BioMetals. 2010;23:623–632.

[99] Lee D, Bae S, Hong D, et al. H2O2-responsive molecularly engineered polymer nanoparticles as ischemia/reperfusion-targeted nanotherapeutic agents. Sci. Rep. 2013;3:2233.

[100] Yoo D, Guk K, Kim H, et al. Antioxidant polymeric nanoparticles as novel therapeutics for airway inflammatory diseases. Int. J. Pharm. 2013;450:87–94.

[101] Ballance WC, Qin EC, Chung HJ, et al. Reactive oxygen species-responsive drug delivery systems for the treatment of neurodegenerative diseases. Biomaterials. 2019;217:119292.

[102] Phromviyo N, Lert-itthiporn A, Swatsitang E, et al. Biodegradable poly(vinyl alcohol)/polyoxalate electrospun nanofibers for hydrogen peroxide-triggered drug release. J. Biomater. Sci. Polym. Ed. 2015;26:975–987.

[103] Lee D, Bae S, Ke Q, et al. Hydrogen peroxide-responsive copolyoxalate nanoparticles for detection and therapy of ischemia–reperfusion injury. J. Controlled Release. 2013;172:1102–1110.

[104] Rajan M, Murugan M, Ponnamma D, et al. Poly-carboxylic acids functionalized chitosan nanocarriers for controlled and targeted anti-cancer drug delivery. Biomed. Pharmacother. 2016;83:201–211.

[105] Kim S, Lee Y, Park H, et al. Reduced inflammatory responses to poly(lactic-co-glycolic acid) by the incorporation of hydroxybenzyl alcohol releasing polyoxalate. Macromol. Res. 2011;19:1242–1249.

[106] Yu SS, Koblin RL, Zachman AL, et al. Physiologically relevant oxidative degradation of oligo(proline) cross-linked polymeric scaffolds. Biomacromolecules. 2011;12:4357–4366.

[107] Lee SH, Boire TC, Lee JB, et al. ROS-cleavable proline oligomer crosslinking of polycaprolactone for pro-angiogenic host response. J. Mater. Chem. B. 2014;2:7109–7113.

[108] Gupta MK, Lee SH, Crowder SW, et al. Oligoproline-derived nanocarrier for dual stimuli-responsive gene delivery. J. Mater. Chem. B. 2015;3:7271–7280.

[109] Song C-C, Ji R, Du F-S, et al. Oxidation-Responsive Poly(amino ester)s Containing Arylboronic Ester and Self-Immolative Motif: Synthesis and Degradation Study. Macromolecules. 2013;46:8416–8425.

[110] Luo C-Q, Zhou Y-X, Zhou T-J, et al. Reactive oxygen species-responsive nanoprodrug with quinone methides-mediated GSH depletion for improved chlorambucil breast cancers therapy. J. Control. Release Off. J. Control. Release Soc. 2018;274:56–68.

[111] Zhang D, Wei Y, Chen K, et al. Biocompatible Reactive Oxygen Species (ROS)-Responsive Nanoparticles as Superior Drug Delivery Vehicles. Adv. Healthc. Mater. 2015;4:69–76.

[112] Liu H, Jiang W, Wang Q, et al. Biomater. Sci. 2019;7:3706–3716.

[113] Bertoni S, Liu Z, Correia A, et al. pH and Reactive Oxygen Species-Sequential Responsive Nano-in-Micro Composite for Targeted Therapy of Inflammatory Bowel Disease. Adv. Funct. Mater. 2018;28:1806175.

[114] Li Y, Bai H, Wang H, et al. Reactive oxygen species (ROS)-responsive nanomedicine for RNAi-based cancer therapy. Nanoscale [Internet]. 2017 [cited 2017 Dec 14]; Available from: http://pubs.rsc.org/en/content/articlelanding/2018/nr/c7nr06689a.

[115] McEnery MAP, Lu S, Gupta MK, et al. Oxidatively degradable poly(thioketal urethane)/ceramic composite bone cements with bone-like strength. RSC Adv. 2016;6:109414–109424.

[116] El-Mohtadi F, d'Arcy R, Tirelli N. Oxidation-Responsive Materials: Biological Rationale, State of the Art, Multiple Responsiveness, and Open Issues. Macromol. Rapid Commun. 2019;40:1800699.

[117] Zheng N, Xie D, Zhang Z, et al. Thioketal-crosslinked: ROS-degradable polycations for enhanced in vitro and in vivo gene delivery with self-diminished cytotoxicity. J. Biomater. Appl. 2019;34:326–338.

[118] Tang T, Jiang H, Yu Y, et al. A new method of wound treatment: targeted therapy of skin wounds with reactive oxygen species-responsive nanoparticles containing SDF-1α. Int. J. Nanomedicine. 2015;10:6571–6585.

[119] Kim JS, Jo SD, Seah GL, et al. ROS-induced biodegradable polythioketal nanoparticles for intracellular delivery of anti-cancer therapeutics. J. Ind. Eng. Chem. 2015;21:1137–1142.

[120] Shim MS, Xia Y. A Reactive Oxygen Species (ROS)-Responsive Polymer for Safe, Efficient, and Targeted Gene Delivery in Cancer Cells. Angew. Chem. Int. Ed. 2013;52:6926–6929.

[121] Martin JR, Gupta MK, Page JM, et al. A porous tissue engineering scaffold selectively degraded by cell-generated reactive oxygen species. Biomaterials. 2014;35:3766–3776.

[122] Zhang Y, Zhang H, Mao Z, et al. ROS-Responsive Nanoparticles for Suppressing the Cytotoxicity and Immunogenicity Caused by PM2.5 Particulates. Biomacromolecules. 2019;20:1777–1788.

[123] Regmi S, Pathak S, Nepal MR, et al. Inflammation-triggered local drug release ameliorates colitis by inhibiting dendritic cell migration and Th1/Th17 differentiation. J. Controlled Release. 2019;316:138–149.

[124] Chen B, Zhang Y, Ran R, et al. Reactive oxygen species-responsive nanoparticles based on a thioketal-containing poly(β-amino ester) for combining photothermal/photodynamic therapy and chemotherapy. Polym. Chem. 2019;10:4746–4757.

[125] Sun C, Liang Y, Hao N, et al. A ROS-responsive polymeric micelle with a π-conjugated thioketal moiety for enhanced drug loading and efficient drug delivery. Org. Biomol. Chem. 2017;15:9176–9185.

[126] Lin G-Q, Yi W-J, Liu Q, et al. Aromatic Thioacetal-Bridged ROS-Responsive Nanoparticles as Novel Gene Delivery Vehicles. Mol. J. Synth. Chem. Nat. Prod. Chem. [Internet]. 2018 [cited 2019 Aug 29];23. Available from: https://www.ncbi.nlm.nih.gov/pmc/articles/PMC6225261/.

[127] Liu X, Wang Y, Chen C, et al. A Fluorinated Bola-Amphiphilic Dendrimer for On-Demand Delivery of siRNA, via Specific Response to Reactive Oxygen Species. Adv. Funct. Mater. 2016;26:8594–8603.

[128] Ling X, Zhang S, Shao P, et al. Synthesis of a reactive oxygen species responsive heterobifunctional thioketal linker. Tetrahedron Lett. 2015;56:5242–5244.

[129] Yin W, Ke W, Chen W, et al. Integrated block copolymer prodrug nanoparticles for combination of tumor oxidative stress amplification and ROS-responsive drug release. Biomaterials. 2019;195:63–74.

[130] Oddone N, Pederzoli F, Duskey JT, et al. ROS-responsive “smart” polymeric conjugate: Synthesis, characterization and proof-of-concept study. Int. J. Pharm. 2019;570:118655.

[131] Shi J, Chen Z, Wang B, et al. Reactive Oxygen Species-Manipulated Drug Release from a Smart Envelope-Type Mesoporous Titanium Nanovehicle for Tumor Sonodynamic-Chemotherapy. ACS Appl. Mater. Interfaces. 2015;7:28554–28565.

[132] Sun C-Y, Cao Z, Zhang X-J, et al. Cascade-amplifying synergistic effects of chemo-photodynamic therapy using ROS-responsive polymeric nanocarriers. Theranostics. 2018;8:2939–2953.

[133] Li J, Sun C, Tao W, et al. Photoinduced PEG deshielding from ROS-sensitive linkage-bridged block copolymer-based nanocarriers for on-demand drug delivery. Biomaterials. 2018;170:147–155.

[134] Zheng N, Zhang Z, Kuang J, et al. Poly(photosensitizer) Nanoparticles for Enhanced in Vivo Photodynamic Therapy by Interrupting the π–π Stacking and Extending Circulation Time. ACS Appl. Mater. Interfaces. 2019;11:18224–18232.

[135] Li Y, Hu J, Liu X, et al. Photodynamic therapy-triggered on-demand drug release from ROS-responsive core-cross-linked micelles toward synergistic anti-cancer treatment. Nano Res. 2019;12:999–1008.

[136] McGough MAP, Shiels SM, Boller LA, et al. Poly(Thioketal Urethane) Autograft Extenders in an Intertransverse Process Model of Bone Formation. Tissue Eng. Part A. 2018;25:949–963.

[137] Liu L, Pei Y, Zhang Y, et al. Guanine-cytosine base-pairings crosslinked ROS-sensitive supramolecular hydrogels with improved rheological properties. Eur. Polym. J. 2018;102:75–81.

[138] Xu X, Zeng Z, Huang Z, et al. Near-infrared light-triggered degradable hyaluronic acid hydrogel for on-demand drug release and combined chemo-photodynamic therapy. Carbohydr. Polym. 2020;229:115394.

[139] Zhou F, Feng B, Wang T, et al. Theranostic Prodrug Vesicles for Reactive Oxygen Species-Triggered Ultrafast Drug Release and Local-Regional Therapy of Metastatic Triple-Negative Breast Cancer. Adv. Funct. Mater. 2017;27:1703674.

[140] Liang C, Chang J, Jiang Y, et al. Selective RNA interference and gene silencing using reactive oxygen species-responsive lipid nanoparticles. Chem. Commun. 2019;55:8170–8173.

[141] Shi S, Zhang L, Zhu M, et al. Reactive Oxygen Species-Responsive Nanoparticles Based on PEGlated Prodrug for Targeted Treatment of Oral Tongue Squamous Cell Carcinoma by Combining Photodynamic Therapy and Chemotherapy. ACS Appl. Mater. Interfaces. 2018;10:29260–29272.

[142] Lin C, Tao Y, Saw PE, et al. A polyprodrug-based nanoplatform for cisplatin prodrug delivery and combination cancer therapy. Chem. Commun. 2019;55:13987–13990.

[143] Li Q, Wen Y, Wen J, et al. A new biosafe reactive oxygen species (ROS)-responsive nanoplatform for drug delivery. RSC Adv. 2016;6:38984–38989.

[144] Li Q, Wen Y, You X, et al. Development of a reactive oxygen species (ROS)-responsive nanoplatform for targeted oral cancer therapy. J. Mater. Chem. B. 2016;4:4675–4682.

[145] Mohammed F, Ke W, Mukerabigwi JF, et al. ROS-Responsive Polymeric Nanocarriers with Photoinduced Exposure of Cell-Penetrating Moieties for Specific Intracellular Drug Delivery. ACS Appl. Mater. Interfaces. 2019;11:31681–31692.

[146] Cheng D-B, Zhang X-H, Gao Y-J, et al. Endogenous Reactive Oxygen Species-Triggered Morphology Transformation for Enhanced Cooperative Interaction with Mitochondria. J. Am. Chem. Soc. 2019;141:7235–7239.

[147] Wang J, He X, Shen S, et al. ROS-Sensitive Cross-Linked Polyethylenimine for Red-Light-Activated siRNA Therapy. ACS Appl. Mater. Interfaces. 2019;11:1855–1863.

[148] Zhang Y, Guo Q, An S, et al. ROS-Switchable Polymeric Nanoplatform with Stimuli-Responsive Release for Active Targeted Drug Delivery to Breast Cancer. ACS Appl. Mater. Interfaces. 2017;9:12227–12240.

[149] Hu J-J, Lei Q, Peng M-Y, et al. A positive feedback strategy for enhanced chemotherapy based on ROS-triggered self-accelerating drug release nanosystem. Biomaterials. 2017;128:136–146.

[150] Zhang T, Lin H, Cui L, et al. Near Infrared Light Triggered Reactive Oxygen Species Responsive Upconversion Nanoplatform for Drug Delivery and Photodynamic Therapy. Eur. J. Inorg. Chem. 2016;2016:1206–1213.

[151] Chen G, Jiang M. Cyclodextrin-based inclusion complexation bridging supramolecular chemistry and macromolecular self-assembly. Chem. Soc. Rev. 2011;40:2254–2266.

[152] Yang G-G, Zhang H, Zhang D-Y, et al. Cancer-specific chemotherapeutic strategy based on the vitamin K3 mediated ROS regenerative feedback and visualized drug release in vivo. Biomaterials. 2018;185:73–85.

[153] Jin H, Zhu T, Huang X, et al. ROS-responsive nanoparticles based on amphiphilic hyperbranched polyphosphoester for drug delivery: Light-triggered size-reducing and enhanced tumor penetration. Biomaterials. 2019;211:68–80.

[154] Liu R, Yu M, Yang X, et al. Linear Chimeric Triblock Molecules Self-Assembled Micelles with Controllably Transformable Property to Enhance Tumor Retention for Chemo-Photodynamic Therapy of Breast Cancer. Adv. Funct. Mater. 2019;29:1808462.

[155] Wang X, Meng G, Zhang S, et al. A Reactive $^{1}O_2$ - Responsive Combined Treatment System of Photodynamic and Chemotherapy for Cancer. Sci. Rep. 2016;6:srep29911.

[156] Yuan Y, Liu J, Liu B. Conjugated-Polyelectrolyte-Based Polyprodrug: Targeted and Image-Guided Photodynamic and Chemotherapy with On-Demand Drug Release upon Irradiation with a Single Light Source. Angew. Chem. Int. Ed. 2014;53:7163–7168.

[157] Zhao Z, Wang W, Li C, et al. Reactive Oxygen Species–Activatable Liposomes Regulating Hypoxic Tumor Microenvironment for Synergistic Photo/Chemodynamic Therapies. Adv. Funct. Mater. 2019;29:1905013.

[158] Seah GL, Yu JH, Yang MY, et al. Low-power and low-drug-dose photodynamic chemotherapy via the breakdown of tumor-targeted micelles by reactive oxygen species. J. Controlled Release. 2018;286:240–253.

[159] Seah GL, Yu JH, Koo BI, et al. Cancer-targeted reactive oxygen species-degradable polymer nanoparticles for near infrared light-induced drug release. J. Mater. Chem. B. 2018;6:7737–7749.

[160] Chen W-H, Luo G-F, Qiu W-X, et al. Programmed Nanococktail for Intracellular Cascade Reaction Regulating Self-Synergistic Tumor Targeting Therapy. Small. 2016;12:733–744.

[161] Bao Y, Yin L, Liu L, et al. Acid-sensitive ROS-triggered dextran-based drug delivery system for advanced chemo-photodynamic synergistic therapy. J. Biomed. Mater. Res. A. 2020;108:148–156.

[162] Cao Z, Li D, Wang J, et al. Direct Nucleus-Targeted Drug Delivery Using Cascade pHe/Photo Dual-Sensitive Polymeric Nanocarrier for Cancer Therapy. Small. 2019;15:1902022.

[163] Li C, Lin W, Liu S, et al. Self-destructive PEG–BODIPY nanomaterials for photodynamic and photothermal therapy. J. Mater. Chem. B. 2019;7:4655–4660.

[164] Li J, Wei K, Zuo S, et al. Light-Triggered Clustered Vesicles with Self-Supplied Oxygen and Tissue Penetrability for Photodynamic Therapy against Hypoxic Tumor. Adv. Funct. Mater. 2017;27:n/a-n/a.

[165] Wang S, Yu G, Wang Z, et al. Enhanced Antitumor Efficacy by a Cascade of Reactive Oxygen Species Generation and Drug Release. Angew. Chem. 2019;131:14900–14905.

[166] Wang J, He H, Xu X, et al. Far-red light-mediated programmable anti-cancer gene delivery in cooperation with photodynamic therapy. Biomaterials. 2018;171:72–82.

[167] Li S, Xie A, Li H, et al. A self-assembled, ROS-responsive Janus-prodrug for targeted therapy of inflammatory bowel disease. J. Controlled Release. 2019;316:66–78.

[168] Maras JS, Das S, Sharma S, et al. Iron-Overload triggers ADAM-17 mediated inflammation in Severe Alcoholic Hepatitis. Sci. Rep. 2018;8:1–14.

[169] Liu Z, Qiao J, Nagy T, et al. ROS-triggered degradable iron-chelating nanogels: Safely improving iron elimination in vivo. J. Controlled Release. 2018;283:84–93.

[170] Chen D, Zhang G, Li R, et al. Biodegradable, Hydrogen Peroxide, and Glutathione Dual Responsive Nanoparticles for Potential Programmable Paclitaxel Release. J. Am. Chem. Soc. 2018;140:7373–7376.

[171] Tiwari G, Tiwari R, Sriwastawa B, et al. Drug delivery systems: An updated review. Int. J. Pharm. Investig. 2012;2:2–11.

[172] Dragojevic S, Ryu JS, Raucher D. Polymer-Based Prodrugs: Improving Tumor Targeting and the Solubility of Small Molecule Drugs in Cancer Therapy. Molecules. 2015;20:21750–21769.

[173] Xu L, Yang Y, Zhao M, et al. A reactive oxygen species–responsive prodrug micelle with efficient cellular uptake and excellent bioavailability. J. Mater. Chem. B. 2018;6:1076–1084.

[174] Chakraborty C, Sharma AR, Sharma G, et al. The novel strategies for next-generation cancer treatment: miRNA combined with chemotherapeutic agents for the treatment of cancer. Oncotarget. 2018;9:10164–10174.

[175] Salim S. Oxidative Stress and the Central Nervous System. J. Pharmacol. Exp. Ther. 2017;360:201–205.

[176] Sharma V, Joseph C, Ghosh S, et al. Kaempferol induces apoptosis in glioblastoma cells through oxidative stress. Mol. Cancer Ther. 2007;6:2544–2553.

[177] Lee Y, Kataoka K. Biosignal-sensitive polyion complex micelles for the delivery of biopharmaceuticals. Soft Matter. 2009;5:3810–3817.

[178] Shim MS, Xia Y. A Reactive Oxygen Species (ROS)-Responsive Polymer for Safe, Efficient, and Targeted Gene Delivery in Cancer Cells. Angew. Chem. Int. Ed. 2013;52:6926–6929.

[179] Turecek PL, Bossard MJ, Schoetens F, et al. PEGylation of Biopharmaceuticals: A Review of Chemistry and Nonclinical Safety Information of Approved Drugs. J. Pharm. Sci. 2016;105:460–475.

[180] Li F, Mahato RI. Bioconjugate Therapeutics: Current Progress and Future Perspective. Mol. Pharm. 2017;14:1321–1324.

[181] Goldstein S, Meyerstein D, Czapski G. The Fenton reagents. Free Radic. Biol. Med. 1993;15:435–445.

[182] Hwang E, Sim S, Park SH, et al. Anti-proliferative effect of Zea mays L. cob extract on rat C6 glioma cells through regulation of glycolysis, mitochondrial ROS, and apoptosis. Biomed. Pharmacother. 2018;98:726–732.

[183] Kim S-J, Hwang E, Yi SS, et al. Sea Buckthorn Leaf Extract Inhibits Glioma Cell Growth by Reducing Reactive Oxygen Species and Promoting Apoptosis. Appl. Biochem. Biotechnol. 2017;182:1663–1674.

[184] Zong H, Verhaak RG, Canoll P. The cellular origin for malignant glioma and prospects for clinical advancements. Expert Rev. Mol. Diagn. 2012;12:383–394.

[185] Pellerin L, Stolz M, Sorg O, et al. Regulation of energy metabolism by neurotransmitters in astrocytes in primary culture and in an immortalized cell line. Glia. 1997;21:74–83.

[186] Philippe J-M, Dubois J-M, Rouzaire-Dubois B, et al. Functional expression of V-ATPases in the plasma membrane of glial cells. Glia. 2002;37:365–373.

[187] Lee D, Park S, Bae S, et al. Hydrogen peroxide-activatable antioxidant prodrug as a targeted therapeutic agent for ischemia-reperfusion injury. Sci. Rep. 2015;5:16592.

[188] Swiecicki J-M, Thiebaut F, Di Pisa M, et al. How to unveil self-quenched fluorophores and subsequently map the subcellular distribution of exogenous peptides. Sci. Rep. 2016;6:20237.

[189] Resende FFB, Titze-de-Almeida SS, Titze-de-Almeida R. Function of neuronal nitric oxide synthase enzyme in temozolomide-induced damage of astrocytic tumor cells. Oncol. Lett. 2018;15:4891–4899.

[190] Majewska P, Ioannidis S, Raza MH, et al. Postprogression survival in patients with glioblastoma treated with concurrent chemoradiotherapy: a routine care cohort study. CNS Oncol. 2017;6:307–313.

[191] Raucher D, Dragojevic S, Ryu J. Macromolecular Drug Carriers for Targeted Glioblastoma Therapy: Preclinical Studies, Challenges, and Future Perspectives. Front. Oncol. [Internet]. 2018 [cited 2019 Oct 24];8. Available from: https://www.ncbi.nlm.nih.gov/pmc/articles/PMC6304427/.

[192] Mahase E. Cancer overtakes CVD to become leading cause of death in high income countries. BMJ. 2019;366:l5368.

[193] Lee B-S, Amano T, Wang HQ, et al. Reactive oxygen species responsive nanoprodrug to treat intracranial glioblastoma. ACS Nano. 2013;7:3061–3077.

[194] Tsai C-F, Yeh W-L, Huang SM, et al. Wogonin Induces Reactive Oxygen Species Production and Cell Apoptosis in Human Glioma Cancer Cells. Int. J. Mol. Sci. 2012;13:9877–9892.

[195] Yang J, Li Y, Zhang T, et al. Development of bioactive materials for glioblastoma therapy. Bioact. Mater. 2016;1:29–38.

[196] Legendre C, Avril S, Guillet C, et al. Low oxygen tension reverses antineoplastic effect of iron chelator deferasirox in human glioblastoma cells. BMC Cancer [Internet]. 2016 [cited 2019 Oct 20];16. Available from: https://www.ncbi.nlm.nih.gov/pmc/articles/PMC4736662/.

[197] Gramatzki D, Herrmann C, Happold C, et al. Glioma Cell Death Induced by Irradiation or Alkylating Agent Chemotherapy Is Independent of the Intrinsic Ceramide Pathway. PLoS ONE [Internet]. 2013 [cited 2019 May 2];8. Available from: https://www.ncbi.nlm.nih.gov/pmc/articles/PMC3646759/.

[198] Haar CP, Hebbar P, Wallace GC, et al. Drug Resistance in Glioblastoma: A Mini Review. Neurochem. Res. 2012;37:1192–1200.

[199] Gonda A, Zhao N, Shah JV, et al. Engineering Tumor-Targeting Nanoparticles as Vehicles for Precision Nanomedicine. Med One [Internet]. 2019 [cited 2019 Dec 11];4. Available from: https://www.ncbi.nlm.nih.gov/pmc/articles/PMC6779336/.

[200] Farokhzad OC, Langer R. Nanomedicine: Developing smarter therapeutic and diagnostic modalities. Adv. Drug Deliv. Rev. 2006;58:1456–1459.

[201] Meel R van der, Sulheim E, Shi Y, et al. Smart cancer nanomedicine. Nat. Nanotechnol. 2019;14:1007–1017.

[202] Cobo I, Li M, Sumerlin BS, et al. Smart hybrid materials by conjugation of responsive polymers to biomacromolecules. Nat. Mater. 2015;14:143–159.

[203] Pelicano H, Carney D, Huang P. ROS stress in cancer cells and therapeutic implications. Drug Resist. Updat. 2004;7:97–110.

[204] Wang Y, Zhang Y, Ru Z, et al. A ROS-responsive polymeric prodrug nanosystem with self-amplified drug release for PSMA (−) prostate cancer specific therapy. J. Nanobiotechnology. 2019;17:91.

[205] Tseng Y-Y, Wang Y-C, Su C-H, et al. Concurrent delivery of carmustine, irinotecan, and cisplatin to the cerebral cavity using biodegradable nanofibers: In vitro and in vivo studies. Colloids Surf. B Biointerfaces. 2015;134:254–261.

[206] Wang D, Wang C, Wang L, et al. A comprehensive review in improving delivery of small-molecule chemotherapeutic agents overcoming the blood-brain/brain tumor barriers for glioblastoma treatment. Drug Deliv. 2019;26:551–565.

[207] Sousa F, Dhaliwal HK, Gattacceca F, et al. Enhanced anti-angiogenic effects of bevacizumab in glioblastoma treatment upon intranasal administration in polymeric nanoparticles. J. Controlled Release. 2019;309:37–47.

[208] Ajazuddin, Alexander A, Amarji B, et al. Synthesis, characterization and in vitro studies of pegylated melphalan conjugates. Drug Dev. Ind. Pharm. 2013;39:1053–1062.

[209] Colvin M. Alkylating Agents. Holl.-Frei Cancer Med. 6th Ed. [Internet]. 2003 [cited 2019 Oct 21]; Available from: https://www.ncbi.nlm.nih.gov/books/NBK12772/.

[210] Gahramanov S, Varallyay C, Tyson RM, et al. Diagnosis of pseudoprogression using MRI perfusion in patients with glioblastoma multiforme may predict improved survival. CNS Oncol. 2014;3:389–400.

[211] Bottom KS, Ashley DM, Friedman HS, et al. Evaluation of Pre-radiotherapy Cyclophosphamide in Patients with Newly Diagnosed Glioblastoma Multiforme. J. Neurooncol. 2000;46:151–156.

[212] Swierczewska M, Lee KC, Lee S. What is the future of PEGylated therapies? Expert Opin. Emerg. Drugs. 2015;20:531–536.

[213] Kirtane A, Kalscheuer S, Panyam J. Exploiting Nanotechnology to Overcome Tumor Drug Resistance: Challenges and Opportunities. Adv. Drug Deliv. Rev. [Internet]. 2013 [cited 2019 Nov 4];65. Available from: https://www.ncbi.nlm.nih.gov/pmc/articles/PMC3849460/.

[214] Batra J, Robinson J, Mehner C, et al. PEGylation Extends Circulation Half-Life While Preserving In Vitro and In Vivo Activity of Tissue Inhibitor of Metalloproteinases-1 (TIMP-1). PLOS ONE. 2012;7:e50028.

[215] Kuczma M, Ding Z-C, Zhou G. Immunostimulatory Effects of Melphalan and Usefulness in Adoptive Cell Therapy with Antitumor CD4+ T Cells. Crit. Rev. Immunol. 2016;36:179–191.

[216] Zeng Y, Ma J, Zhan Y, et al. Hypoxia-activated prodrugs and redox-responsive nanocarriers [Internet]. Int. J. Nanomedicine. 2018 [cited 2019 Dec 18]. Available from: https://www.dovepress.com/hypoxia-activated-prodrugs-and-redox-responsive-nanocarriers-peer-reviewed-fulltext-article-IJN.

[217] Taresco V, Alexander C, Singh N, et al. Stimuli-Responsive Prodrug Chemistries for Drug Delivery. Adv. Ther. 2018;1:1800030.

[218] Weidle UH, Tiefenthaler G, Georges G. Proteases as Activators for Cytotoxic Prodrugs in Antitumor Therapy. Cancer Genomics - Proteomics. 2014;11:67–79.

[219] Zheng M, Liu Y, Wang Y, et al. ROS-Responsive Polymeric siRNA Nanomedicine Stabilized by Triple Interactions for the Robust Glioblastoma Combinational RNAi Therapy. Adv. Mater. 0:1903277.

[220] Yamamori T, Yasui H, Yamazumi M, et al. Ionizing radiation induces mitochondrial reactive oxygen species production accompanied by upregulation of mitochondrial electron transport chain function and mitochondrial content under control of the cell cycle checkpoint. Free Radic. Biol. Med. 2012;53:260–270.

[221] Oddone N, Lecot N, Fernández M, et al. In vitro and in vivo uptake studies of PAMAM G4.5 dendrimers in breast cancer. J. Nanobiotechnology [Internet]. 2016 [cited 2019 May 9];14. Available from: https://www.ncbi.nlm.nih.gov/pmc/articles/PMC4906583/.

[222] Souza TGF, Ciminelli VST, Mohallem NDS. A comparison of TEM and DLS methods to characterize size distribution of ceramic nanoparticles. J. Phys. Conf. Ser. 2016;733:012039.

[223] Single A, Beetham H, Telford BJ, et al. A Comparison of Real-Time and Endpoint Cell Viability Assays for Improved Synthetic Lethal Drug Validation. J. Biomol. Screen. 2015;20:1286–1293.

[224] Kupczyk-Subotkowska L, Siahaan TJ, Basile AS, et al. Modulation of Melphalan Resistance in Glioma Cells with a Peripheral Benzodiazepine Receptor Ligand−Melphalan Conjugate. J. Med. Chem. 1997;40:1726–1730.

[225] Kühne A, Tzvetkov MV, Hagos Y, et al. Influx and efflux transport as determinants of melphalan cytotoxicity: Resistance to melphalan in MDR1 overexpressing tumor cell lines. Biochem. Pharmacol. 2009;78:45–53.

[226] Xiong T, Wei H, Chen X, et al. PJ34, a poly(ADP-ribose) polymerase (PARP) inhibitor, reverses melphalan-resistance and inhibits repair of DNA double-strand breaks by targeting the FA/BRCA pathway in multidrug resistant multiple myeloma cell line RPMI8226/R. Int. J. Oncol. 2015;46:223–232.

[227] Lin J, Raoof DA, Thomas DG, et al. L-Type Amino Acid Transporter-1 Overexpression and Melphalan Sensitivity in Barrett's Adenocarcinoma. Neoplasia. 2004;6:74–84.

[228] Nawashiro H, Otani N, Uozumi Y, et al. High expression of L-type amino acid transporter 1 in infiltrating glioma cells. Brain Tumor Pathol. 2005;22:89–91.

[229] Nawashiro H, Otani N, Shinomiya N, et al. L-type amino acid transporter 1 as a potential molecular target in human astrocytic tumors. Int. J. Cancer. 2006;119:484–492.

[230] Zhang R, Qin X, Kong F, et al. Improving cellular uptake of therapeutic entities through interaction with components of cell membrane. Drug Deliv. 2019;26:328–342.

[231] Sampaio-Maia B, Serrão MP, Soares-da-Silva P. Regulatory pathways and uptake ofl-DOPA by capillary cerebral endothelial cells, astrocytes, and neuronal cells. Am. J. Physiol.-Cell Physiol. 2001;280:C333–C342.

[232] Lenting K, Verhaak R, ter Laan M, et al. Glioma: experimental models and reality. Acta Neuropathol. (Berl.). 2017;133:263–282.

[233] Wojtala A, Bonora M, Malinska D, et al. Chapter Thirteen - Methods to Monitor ROS Production by Fluorescence Microscopy and Fluorometry. In: Galluzzi L, Kroemer G, editors. Methods Enzymol. [Internet]. Academic Press; 2014 [cited 2019 Nov 7]. p. 243–262. Available from: http://www.sciencedirect.com/science/article/pii/B9780124166189000133.

[234] Kawamura K, Qi F, Kobayashi J. Potential relationship between the biological effects of low-dose irradiation and mitochondrial ROS production. J. Radiat. Res. (Tokyo). 2018;59:ii91–ii97.

[235] McKelvey KJ, Hudson AL, Back M, et al. Radiation, inflammation and the immune response in cancer. Mamm. Genome. 2018;29:843–865.

[236] Gill MR, Vallis KA. Transition metal compounds as cancer radiosensitizers. Chem. Soc. Rev. 2019;48:540–557.

[237] Nam L, Coll C, Erthal LCS, et al. Drug Delivery Nanosystems for the Localized Treatment of Glioblastoma Multiforme. Materials [Internet]. 2018 [cited 2019 Oct 24];11. Available from: https://www.ncbi.nlm.nih.gov/pmc/articles/PMC5978156/.

[238] Anderson CP, Matthay KK, Perentesis JP, et al. Pilot study of intravenous melphalan combined with continuous infusion L-S,R-buthionine sulfoximine for children with recurrent neuroblastoma. Pediatr. Blood Cancer. 2015;62:1739–1746.

[239] Hans ML, Lowman AM. Biodegradable nanoparticles for drug delivery and targeting. Curr. Opin. Solid State Mater. Sci. 2002;6:319–327.

[240] Astete CE, Sabliov CM. Synthesis and characterization of PLGA nanoparticles. J. Biomater. Sci. Polym. Ed. 2006;17:247–289.

[241] Martins C, Sousa F, Araújo F, et al. Functionalizing PLGA and PLGA Derivatives for Drug Delivery and Tissue Regeneration Applications. Adv. Healthc. Mater. 2018;7:1701035.

[242] Colzani B, Biagiotti M, Speranza G, et al. Smart Biodegradable Nanoparticulate Materials: Poly-lactide-co-glycolide Functionalization with Selected Peptides [Internet]. 2016 [cited 2019 Nov 24]. Available from: https://www.ingentaconnect.com/contentone/ben/cnano/2016/00000012/00000003/art00014.

[243] Xu Y, Kim C-S, Saylor DM, et al. Polymer degradation and drug delivery in PLGA-based drug–polymer applications: A review of experiments and theories. J. Biomed. Mater. Res. B Appl. Biomater. 2017;105:1692–1716.

[244] Makadia HK, Siegel SJ. Poly Lactic-co-Glycolic Acid (PLGA) as Biodegradable Controlled Drug Delivery Carrier. Polymers. 2011;3:1377–1397.

[245] Cu Y, Saltzman WM. Controlled Surface Modification with Poly(ethylene)glycol Enhances Diffusion of PLGA Nanoparticles in Human Cervical Mucus. Mol. Pharm. 2009;6:173–181.

[246] Kim K-T, Lee J-Y, Kim D-D, et al. Recent Progress in the Development of Poly(lactic-co-glycolic acid)-Based Nanostructures for Cancer Imaging and Therapy. Pharmaceutics. 2019;11:280.

[247] Sah H, Thoma LA, Desu HR, et al. Concepts and practices used to develop functional PLGA-based nanoparticulate systems. Int. J. Nanomedicine. 2013;8:747–765.

[248] Onishi H, Machida Y. In Vitro and In Vivo Evaluation of Microparticulate Drug Delivery Systems Composed of Macromolecular Prodrugs. Molecules. 2008;13:2136–2155.

[249] Nicolas J, Mura S, Brambilla D, et al. Design, functionalization strategies and biomedical applications of targeted biodegradable/biocompatible polymer-based nanocarriers for drug delivery. Chem. Soc. Rev. 2013;42:1147–1235.

[250] Costantino L, Gandolfi F, Tosi G, et al. Peptide-derivatized biodegradable nanoparticles able to cross the blood-brain barrier. J. Control. Release Off. J. Control. Release Soc. 2005;108:84–96.

[251] Karra N, Nassar T, Ripin AN, et al. Antibody Conjugated PLGA Nanoparticles for Targeted Delivery of Paclitaxel Palmitate: Efficacy and Biofate in a Lung Cancer Mouse Model. Small. 2013;9:4221–4236.

[252] Bertram JP, Jay SM, Hynes SR, et al. Functionalized Poly(lactic-co-glycolic acid) Enhances Drug Delivery and Provides Chemical Moieties for Surface Engineering while Preserving Biocompatibility. Acta Biomater. 2009;5:2860–2871.

[253] Determination of primary amine endgroups on polymers with fluorescamine in nonaqueous solvents [Internet]. [cited 2019 Nov 24]. Available from: https://pubs.acs.org/doi/pdf/10.1021/ac50053a037.

[254] Barbara R, Belletti D, Pederzoli F, et al. Novel Curcumin loaded nanoparticles engineered for Blood-Brain Barrier crossing and able to disrupt Abeta aggregates. Int. J. Pharm. 2017;526:413–424.

[255] Pederzoli F, Ruozi B, Duskey J, et al. Nanomedicine against Aβ Aggregation by β–Sheet Breaker Peptide Delivery: In Vitro Evidence. Pharmaceutics. 2019;11:572.

[256] Udenfriend S, Stein S, Böhlen P, et al. Fluorescamine: A Reagent for Assay of Amino Acids, Peptides, Proteins, and Primary Amines in the Picomole Range. Science. 1972;178:871–872.

[257] Öztürk AA, Yenilmez E, Özarda MG. Clarithromycin-Loaded Poly (Lactic-co-glycolic Acid) (PLGA) Nanoparticles for Oral Administration: Effect of Polymer Molecular Weight and Surface Modification with Chitosan on Formulation, Nanoparticle Characterization and Antibacterial Effects. Polymers [Internet]. 2019 [cited 2020 Jan 15];11. Available from: https://www.ncbi.nlm.nih.gov/pmc/articles/PMC6835525/.

[258] Govender T, Stolnik S, Garnett MC, et al. PLGA nanoparticles prepared by nanoprecipitation: drug loading and release studies of a water soluble drug. J. Controlled Release. 1999;57:171–185.

[259] Sakai K, Hayashi C, Yamaji H, et al. Use of nonionic surfactants for effective supply of phosphatidic acid in serum-free culture of Chinese hamster ovary cells. J. Biosci. Bioeng. 2001;92:256–261.

[260] Madani F, Goodarzi A, Hashemi M, et al. Preparation of Methotrexate loaded PLGA nanoparticles coated with PVA and Poloxamer188. Nanomedicine Res. J. 2018;3:19–24.

[261] Santander-Ortega MJ, Jódar-Reyes AB, Csaba N, et al. Colloidal stability of pluronic F68-coated PLGA nanoparticles: a variety of stabilisation mechanisms. J. Colloid Interface Sci. 2006;302:522–529.

[262] Ratner BD, Castner DG. Electron Spectroscopy for Chemical Analysis. Surf. Anal. – Princ. Tech. [Internet]. John Wiley & Sons, Ltd; 2009 [cited 2020 Jan 17]. p. 47–112. Available from: https://onlinelibrary.wiley.com/doi/abs/10.1002/9780470721582.ch3.

[263] Lee L-H. Characterization of Metal and Polymer Surfaces V1: Metal Surfaces. Elsevier; 2012.

[264] Mourdikoudis S, Pallares RM, Thanh NTK. Characterization techniques for nanoparticles: comparison and complementarity upon studying nanoparticle properties. Nanoscale. 2018;10:12871–12934.

[265] Wang GD, Nguyen HT, Chen H, et al. X-Ray Induced Photodynamic Therapy: A Combination of Radiotherapy and Photodynamic Therapy. Theranostics. 2016;6:2295–2305.

[266] Mann J, Ramakrishna R, Magge R, et al. Advances in Radiotherapy for Glioblastoma. Front. Neurol. [Internet]. 2018 [cited 2019 Oct 20];8. Available from: https://www.ncbi.nlm.nih.gov/pmc/articles/PMC5775505/.